Draft version September 12, 2016
Preprint typeset using LaTeX style emulateapj v. 5/2/11

arXiv:1609.02767v1 [astro-ph.EP] 9 Sep 2016

HAT-P-65b AND HAT-P-66b: TWO TRANSITING INFLATED HOT JUPITERS AND OBSERVATIONAL EVIDENCE FOR THE RE-INFLATION OF CLOSE-IN GIANT PLANETS†

J. D. Hartman[1], G. Á. Bakos[1,*,**], W. Bhatti[1], K. Penev[1], A. Bieryla[2], D. W. Latham[2], G. Kovács[3], G. Torres[2], Z. Csubry[1], M. de Val-Borro[1], L. Buchhave[4], T. Kovács[3], S. Quinn[5], A. W. Howard[6], H. Isaacson[7], B. J. Fulton[6], M. E. Everett[8], G. Esquerdo[2], B. Béky[9], T. Szklenar[10], E. Falco[2], A. Santerne[12], I. Boisse[11], G. Hébrard[13], A. Burrows[1], J. Lázár[10], I. Papp[10], P. Sári[10]

Draft version September 12, 2016

ABSTRACT

We present the discovery of the transiting exoplanets HAT-P-65b and HAT-P-66b, with orbital periods of 2.6055 d and 2.9721 d, masses of $0.527 \pm 0.083\,M_{\rm J}$ and $0.783 \pm 0.057\,M_{\rm J}$, and inflated radii of $1.89 \pm 0.13\,R_{\rm J}$ and $1.59^{+0.16}_{-0.10}\,R_{\rm J}$, respectively. They orbit moderately bright ($V = 13.145 \pm 0.029$, and $V = 12.993 \pm 0.052$) stars of mass $1.212 \pm 0.050\,M_{\odot}$ and $1.255^{+0.107}_{-0.054}\,M_{\odot}$. The stars are at the main sequence turnoff. While it is well known that the radii of close-in giant planets are correlated with their equilibrium temperatures, whether or not the radii of planets increase in time as their hosts evolve and become more luminous is an open question. Looking at the broader sample of well-characterized close-in transiting giant planets, we find that there is a statistically significant correlation between planetary radii and the fractional ages of their host stars, with a false alarm probability of only 0.0041%. We find that the correlation between the radii of planets and the fractional ages of their hosts is fully explained by the known correlation between planetary radii and their present day equilibrium temperatures, however if the zero-age main sequence equilibrium temperature is used in place of the present day equilibrium temperature then a correlation with age must also be included to explain the planetary radii. This suggests that, after contracting during the pre-main-sequence, close-in giant planets are re-inflated over time due to the increasing level of irradiation received from their host stars. Prior theoretical work indicates that such a dynamic response to irradiation requires a significant fraction of the incident energy to be deposited deep within the planetary interiors.

Subject headings: planetary systems — stars: individual (HAT-P-65, GSC 1111-00383, HAT-P-66, GSC 3814-00307) techniques: spectroscopic, photometric

[1] Department of Astrophysical Sciences, Princeton University, Princeton, NJ 08544, USA; email: jhartman@astro.princeton.edu
[*] Alfred P. Sloan Research Fellow
[**] Packard Fellow
[2] Harvard-Smithsonian Center for Astrophysics, Cambridge, MA 02138, USA
[3] Konkoly Observatory of the Hungarian Academy of Sciences, Budapest, Hungary
[4] Centre for Star and Planet Formation, Natural History Museum of Denmark, University of Copenhagen, DK-1350 Copenhagen, Denmark
[5] Department of Physics and Astronomy, Georgia State University, Atlanta, GA 30303, USA
[6] Institute for Astronomy, University of Hawaii, Honolulu, HI 96822, USA
[7] Department of Astronomy, University of California, Berkeley, CA, USA
[8] National Optical Astronomy Observatory, Tucson, AZ, USA
[9] Google
[10] Hungarian Astronomical Association, Budapest, Hungary
[11] Aix Marseille Université, CNRS, LAM (Laboratoire d'Astrophysique de Marseille) UMR 7326, F-13388, Marseille, France
[12] Instituto de Astrofisica e Ciências do Espaço, Universidade do Porto, CAUP, Rua das Estrelas, PT4150-762 Porto, Portugal
[13] Institut d'Astrophysique de Paris, UMR7095 CNRS, Université Pierre & Marie Curie, 98bis boulevard Arago, 75014 Paris, France

† Based on observations obtained with the Hungarian-made Automated Telescope Network. Based on observations obtained at the W. M. Keck Observatory, which is operated by the University of California and the California Institute of Technology. Keck time has been granted by NOAO (A289Hr, A245Hr) and NASA (N029Hr, N154Hr, N130Hr, N133Hr, N169Hr, N186Hr). Based on observations obtained with the Tillinghast Reflector 1.5 m telescope and the 1.2 m telescope, both operated by the Smithsonian Astrophysical Observatory at the Fred Lawrence Whipple Observatory in AZ. Based on observations made with the Nordic Optical Telescope, operated on the island of La Palma jointly by Denmark, Finland, Norway, Sweden, in the Spanish Observatorio del Roque de los Muchachos of the Intituto de Astrofísica de Canarias. Based on observations made with the SOPHIE spectrograph on the 1.93 m telescope at Observatoire de Haute-Provence (OHP, CNRS/AMU), France (programs 15A.PNP.HEBR and 15B.PNP.HEBR). Data presented herein were obtained at the WIYN Observatory from telescope time allocated to NN-EXPLORE through the scientific partnership of the National Aeronautics and Space Administration, the National Science Foundation, and the National Optical Astronomy Observatory. This work was supported by a NASA WIYN PI Data Award, administered by the NASA Exoplanet Science Institute.

1. INTRODUCTION

The first transiting exoplanet (TEP) discovered, HD 209458b (Henry et al. 2000; Charbonneau et al. 2000), surprised the community in having a radius much larger than expected based on theoretical planetary structure models (e.g., Burrows et al. 2000; Bodenheimer et al. 2001). Since then many more inflated transiting planets have been discovered, the largest being WASP-79b with $R_P = 2.09 \pm 0.14\,R_{\rm J}$ (Smalley et al. 2012). It has also become apparent that the degree of planet inflation is closely tied to a planet's proximity to its host star (e.g., Fortney et al. 2007; Enoch et al. 2011b; Kovács et al. 2010; Béky et al. 2011; Enoch et al. 2012). This is expected on theoretical grounds, as some additional energy, beyond the initial heat from formation, must be responsible for making the planet so large, and in principle there is more than enough energy available from stellar irradiation or tidal forces to inflate close-in planets at $a < 0.1\,{\rm AU}$ (Bodenheimer et al. 2001). Whether and how the energy is transfered into planetary interiors remains a mystery, however, despite a large amount of theoretical work devoted to the subject (see, e.g., Spiegel & Burrows 2013 for a review). The problem is intrinsically challenging, requiring the simultaneous treatment of molecular chemistry, radiative transport, and turbulent (magneto-)hydrodynamics, carried out over pressures, densities, temperatures, and length-scales that span many orders of magnitude. Theoretical models of planet inflation have thus, by necessity, made numerous simplifying assumptions, often introducing free parameters whose values are unknown, or poorly known. One way to make further progress on this problem is to build up a larger sample of inflated planets to identify patterns in their properties that may be used to discriminate between different theories.

Recently Lopez & Fortney (2016) proposed an observational test to distinguish between two broad classes of models. Noting that once a star leaves the main sequence, the irradiation of its planets with periods of tens of days becomes comparable to the irradiation of very short period planets around main sequence stars, they suggested searching for inflated planets with periods of tens of days around giant stars. Planets at these orbital periods are not inflated when found around main sequence stars (Demory & Seager 2011), so finding them to be inflated around giants would indicate that the enhanced irradiation is able to directly inflate the planets. As shown, for example, by Liu et al. (2008) and also by Spiegel & Burrows (2013), this in turn would imply that energy must be transferred deep into the planetary interior, and would rule out models where the energy is deposited only in the outer layers of the planet, and serves simply to slow the planet's contraction from its initial highly inflated state. The recently discovered planet EPIC 211351816.01 (Grunblatt et al. 2016, found using *K2*) is a possible example of a re-inflated planet around a giant star, with the planet having a larger than usual radius of $1.27 \pm 0.09\,R_{\rm J}$ given its orbital period of 8.4 days. The planet K2-39b (Van Eylen et al. 2016), on the other hand, does not appear to be exceptionally inflated ($R_p = 0.732 \pm 0.098\,R_{\rm J}$) despite being found on a very short period orbit around a sub-giant star. This planet, however, is in the Super-Neptune mass range ($M_p = 0.158 \pm 0.031\,M_{\rm J}$) and may not have a gas-dominated composition.

Here we present the discovery of two transiting inflated planets by the Hungarian-made Automated Telescope Network (HATNet; Bakos et al. 2004). As we will show, the planets have radii of $1.89 \pm 0.13\,R_{\rm J}$ and $1.59^{+0.16}_{-0.10}\,R_{\rm J}$, and are around a pair of stars that are leaving the main sequence. HATNet, together with its southern counterpart HATSouth (Bakos et al. 2013), has now discovered 17 highly inflated planets with $R \geq 1.5\,R_{\rm J}$[17]. Adding those found by WASP (Pollacco et al. 2006), *Kepler* (Borucki et al. 2010), TrES (e.g., Mandushev et al. 2007) and KELT (e.g., Siverd et al. 2012), a total of 45 well-characterized highly inflated planets are now known, allowing us to explore some of their statistical properties. In this paper we find that inflated planets are more commonly found around moderately evolved stars that are more than 50% of the way through their main sequence lifetimes. Smaller radius close-in giant planets, by contrast, are generally found around less evolved stars. Taken at face value, this suggests that planets are re-inflated as they age, and indicates that energy must be transferred deep into the planetary interiors (e.g., Liu et al. 2008).

Of course, observational selection effects or systematic errors in the determination of stellar and planetary properties could potentially be responsible for the correlation as well. We therefore consider a variety of potentially important effects, such as the effect of stellar evolution on the detectability of transits and our ability to confirm planets through follow-up observations, and systematic errors in the orbital eccentricity, transit parameters, stellar atmospheric parameters, or in the comparison to stellar evolution models. We conclude that the net selection effect would, if anything, tend to favor the discovery of large planets around less evolved stars, while potential systematic errors are too small to explain the correlation. We also show that the correlation remains significant even after accounting for non-trivial truncations placed on the data as a result of the observational selection biases. We are therefore confident in the robustness of this result.

The organization of the paper is as follows. In Section 2 we describe the photometric and spectroscopic observations made to discover and characterize HAT-P-65b and HAT-P-66b. In Section 3 we present the analysis carried out to determine the stellar and planetary parameters and to rule out blended stellar eclipsing binary false positive scenarios. In Section 4 we place these planets into context, and find that large radius planets are more commonly found around moderately evolved, brighter stars. We provide a brief summary of the results in Section 5.

2. OBSERVATIONS

2.1. *Photometric detection*

Both HAT-P-65 (R.A. $=21^{\rm h}03^{\rm m}37.44$s, Dec. $=+11^\circ59'21.9''$ (J2000), $V = 13.145 \pm 0.029$ mag, spectral type G2) and HAT-P-66 (R.A. $=10^{\rm h}02^{\rm m}17.52$s, Dec. $=+53^\circ57'03.1''$ (J2000), $V = 12.993 \pm 0.052$ mag,

[17] This radius is chosen simply for illustrative purposes, and is not meant to imply that planets with radii above this value are physically distinct from those with radii below this value.

spectral type G0) were selected as candidate transiting planet systems based on Sloan r-band photometric time series observations carried out with the HATNet telescope network (Bakos et al. 2004).

HATNet consists of six 11 cm aperture telephoto lenses, each coupled to an APOGEE front-side-illuminated CCD camera, and each placed on a fully-automated telescope mount. Four of the instruments are located at Fred Lawrence Whipple Observatory (FLWO) in Arizona, USA, while two are located on the roof of the Submillimeter Array hangar building at Mauna Kea Observatory (MKO) on the island of Hawaii, USA. Each instrument observes a $10.6^\circ \times 10.6^\circ$ field of view, and continuously monitors one or two fields each night, where a field corresponds to one of 838 fixed pointings used to cover the full 4π celestial sphere. A typical field is observed for approximately three months using one or two instruments (e.g., field G342 containing HAT-P-65), while a handful of fields have been observed extensively using all six instruments in the network and with observations repeated in multiple seasons (e.g., field G101 containing HAT-P-66). The former observing strategy maximizes the sky coverage of the survey, while maintaining nearly complete sensitivity to transiting giant planets with orbital periods of a few days. The latter strategy substantially increases the sensitivity to Neptune and Super-Earth-size planets, as well as planets with periods greater than 10 days, but with the trade-off of covering a smaller area of the sky.

Table 1 summarizes the properties of the HATNet observations collected for each system, including which HAT instruments were used, the date ranges over which each target was observed, the median cadence of the observations, and the per-point photometric precision after trend filtering.

We reduce the HATNet observations to light curves, for all stars in a field with $r < 14.5$, following Bakos et al. (2004). We used aperture photometry routines based on the FITSH software package (Pál 2012), and filtered systematic trends from the light curves following Kovács et al. (2005) (i.e., TFA) and Bakos et al. (2010) (i.e., EPD). Transits were identified in the filtered light curves using the Box-Least Squares method (BLS; Kovács et al. 2002). After identifying the transits we then re-applied TFA while preserving the shape of the transit signal as described in Kovács et al. (2005). This procedure is referred to as signal-reconstruction TFA. The final trend-filtered, and signal-reconstructed light curves are shown phase-folded in Figure 1, while the measurements are available in Table 3.

We searched the residual HATNet light curves of both objects for additional periodic signals using BLS. Neither target shows evidence for additional transits with BLS, however this conclusion depends on the set of template light curves used in applying signal-reconstruction TFA to remove systematics. For HAT-P-65 we find that with an alternative set of templates the residuals display a marginally significant transit signal with a period of 2.573 days, which is only slightly different from the main transit period of 2.6054552 ± 0.0000031 days. The transits detected at this period come from data points near orbital phase 0.25 when phased at the primary transit period. Since the detection of this additional signal depends on the template set used, and since any planet orbiting with a period so close to (but not equal to) that of the hot Jupiter HAT-P-65b would almost certainly be unstable, we suspect that the $P = 2.573$ day transit signal is not of physical origin.

We also searched the residual light curves for periodic signals using the Generalized Lomb-Scargle method (GLS; Zechmeister & Kürster 2009). For HAT-P-65 no statistically significant signal is detected in the GLS periodogram either. The highest peak in the periodogram is at a period of 0.035 d and has a semi-amplitude of 1.2 mmag (using a Markov-Chain Monte Carlo procedure to fit a sinusoid with a variable period yields a 95% confidence upper limit of 1.7 mmag on the semi-amplitude). For HAT-P-66, for our default light curve (i.e., the one included in Table 3), we do see significant peaks in the periodogram at periods of $P = 83.3029$ d and 0.98664 d (and its harmonics) and with formal false alarm probabilities of 10^{-11}, and semi-amplitudes of ~ 0.02 mag. Given the effective sampling rate of the observations, the two signals are aliases of each other. Based on an inspection of the light curve, we conclude that this detected variability is likely due to additional systematic errors in the photometry which were not effectively removed by our filtering procedures, and that the signal is not astrophysical in nature. Indeed if we use an alternative TFA template set in filtering the HAT-P-66 light curve, we detect no significant signal in the GLS spectrum, and place an upper limit on the amplitude of any periodic signal of 1 mmag.

2.2. *Spectroscopic Observations*

Spectroscopic observations of both HAT-P-65 and HAT-P-66 were carried out using the Tillinghast Reflector Echelle Spectrograph (TRES; Fűresz 2008) on the 1.5 m Tillinghast Reflector at FLWO, and HIRES (Vogt et al. 1994) on the Keck-I 10 m at MKO. For HAT-P-65 we also obtained observations using the FIbre-fed Échelle Spectrograph (FIES) on the 2.5 m Nordic Optical Telescope (NOT; Djupvik & Andersen 2010) at the Observatorio del Roque de los Muchachos on the Spanish island of La Palma. For HAT-P-66 spectroscopic observations were also collected using the SOPHIE spectrograph on the 1.93 m telescope at the Observatoire de Haute-Provence (OHP; Bouchy et al. 2009) in France. The spectroscopic observations collected for each system are summarized in Table 2. Phase-folded high-precision RV and spectral line bisector span (BS) measurements are plotted in Figure 2 together with our best-fit models for the RV orbital wobble of the host stars (Section 3.3). The individual RV and BS measurements are made available in Table 7 at the end of the paper.

The TRES observations were reduced to spectra and cross-correlated against synthetic stellar templates to measure the RVs and to estimate $T_{\rm eff\star}$, $\log g_\star$, and $v \sin i$. Here we followed the procedure of Buchhave et al. (2010), initially making use of a single order containing the gravity and temperature-sensitive Mg b lines. Based on these "reconnaissance" observations we quickly ruled out common false positive scenarios, such as transiting M dwarf stars, or blends between giant stars and pairs of eclipsing dwarf stars (e.g., Latham et al. 2009). For HAT-P-65 we only obtained a single TRES observation which, in combination with the FIES observations dis-

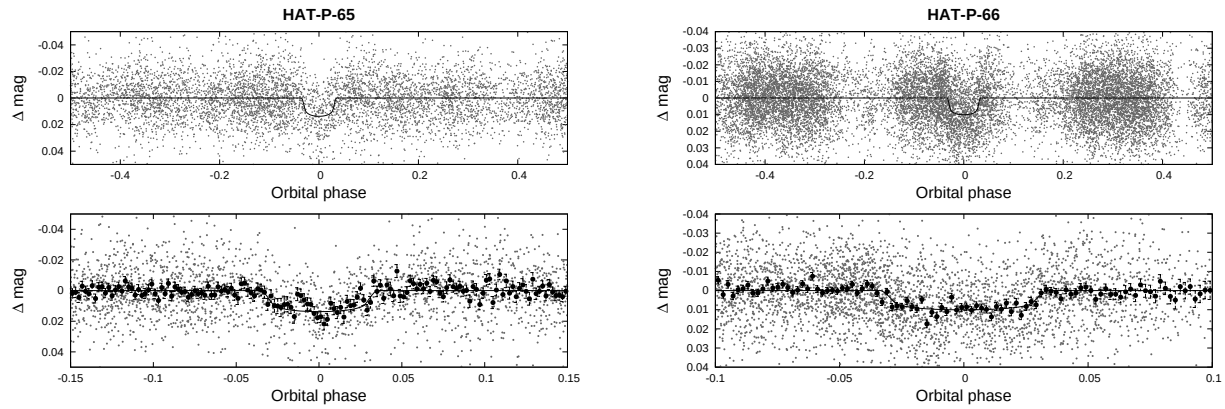

Figure 1. Phase-folded unbinned HATNet light curves for HAT-P-65 (left) and HAT-P-66 (right). In each case we show two panels. The top panel shows the full light curve, while the bottom panel shows the light curve zoomed-in on the transit. The solid lines show the model fits to the light curves. The dark filled circles in the bottom panels show the light curves binned in phase with a bin size of 0.002.

Table 1
Summary of photometric observations

Instrument/Field[a]	Date(s)	# Images	Cadence[b] (sec)	Filter	Precision[c] (mmag)
HAT-P-65					
HAT-6/G342	2009 Sep–2009 Dec	2738	231	r	16.7
HAT-8/G342	2009 Sep–2009 Dec	3174	235	r	16.6
FLWO 1.2 m/KeplerCam	2011 Jun 10	86	124	i	1.6
FLWO 1.2 m/KeplerCam	2011 Jun 26	108	135	i	1.3
FLWO 1.2 m/KeplerCam	2011 Jul 14	73	133	i	2.3
FLWO 1.2 m/KeplerCam	2011 Sep 20	117	124	i	1.9
FLWO 1.2 m/KeplerCam	2013 Sep 16	188	60	z	3.3
FLWO 1.2 m/KeplerCam	2013 Sep 29	295	60	i	1.4
FLWO 1.2 m/KeplerCam	2013 Oct 04	294	60	i	1.3
HAT-P-66					
HAT-10/G101	2011 Feb–2012 Mar	2029	212	r	16.8
HAT-5/G101	2011 Feb–2012 Apr	1520	214	r	18.1
HAT-6/G101	2011 Feb–2012 Mar	1178	214	r	16.9
HAT-7/G101	2011 Feb–2012 Mar	4931	212	r	14.9
HAT-8/G101	2011 May–2012 Jun	4157	212	r	14.5
HAT-9/G101	2011 Oct–2012 Jan	260	212	r	13.6
FLWO 1.2 m/KeplerCam	2015 Apr 29	204	59	i	1.9
FLWO 1.2 m/KeplerCam	2015 Nov 26	273	60	z	1.9
FLWO 1.2 m/KeplerCam	2015 Dec 08	131	60	i	1.9

[a] For HATNet data we list the HATNet unit and field name from which the observations are taken. HAT-5, -6, -7 and -10 are located at Fred Lawrence Whipple Observatory in Arizona. HAT-8 and -9 are located on the roof of the Smithsonian Astrophysical Observatory Submillimeter Array hangar building at Mauna Kea Observatory in Hawaii. Each field corresponds to one of 838 fixed pointings used to cover the full 4π celestial sphere. All data from a given HATNet field are reduced together, while detrending through External Parameter Decorrelation (EPD) is done independently for each unique unit+field combination.
[b] The median time between consecutive images rounded to the nearest second. Due to factors such as weather, the day–night cycle, guiding and focus corrections the cadence is only approximately uniform over short timescales.
[c] The RMS of the residuals from the best-fit model.

cussed below, rules out these false positive scenarios. For HAT-P-66 the initial TRES RVs showed evidence of an orbital variation consistent with a planetary-mass companion producing the transits detected by HATNet, so we continued collecting higher S/N observations of this system with TRES. High precision RVs and BSs were measured from these spectra via a multi-order analysis (e.g., Bieryla et al. 2014).

The FIES spectra of HAT-P-65 were reduced in a similar manner to the TRES data (Buchhave et al. 2010), and were used for reconnaissance. Two exposures were obtained using the medium-resolution fiber, while the third was obtained with the high-resolution fiber. One of the two medium resolution observations had sufficiently high S/N to be used for characterizing the stellar atmospheric parameters (Section 3.1).

The HIRES observations of HAT-P-65 and HAT-P-66 were reduced to relative RVs in the Solar System barycenter frame following the method of Butler et al. (1996), and to BSs following Torres et al. (2007). We also measured Ca II HK chromospheric emission indices (the so-called S and $\log_{10} R'_{\rm HK}$ indices) following Isaacson & Fischer (2010) and Noyes et al. (1984). The I_2-free template observations of each system were also

used to determine the adopted stellar atmospheric parameters (Section 3.1).

The SOPHIE spectra of HAT-P-66 were collected as described in Boisse et al. (2013) and reduced following Santerne et al. (2014). One of the observations was obtained during a planetary transit and is excluded from the analysis.

2.3. *Photometric follow-up observations*

In order to better determine the physical parameters of each TEP system, and to aid in excluding blended stellar eclipsing binary false positive scenarios, we conducted follow-up photometric time-series observations of each object using KeplerCam on the 1.2 m telescope at FLWO. These observations are summarized in Table 1, where we list the dates of the observed transit events, the number of images collected for each event, the cadence of the observations, the filters used, and the per-point photometric precision achieved after trend-filtering. The images were reduced to light curves via aperture photometry based on the FITSH package (following Bakos et al. (2010)), and filtered for trends, which were fit to the light curves simultaneously with the transit model (Section 3.3). The resulting trend filtered light curves are plotted together with the best-fit transit model in Figure 3 for HAT-P-65 and in Figure 4 for HAT-P-66. The data are made available in Table 3.

2.4. *Imaging Constraints on Resolved Neighbors*

In order to detect possible neighboring stars which may be diluting the transit signals we obtained J and K_S-band snapshot images of both targets using the WIYN High-Resolution Infrared Camera (WHIRC) on the WIYN 3.5 m telescope at Kitt Peak National Observatory (KPNO) in AZ. Observations were obtained on the nights of 2016 April 24, 27 and 28, with seeing varying between $\sim 0\farcs5$ and $\sim 1''$. Images were collected at different nod positions. These were calibrated, background-subtracted, registered and median-combined using the same tools that we used for reducing the KeplerCam images.

We find that HAT-P-65 has a neighbor located $3\farcs6$ to the west with a magnitude difference of $\Delta J = 4.91 \pm 0.01$ mag and $\Delta K = 4.95 \pm 0.03$ mag relative to HAT-P-65 (Figure 5). The neighbor is too faint and distant to be responsible for the transits detected in either the HATNet or KeplerCam observations. The neighbor has a $J - K$ color that is the same as HAT-P-65 to within the uncertainties, and is thus a background star with an effective temperature that is similar to that of HAT-P-65, and not a physical companion. No neighbor is detected within $10''$ of HAT-P-66.

Figure 6 shows the J and K-band magnitude contrast curves for HAT-P-65 and HAT-P-66 based on these observations. These curves are calculated using the method and software described by Espinoza et al. (2016). The bands shown in these images represent the variation in the contrast limits depending on the position angle of the putative neighbor.

3. ANALYSIS

3.1. *Properties of the parent star*

High-precision atmospheric parameters, including the effective surface temperature $T_{\rm eff\star}$, the surface gravity $\log g_\star$, the metallicity [Fe/H], and the projected rotational velocity $v \sin i$, were determined by applying the Stellar Parameter Classification (SPC; Buchhave et al. 2012) procedure to our high resolution spectra. For HAT-P-65 this analysis was performed on the highest S/N FIES spectrum and on our Keck-I/HIRES I_2-free template spectrum (we adopt the weighted average of each parameter determined from the two spectra). For HAT-P-66 this analysis was performed on our Keck-I/HIRES I_2-free template spectrum. We assume a minimum uncertainty of 50 K on $T_{\rm eff\star}$, 0.10 dex on $\log g_\star$, 0.08 dex on [Fe/H], and 0.5 km s^{-1} on $v \sin i$, which reflects the systematic uncertainty in the method, and is based on applying the SPC analysis to observations of spectroscopic standard stars.

Following Sozzetti et al. (2007) we combine the $T_{\rm eff\star}$ and [Fe/H] values measured from the spectra with the stellar densities ($\rho_\star$) determined from the light curves (based on the analysis in Section 3.3) to determine the physical parameters of the host stars (i.e., their masses, radii, surface gravities, ages, luminosities, and broadband absolute magnitudes) via interpolation within the Yonsei-Yale theoretical stellar isochrones (YY; Yi et al. 2001). Figure 7 compares the model isochrones to the measured $T_{\rm eff\star}$ and $\rho_\star$ values for each system.

For HAT-P-65 the $\log g_\star$ value determined from this analysis differed by 0.19 dex ($\sim 1.9\sigma$) from the initial value determined through SPC. A difference of this magnitude is typical and reflects the difficulty of accurately measuring all four atmospheric parameters simultaneously via cross-correlation with synthetic templates (e.g., Torres et al. 2012). We therefore carried out a second SPC analysis of HAT-P-65 with $\log g_\star$ fixed based on this analysis, and then repeated the light curve analysis and stellar parameter determination, finding no appreciable change in $\log g_\star$. For HAT-P-66 the $\log g_\star$ value determined from the YY isochrones differed by only 0.007 dex from the initial spectroscopically determined value, so we did not carry out a second SPC iteration in this case.

The adopted stellar parameters for HAT-P-65 and HAT-P-66 are listed in Table 4. We also collect in this table a variety of photometric and kinematic properties for each system from catalogs. Distances are determined using the listed photometry and assuming a $R_V = 3.1$ Cardelli et al. (1989) extinction law.

The two stars are quite similar, with masses of $1.212 \pm 0.050\,M_\odot$ and $1.255^{+0.107}_{-0.054}\,M_\odot$ for HAT-P-65 and HAT-P-66, respectively, and with respective radii of $1.860 \pm 0.096\,R_\odot$ and $1.881^{+0.151}_{-0.095}\,R_\odot$. The stars are moderately evolved, with ages of 5.46 ± 0.61 Gyr and $4.66^{+0.52}_{-1.12}$ Gyr (these are $84 \pm 10\%$ and $83^{+9}_{-20}\%$ of each star's full lifetime, respectively). As we point out in Section 4, there appears to be a general trend among the host stars of highly inflated planets in which the largest planets are preferentially found around moderately evolved stars. HAT-P-65 and HAT-P-66 are in line with this trend.

3.2. *Excluding blend scenarios*

In order to exclude blend scenarios we carried out an analysis following Hartman et al. (2012). Here we attempt to model the available photometric data (in-

Table 2
Summary of spectroscopy observations

Instrument	UT Date(s)	# Spec.	Res. $(\lambda/\Delta\lambda)/1000$	S/N Range[a]	$\gamma_{\rm RV}$[b] ($\rm km\,s^{-1}$)	RV Precision[c] ($\rm m\,s^{-1}$)
HAT-P-65						
NOT 2.5 m/FIES	2010 Aug 21–22	2	46	24–28	−48.131	100
FLWO 1.5 m/TRES	2010 Oct 27	1	44	16.5	−47.768	100
NOT 2.5 m/FIES	2011 Oct 8	1	67	15	−47.799	1000
Keck-I/HIRES	2010 Dec 14	1	55	80	···	···
Keck-I/HIRES+I_2	2010 Dec–2013 Aug	12	55	64–106	···	25
HAT-P-66						
FLWO 1.5 m/TRES	2014 Nov–2015 Jun	10	44	17–22	7.973	43
OHP 1.93 m/SOPHIE	2015 Mar–2016 Jan	14	39	12–33	7.226	20
Keck-I/HIRES+I_2	2015 Dec–2016 Jan	5	55	78–119	···	12
Keck-I/HIRES	2016 Feb 3	1	55	148	···	···

[a] S/N per resolution element near 5180 Å.
[b] For high-precision RV observations included in the orbit determination this is the zero-point RV from the best-fit orbit. For other instruments it is the mean value. We do not provide this information for Keck-I/HIRES for which only relative velocities are measured.
[c] For high-precision RV observations included in the orbit determination this is the scatter in the RV residuals from the best-fit orbit (which may include astrophysical jitter), for other instruments this is either an estimate of the precision (not including jitter), or the measured standard deviation. We do not provide this quantity for the I_2-free templates obtained with Keck-I/HIRES.

Table 3
Light curve data for HAT-P-65 and HAT-P-66.

Object[a]	BJD[b] (2,400,000+)	Mag[c]	$\sigma_{\rm Mag}$	Mag(orig)[d]	Filter	Instrument
HAT-P-65	55128.75175	−0.00921	0.01482	···	r	HATNet
HAT-P-65	55115.72468	−0.00946	0.01149	···	r	HATNet
HAT-P-65	55120.93574	−0.02459	0.01224	···	r	HATNet
HAT-P-65	55115.72489	−0.01377	0.01518	···	r	HATNet
HAT-P-65	55094.88211	−0.01227	0.01156	···	r	HATNet
HAT-P-65	55128.75370	−0.00283	0.01249	···	r	HATNet
HAT-P-65	55154.80831	−0.01096	0.01202	···	r	HATNet
HAT-P-65	55102.69977	−0.00937	0.01341	···	r	HATNet
HAT-P-65	55128.75445	−0.00558	0.01427	···	r	HATNet
HAT-P-65	55115.72734	0.00413	0.01208	···	r	HATNet

Note. — This table is available in a machine-readable form in the online journal. A portion is shown here for guidance regarding its form and content.
[a] Either HAT-P-65 or HAT-P-66.
[b] Barycentric Julian Date is computed directly from the UTC time without correction for leap seconds.
[c] The out-of-transit level has been subtracted. For observations made with the HATNet instruments (identified by "HATNet" in the "Instrument" column) these magnitudes have been corrected for trends using the EPD and TFA procedures applied in signal-reconstruction mode. For observations made with follow-up instruments (anything other than "HATNet" in the "Instrument" column), the magnitudes have been corrected for a quadratic trend in time, for variations correlated with three PSF shape parameters, and with a linear basis of template light curves representing other systematic trends, which are fit simultaneously with the transit.
[d] Raw magnitude values without correction for the quadratic trend in time, or for trends correlated with the shape of the PSF. These are only reported for the follow-up observations.

cluding light curves and catalog broad-band photometric measurements) for each object as a blend between an eclipsing binary star system and a third star along the line of sight (either a physical association, or a chance alignment). The physical properties of the stars are constrained using the Padova isochrones (Girardi et al. 2002), while we also require that the brightest of the three stars in the blend have atmospheric parameters consistent with those measured with SPC. We also simulate composite cross-correlation functions (CCFs) and use them to predict RVs and BSs for each blend scenario considered.

Based on this analysis we rule out blended stellar eclipsing binary scenarios for both HAT-P-65 and HAT-P-66. For HAT-P-65 we are able to exclude blend scenarios, based solely on the photometry, with greater than 3.7σ confidence, while for HAT-P-66 we are able to exclude them with greater than 3.9σ confidence. For both objects, the blend models which come closest to fitting the photometric data (those which could not be rejected with 5σ confidence) can additionally be rejected due to the predicted large amplitude BS and RV variations

Table 4
Stellar parameters for HAT-P-65 and HAT-P-66 [a]

Parameter	**HAT-P-65** Value	**HAT-P-66** Value	Source
Astrometric properties and cross-identifications			
2MASS-ID	21033731+1159218	10021743+5357031	
GSC-ID	GSC 1111-00383	GSC 3814-00307	
R.A. (J2000)	$21^{\rm h}03^{\rm m}37.44$s	$10^{\rm h}02^{\rm m}17.52$s	2MASS
Dec. (J2000)	$+11°59'21.9''$	$+53°57'03.1''$	2MASS
$\mu_{\rm R.A.}$ (mas yr^{-1})	5.5 ± 1.9	-9.2 ± 1.8	UCAC4
$\mu_{\rm Dec.}$ (mas yr^{-1})	-4.0 ± 1.9	-11.4 ± 2.4	UCAC4
Spectroscopic properties			
$T_{\rm eff\star}$ (K)	5835 ± 51	6002 ± 50	SPC[b]
$\log g_\star$ (cgs)	4.18 ± 0.10	3.96 ± 0.10	SPC[c]
[Fe/H]	0.100 ± 0.080	0.035 ± 0.080	SPC
$v \sin i$ (km s^{-1}) ...	7.10 ± 0.50	7.57 ± 0.50	SPC
$v_{\rm mac}$ (km s^{-1})	1.0	1.0	Assumed
$v_{\rm mic}$ (km s^{-1})	2.0	2.0	Assumed
$\gamma_{\rm RV}$ (m s^{-1})	-47.77 ± 0.10	7.97 ± 0.10	TRES[d]
$S_{\rm HK}$	...	...	HIRES
$\log R'_{\rm HK}$	...	...	HIRES
Photometric properties			
B (mag)	13.818 ± 0.021	13.552 ± 0.027	APASS[e]
V (mag)	13.145 ± 0.029	12.993 ± 0.052	APASS[e]
I (mag)	12.46 ± 0.10	12.339 ± 0.084	TASS Mark IV[f]
g (mag)	13.445 ± 0.016	13.209 ± 0.021	APASS[e]
r (mag)	12.948 ± 0.033	12.859 ± 0.064	APASS[e]
i (mag)	12.784 ± 0.097	12.771 ± 0.064	APASS[e]
J (mag)	11.892 ± 0.026	12.001 ± 0.022	2MASS
H (mag)	11.604 ± 0.022	11.735 ± 0.022	2MASS
K_s (mag)	11.528 ± 0.025	11.675 ± 0.022	2MASS
Derived properties			
$M_\star$ ($M_\odot$)	1.212 ± 0.050	$1.255^{+0.107}_{-0.054}$	YY+$\rho_\star$+SPC [g]
$R_\star$ ($R_\odot$)	1.860 ± 0.096	$1.881^{+0.151}_{-0.095}$	YY+$\rho_\star$+SPC
$\log g_\star$ (cgs)	3.983 ± 0.035	3.993 ± 0.045	YY+$\rho_\star$+SPC
$\rho_\star$ (g cm^{-3})	0.266 ± 0.035	0.269 ± 0.040	Light curves
$L_\star$ ($L_\odot$)	3.59 ± 0.40	$4.12^{+0.71}_{-0.46}$	YY+$\rho_\star$+SPC
M_V (mag)	3.43 ± 0.13	3.26 ± 0.15	YY+$\rho_\star$+SPC
M_K (mag,ESO) ..	1.93 ± 0.12	1.86 ± 0.14	YY+$\rho_\star$+SPC
Age (Gyr)	5.46 ± 0.61	$4.66^{+0.52}_{-1.12}$	YY+$\rho_\star$+SPC
A_V (mag)	0.090 ± 0.052	0.0000 ± 0.0062	YY+$\rho_\star$+SPC
Distance (pc)	841 ± 45	927^{+75}_{-49}	YY+$\rho_\star$+SPC

Note. — For both systems the fixed-circular-orbit model has a higher Bayesian evidence than the eccentric-orbit model. We therefore assume a fixed circular orbit in generating the parameters listed here.

[a] We adopt the IAU 2015 Resolution B3 nominal values for the Solar and Jovian parameters (Prša et al. 2016) for all of our calculations, taking $R_{\rm J}$ to be the nominal equatorial radius of Jupiter. Where necessary we assume $G = 6.6408 \times 10^{-11}$ m^{3}kg^{-1}s^{-1}. Because Yi et al. (2001) do not specify the assumed value for G or $M_\odot$, we take the stellar masses from these isochrones at face value without conversion. Any discrepancy results in an error that is less than one percent, which is well below the observational uncertainty. We note that the standard values assumed in prior HAT planet discovery papers are very close to the nominal values adopted here. In all cases the conversion results in changes to measured parameters that are indetectable at the level of precision to which they are listed.

[b] SPC = Stellar Parameter Classification procedure for the analysis of high-resolution spectra (Buchhave et al. 2012), applied to the TRES spectra of HAT-P-65 and the Keck/HIRES spectra of HAT-P-66. These parameters rely primarily on SPC, but have a small dependence also on the iterative analysis incorporating the isochrone search and global modeling of the data.

[c] The spectroscopically determined value of $\log g_\star$ is from our initial SPC analysis where $T_{\rm eff\star}$, $\log g_\star$, [Fe/H] and $v \sin i$ were all varied. Systematic errors are common when all four parameters are varied. The adopted values for $T_{\rm eff\star}$, [Fe/H] and $v \sin i$ stem from a second iteration of SPC, where $\log g_\star$ is fixed to the value determined through the light curve modeling and isochrone comparison. This value is listed under the "Derived Properties" section of the table.

[d] In addition to the uncertainty listed here, there is a ~ 0.1 km s^{-1} systematic uncertainty in transforming the velocities to the IAU standard system.

[e] From APASS DR6 for as listed in the UCAC 4 catalog (Zacharias et al. 2013).

[f] Droege et al. (2006).

[g] YY+$\rho_\star$+SPC = Based on the YY isochrones (Yi et al. 2001), $\rho_\star$ as a luminosity indicator, and the SPC results.

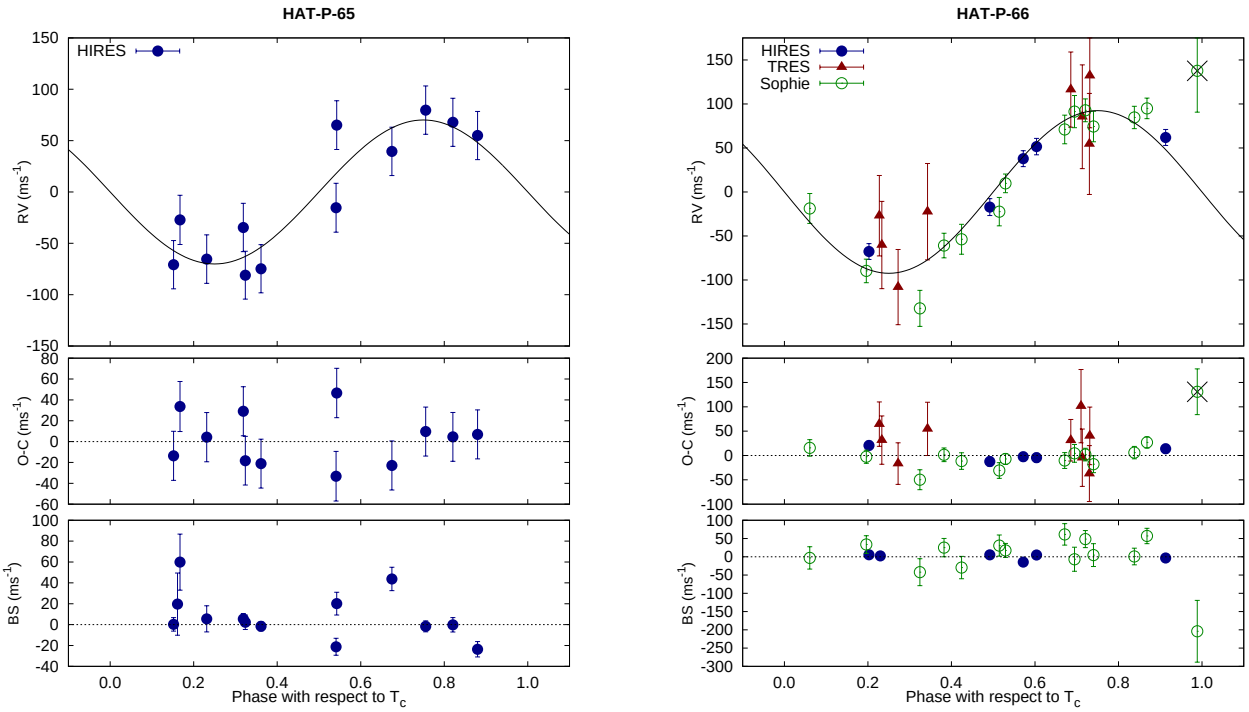

Figure 2. Phase-folded high-precision RV measurements for HAT-P-65 and HAT-P-66. The instruments used are labelled in the plots. In each case we show three panels. The top panel shows the phased measurements together with our best-fit circular-orbit model (see Table 5) for each system. Zero-phase corresponds to the time of mid-transit. The center-of-mass velocity has been subtracted. The second panel shows the velocity $O-C$ residuals from the best fit. The error bars include the jitter terms listed in Table 5 added in quadrature to the formal errors for each instrument. The third panel shows the bisector spans (BS). Note the different vertical scales of the panels. For HAT-P-66 the crossed-out SOPHIE measurement was obtained during transit and is excluded from the analysis.

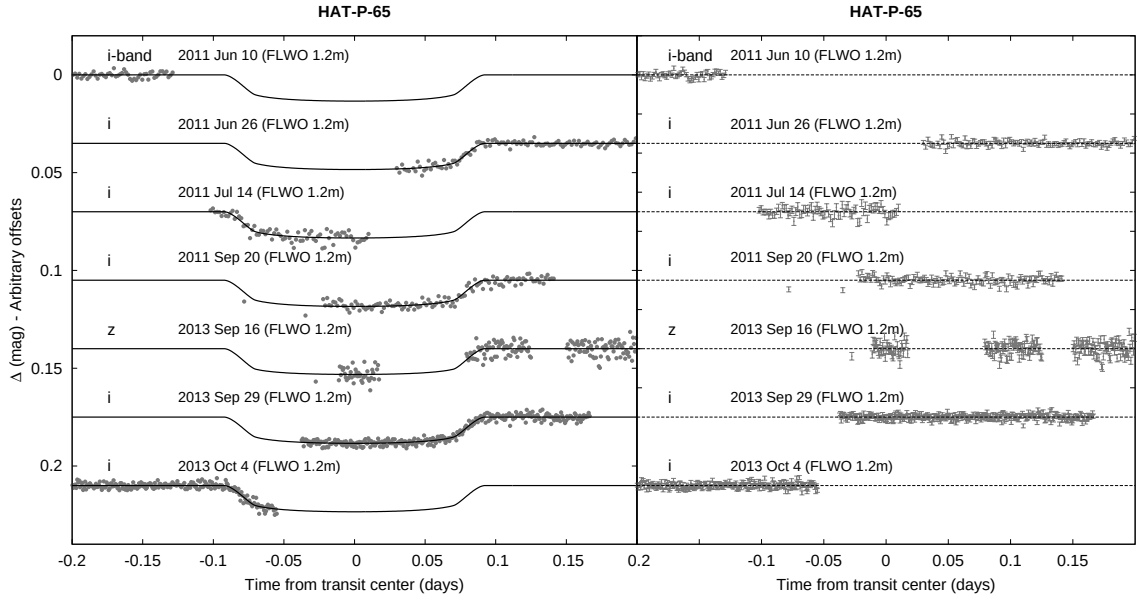
HAT-P-65
HAT-P-65
i-band 2011 Jun 10 (FLWO 1.2m)
i 2011 Jun 26 (FLWO 1.2m)
i 2011 Jul 14 (FLWO 1.2m)
i 2011 Sep 20 (FLWO 1.2m)
z 2013 Sep 16 (FLWO 1.2m)
i 2013 Sep 29 (FLWO 1.2m)
i 2013 Oct 4 (FLWO 1.2m)
Δ (mag) - Arbitrary offsets
Time from transit center (days)
Time from transit center (days)

Figure 3. Left: Unbinned transit light curves for HAT-P-65. The light curves have been filtered of systematic trends, which were fit simultaneously with the transit model. The dates of the events, filters and instruments used are indicated. Light curves following the first are displaced vertically for clarity. Our best fit from the global modeling described in Section 3.3 is shown by the solid lines. Right: The residuals from the best-fit model are shown in the same order as the original light curves. The error bars represent the photon and background shot noise, plus the readout noise.

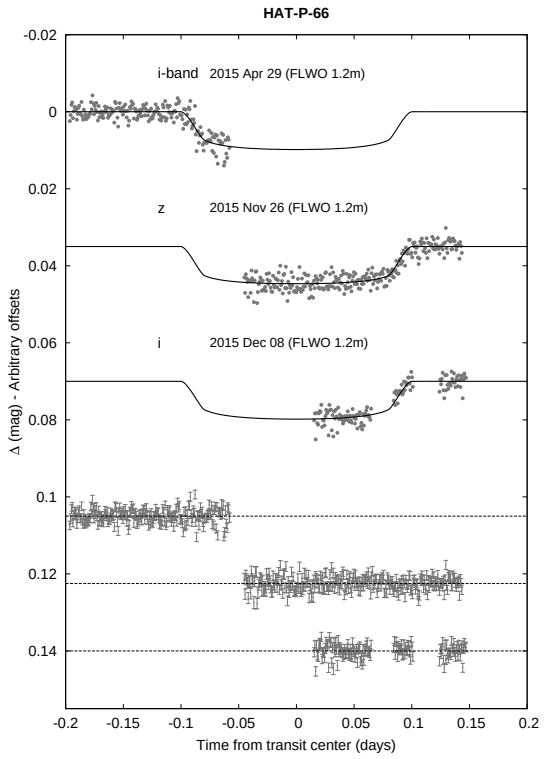
HAT-P-66
i-band 2015 Apr 29 (FLWO 1.2m)
z 2015 Nov 26 (FLWO 1.2m)
i 2015 Dec 08 (FLWO 1.2m)
Δ (mag) - Arbitrary offsets
Time from transit center (days)

Figure 4. Similar to Figure 3, here we show unbinned transit light curves for HAT-P-66. The residuals in this case are shown below in the same order as the original light curves.

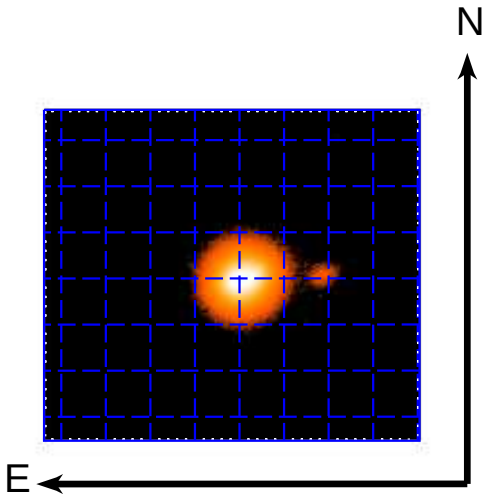

Figure 5. J-band image of HAT-P-65 from WHIRC on the WIYN 3.5 m showing the $\Delta J = 4.91 \pm 0.01$ mag neighbor located 3.″6 to the west. The grid spacing is 2″.

which we do not observe.

3.3. *Global modeling of the data*

In order to determine the physical parameters of the TEP systems, we carried out a global modeling of the HATNet and KeplerCam photometry, and the high-precision RV measurements following Pál et al. (2008); Bakos et al. (2010); Hartman et al. (2012). We use the Mandel & Agol (2002) transit model to fit the light curves, with limb darkening coefficients fixed to the values tabulated by Claret (2004) for the atmospheric parameters of the stars and the broad-band filters used in the observations. For the KeplerCam follow-up light curves we account for instrumental variations by using a set of linear basis vectors in the fit. The vectors that we use include the time of observations, the time squared, three parameters describing the shape of the PSF, and light curves for the twenty brightest non-variable stars in the field (TFA templates). For the TFA templates we use the same linear coefficient (which is varied in the fit) for all light curves collected for a given transiting planet system through a given filter, while for the other basis vectors we use a different coefficient for each light curve. For the HATNet light curves we use a Mandel & Agol (2002) model, and apply the fit to the signal-reconstruction TFA data (see Section 2.1). The RV curves are modeled using a Keplerian orbit, where we allow the zero-point for each instrument to vary independently in the fit, and we include an RV jitter term added in quadrature to the formal uncertainties. The jitter is treated as a free parameter which we fit for, and is taken to be independent for each instrument.

All observations of an individual system are modeled simultaneously using a Differential Evolution Markov Chain Monte Carlo procedure (ter Braak 2006). We visually inspect the Markov Chains and also apply a Geweke (1992) test to verify convergence and determine the burn-in period. For both systems we consider two models: a fixed-circular-orbit model, and an eccentric-orbit model. To determine which model to use we estimate the Bayesian evidence ratio from the Markov Chains following Weinberg et al. (2013), and find that for both systems the fixed-circular model has a greater evidence, and therefore adopt the parameters that come from this model. The resulting parameters for both planetary systems are listed in Table 5. We also list the 95% confidence upper-limit on the eccentricity for each system.

We find that HAT-P-65b has a mass of $0.527 \pm 0.083\,M_{\rm J}$, a radius of $1.89 \pm 0.13\,R_{\rm J}$, an equilibrium temperature (assuming zero albedo, and full redistribution of heat) of 1930 ± 45 K, and is consistent with a circular orbit, with a 95% confidence upper limit on the eccentricity of $e < 0.304$. HAT-P-66b has similar properties, with a mass of $0.783 \pm 0.057\,M_{\rm J}$, a radius of $1.59^{+0.16}_{-0.10}\,R_{\rm J}$, an equilibrium temperature (same assumptions) of 1896^{+66}_{-42} K, and an eccentricity of $e < 0.090$ with 95% confidence.

4. DISCUSSION

4.1. *Large Radius Planets More Commonly Found Around More Evolved Stars*

With radii of $1.89 \pm 0.13\,R_{\rm J}$ and $1.59^{+0.16}_{-0.10}\,R_{\rm J}$, HAT-P-65b and HAT-P-66b are among the largest hot Jupiters known. Both planets are found around moderately evolved stars approaching the end of their main sequence lifetimes. With an estimated age of 5.46 ± 0.61 Gyr, HAT-P-65 is 84 ± 10% of the way through its total lifespan, while HAT-P-66, with an age of $4.66^{+0.52}_{-1.12}$ Gyr, is 83^{+9}_{-20}% of the way through its lifespan. Looking at the broader sample of TEPs that have been discovered to date, we

Table 5
Orbital and planetary parameters for HAT-P-65b and HAT-P-66b [a]

Parameter	**HAT-P-65b** Value	**HAT-P-66b** Value
Light curve parameters		
P (days)	2.6054552 ± 0.0000031	2.9720860 ± 0.0000057
T_c (BJD) [b]	$2456409.33263 \pm 0.00046$	$2457258.79907 \pm 0.00072$
T_{14} (days) [b]	0.1819 ± 0.0022	0.1958 ± 0.0028
$T_{12} = T_{34}$ (days) [b]	0.0215 ± 0.0023	0.0174 ± 0.0025
$a/R_\star$	4.57 ± 0.20	$5.01^{+0.21}_{-0.32}$
$\zeta/R_\star$ [c]	12.438 ± 0.080	11.226 ± 0.096
$R_p/R_\star$	0.1045 ± 0.0024	0.0872 ± 0.0024
b^2	$0.215^{+0.070}_{-0.079}$	$0.110^{+0.106}_{-0.081}$
$b \equiv a\cos i/R_\star$	$0.464^{+0.070}_{-0.094}$	$0.33^{+0.13}_{-0.16}$
i (deg)	84.2 ± 1.3	86.2 ± 1.8
Limb-darkening coefficients [d]		
c_1, r	0.3439	0.3077
c_2, r	0.3359	0.3559
c_1, i	0.2544	0.2249
c_2, i	0.3414	0.3551
c_1, z	0.1949	0.1703
c_2, z	0.3379	0.3491
RV parameters		
K ($\mathrm{m\,s^{-1}}$)	68 ± 11	93.5 ± 5.7
e [e]	< 0.304	< 0.090
RV jitter HIRES ($\mathrm{m\,s^{-1}}$) [f]	26.0 ± 7.1	< 43.2
RV jitter TRES ($\mathrm{m\,s^{-1}}$)	···	< 22.1
RV jitter SOPHIE ($\mathrm{m\,s^{-1}}$)	···	< 16.3
Planetary parameters		
M_p (M_J)	0.527 ± 0.083	0.783 ± 0.057
R_p (R_J)	1.89 ± 0.13	$1.59^{+0.16}_{-0.10}$
$C(M_p, R_p)$ [g]	0.10	0.29
ρ_p ($\mathrm{g\,cm^{-3}}$)	0.096 ± 0.025	$0.242^{+0.045}_{-0.061}$
$\log g_p$ (cgs)	2.560 ± 0.090	$2.884^{+0.051}_{-0.081}$
a (AU)	0.03951 ± 0.00054	$0.04363^{+0.00121}_{-0.00064}$
T_eq (K)	1930 ± 45	1896^{+66}_{-42}
Θ [h]	0.0180 ± 0.0031	0.0336 ± 0.0034
$\log_{10}\langle F\rangle$ (cgs) [i]	9.495 ± 0.041	$9.465^{+0.060}_{-0.039}$

Note. — For both systems the fixed-circular-orbit model has a higher Bayesian evidence than the eccentric-orbit model. We therefore assume a fixed circular orbit in generating the parameters listed here.

[a] We adopt the IAU 2015 Resolution B3 nominal values for the Solar and Jovian parameters (Prša et al. 2016) for all of our calculations, taking R_J to be the nominal equatorial radius of Jupiter. Where necessary we assume $G = 6.6408 \times 10^{-11}\ \mathrm{m^3 kg^{-1} s^{-1}}$. Because Yi et al. (2001) do not specify the assumed value for G or $M_\odot$, we take the stellar masses from these isochrones at face value without conversion. Any discrepancy results in an error that is less than one percent, which is well below the observational uncertainty. We note that the standard values assumed in prior HAT planet discovery papers are very close to the nominal values adopted here. In all cases the conversion results in changes to measured parameters that are indetectable at the level of precision to which they are listed.

[b] Times are in Barycentric Julian Date calculated directly from UTC *without* correction for leap seconds. T_c: Reference epoch of mid transit that minimizes the correlation with the orbital period. T_{14}: total transit duration, time between first to last contact; $T_{12} = T_{34}$: ingress/egress time, time between first and second, or third and fourth contact.

[c] Reciprocal of the half duration of the transit used as a jump parameter in our MCMC analysis in place of $a/R_\star$. It is related to $a/R_\star$ by the expression $\zeta/R_\star = a/R_\star(2\pi(1 + e\sin\omega))/(P\sqrt{1-b^2}\sqrt{1-e^2})$ (Bakos et al. 2010).

[d] Values for a quadratic law, adopted from the tabulations by Claret (2004) according to the spectroscopic (SPC) parameters listed in Table 4.

[e] The 95% confidence upper limit on the eccentricity determined when $\sqrt{e}\cos\omega$ and $\sqrt{e}\sin\omega$ are allowed to vary in the fit.

[f] Term added in quadrature to the formal RV uncertainties for each instrument. This is treated as a free parameter in the fitting routine. In cases where the jitter is consistent with zero we list the 95% confidence upper limit.

[g] Correlation coefficient between the planetary mass M_p and radius R_p estimated from the posterior parameter distribution.

[h] The Safronov number is given by $\Theta = \frac{1}{2}(V_\mathrm{esc}/V_\mathrm{orb})^2 = (a/R_p)(M_p/M_\star)$ (see Hansen & Barman 2007).

[i] Incoming flux per unit surface area, averaged over the orbit.

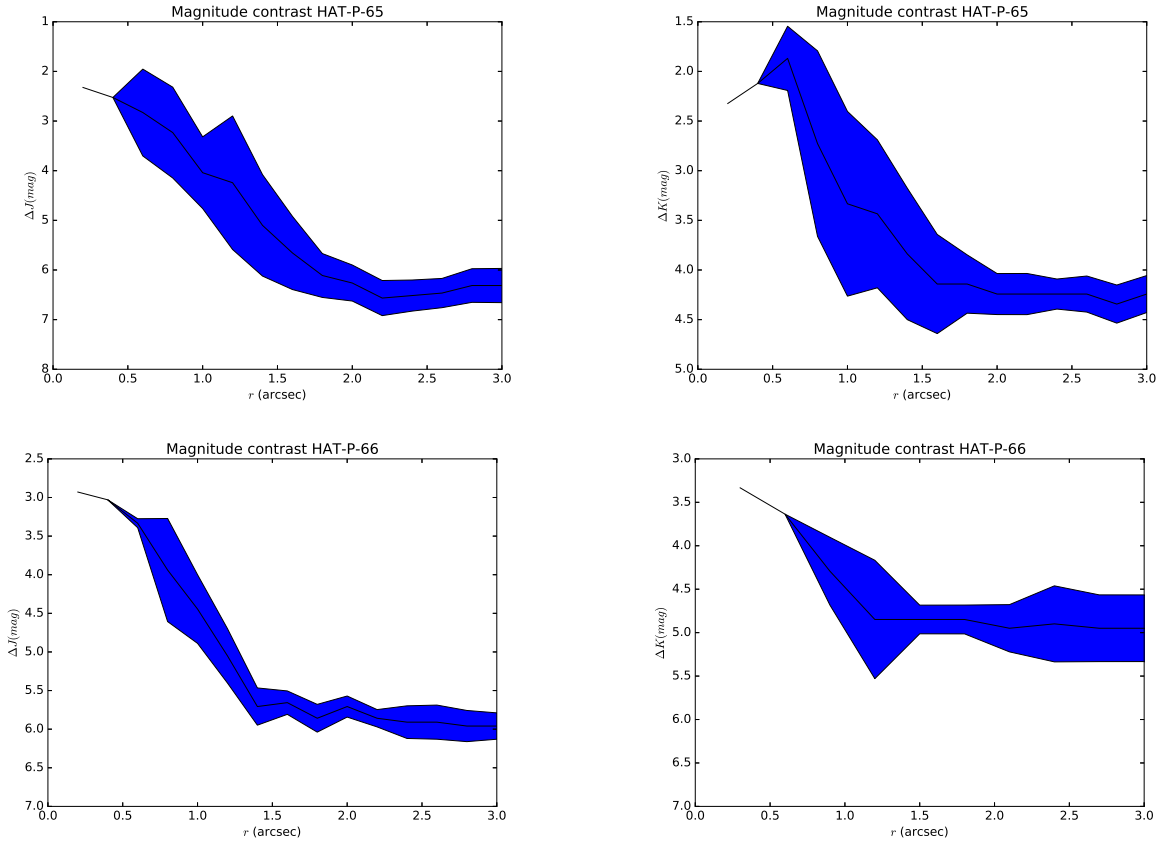

Figure 6. Contrast curves for HAT-P-65 (top) and HAT-P-66 (bottom) in the J-band (left) and K-band (right) based on observations made with WHIRC on the WIYN 3.5 m as described in Section 2.4. The bands show the variation in the contrast limits depending on the position angle of the putative neighbor.

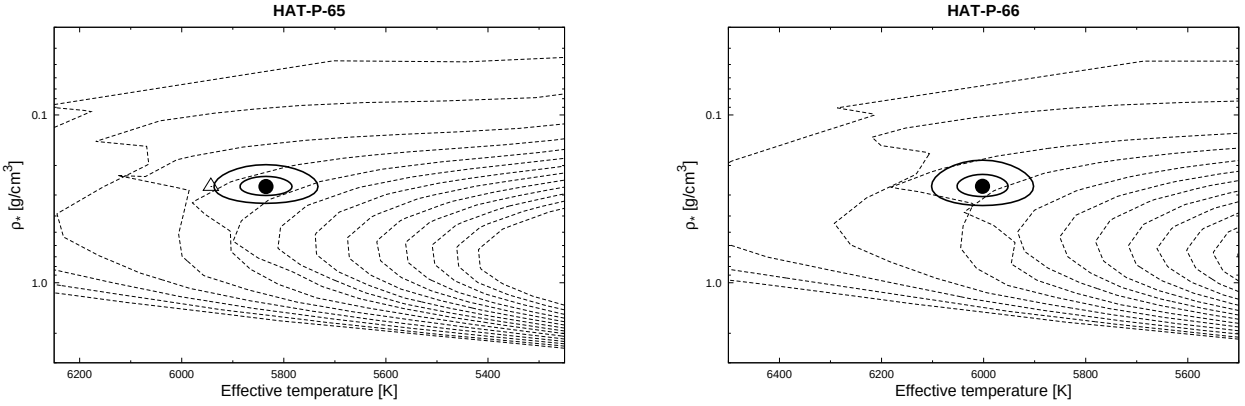

Figure 7. Model isochrones from Yi et al. (2001) for the measured metallicities of HAT-P-65 and HAT-P-66. We show models for ages of 0.2 Gyr and 1.0 to 14.0 Gyr in 1.0 Gyr increments (ages increasing from left to right). The adopted values of $T_{\rm eff\star}$ and $\rho_\star$ are shown together with their 1σ and 2σ confidence ellipsoids. The initial values of $T_{\rm eff\star}$ and $\rho_\star$ for HAT-P-65 from the first SPC and light curve analyses are represented with a triangle.

find that the largest exoplanets are preferentially found around moderately evolved stars.

This effect may be a by-product of the more physically important correlation between planet radius and equilibrium temperature (e.g., Fortney et al. 2007; Enoch et al. 2012; and Spiegel & Burrows 2013), with the planet equilibrium temperature increasing in time as its host star evolves and becomes more luminous. We will address the question of how the correlation between planet radius and host star fractional age which we demonstrate here relates to the radius–equilibrium temperature correlation in Section 4.1.1. While the planet radius–equilibrium temperature correlation is well known, whether or not the radii of planets can actually increase in time as their equilibrium temperatures increase has not been previously established. As discussed in Sections 1 and Sections 4.1.4 the answer to this question has important theoretical implications for understanding the physical mechanism behind the inflation of close-in giant planets. To address this question we will first attempt to determine whether or not there is a statistically signification correlation between planetary radii and the evolutionary status of their host stars.

Figure 8 shows TEP host stars on a $T_{\rm eff\star}$–$\rho_\star$ diagram. These two parameters are directly measured for TEP systems, and together with the [Fe/H] of the star, are the primary parameters used to characterize the stellar hosts. Here we limit the sample to systems with planets having $R_p > 0.5\,R_{\rm J}$ and $P < 10$ days. Because observational selection effects vary from survey to survey, we show separately the systems discovered by HAT (both HATNet and HATSouth), WASP, *Kepler*, TrES and KELT, which are the surveys that have discovered well-characterized planets with $R_p > 1.5\,R_{\rm J}$. The data for the HAT, WASP, TrES and KELT systems are drawn from a database of TEPs which we privately maintain, and are listed, together with references, in Table 8 at the end of this paper. These are planets which have been announced on the arXiv pre-print server as of 2016 June 2, and supplemented by some additional fully confirmed planets from HAT which had not been announced by that date. For *Kepler* we take the data from the NASA Exoplanet archive[18]. In Figure 8 we distinguish between hosts with planets having $R_p > 1.5\,R_{\rm J}$, and hosts with planets having $R_p < 1.5\,R_{\rm J}$. The lower bound in each panel shows the solar metallicity, 200 Myr ZAMS isochrone from the YY models, while the upper bound shows the locus of points for stars having an age that is the lesser of 13.7 Gyr or 90% of their total lifetime, again assuming solar metallicity and using the YY models. For all of the surveys considered, planets with $R > 1.5\,R_{\rm J}$ tend to be found around host stars that are more evolved (closer to the 90% lifetime locus) than planets with $R < 1.5\,R_{\rm J}$. Moreover, very few highly inflated planets have been discovered around stars close to the ZAMS. The largest planets also tend to be found around hot/massive stars, and have the highest level of irradiation.

For another view of the data, in Figure 9 we plot the mass–radius relation of close-in TEPs with the color-scale of each point showing the fractional isochrone-based age of the system (taken to be equal to $\tau = (t - 200\,{\rm Myr})/(t_{\rm tot} - 200\,{\rm Myr})$). Here $t_{\rm tot}$ for a system is the maximum age of a star with a given mass and metallicity according to the YY models (Figure 10). We show the fractional age, rather than the age in Gyr, as the stellar lifetime is a strong function of stellar mass, and the largest planets also tend to be found around more massive stars with shorter total lifetimes. Because the star formation rate in the Galaxy has been approximately constant over the past ~ 8 Gyr (e.g., Snaith et al. 2015), for a star of a given mass we expect τ to be uniformly distributed between 0 and 1. In order to perform a consistent analysis, we re-compute ages for all of the WASP, *Kepler*, TrES and KELT systems using the YY models together with the spectroscopically measured $T_{\rm eff\star}$ and [Fe/H], and transit-inferred stellar densities listed in Table 8. In Figure 9 we focus on systems with $P < 10$ days and $t_{\rm tot} < 10$ Gyr. Again it is apparent that the largest radius planets tend to be around stars that are relatively old. Note that due to the finite age of the Galaxy, there has been insufficient time for stars with $t_{\rm tot} > 10$ Gyr to reach their main sequence lifetimes. The restriction on $t_{\rm tot}$, which is effectively a cut on host star mass, limits the sample to stars which could be discovered at any stage in their evolution. If we do not apply this cut then the apparent correlation between fractional age and planet radius becomes even more significant, but this is likely due to observational bias.

The planets shown in Figure 9 have a variety of orbital separations and host star masses. Because the evolution of a planet depends on its stellar environment, we expect there to be a variance in the planet radius at fixed planet mass. In order to better compare planets likely to have similar histories (but which have different ages, and thus are at different stages in their history), in Figure 11 we re-plot the mass–radius relation, but this time binning by host star mass and orbital semi-major axis. Note that in comparing planets with the same semi-major axis we are assuming that orbital evolution can be neglected. Again we use the color-scale of points to denote the fractional age of the system. We choose a 3×3 binning to allow a sufficient number of planets in at least some of the bins to be able to detect a statistical trend. Unfortunately because we limited by the small sample of planets, we are forced to use relatively large bins, so there is likely to still be significant variation in the evolution of different planets within a bin. Bearing this caveat in mind, we note that the same trend of larger radius planets, at a given planet mass, being found around more evolved stars is seen when comparing only planets with similar host star masses and at similar orbital separations. If anything the gradient in fractional age with planet radius is more pronounced in Figure 11 than it is in Figure 9 (see especially the center row and bottom, center panel of Figure 11). If enhanced irradiation acts to slow a planet's contraction, but does not re-inflate the planet, then we would expect to see the opposite trend in Figure 11. Namely, a planet of a given mass at a given orbital separation around a star of a given mass should decrease, or remain constant, in size over time, despite the increasing irradiation as its host star evolves. This is not what we see. In Section 4.1.1 we follow a more statistically rigorous method to show that planetary radii increase in time with increasing irradiation, rather than being set by the initial

[18] `http://exoplanetarchive.ipac.caltech.edu`, accessed 2016 Mar 4

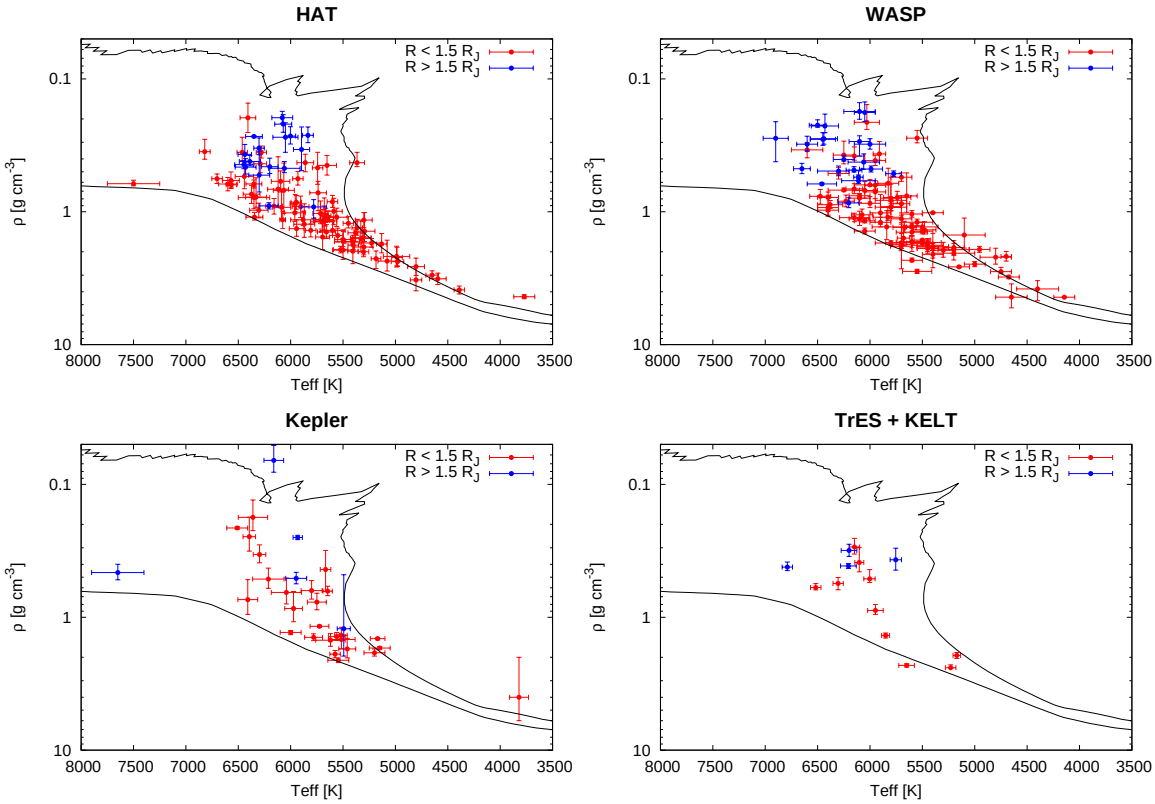

Figure 8. Host stars for TEPs with $R > 0.5\,R_{\rm J}$ and $P < 10$ days from the HAT, WASP, *Kepler*, TrES and KELT surveys. The lower line in each panel is the 200 Myr solar-metallicity isochrone from the YY stellar evolution models, while the upper line is the locus of points for stars having an age that is the lesser of 13.7 Gyr or 90% of their total lifetime, again assuming solar metallicity and using the YY models. Note that the maximum stellar age is a smooth function of stellar mass according to the models (Figure 10), but the 90% lifetime locus in the $T_{\rm eff\star}$–ρ plane is jagged due to the sensitive dependence on mass of the late stages of stellar evolution. We distinguish here between stars with planets having $R_P > 1.5\,R_{\rm J}$ and stars with planets having $R_P < 1.5\,R_{\rm J}$. Large planets have been preferentially discovered around more evolved stars than smaller planets. This appears to be true for all of the surveys considered. Moreover, few, if any, ZAMS stars are known to host planets with $R_P > 1.5\,R_{\rm J}$.

irradiation.

To establish the statistical significance of the trends seen in Figures 8–11, in Figure 12 we plot the fractional isochrone-based age τ against planetary radius, restricted to systems with $t_{\rm tot} < 10$ Gyr. Both the HAT and WASP data have positive correlations between R_P and the fractional age. A Spearman non-parametric rank-order correlation test gives a correlation coefficient of 0.344 between R_P and the fractional age for HAT, with a 1.4% false alarm probability. For the WASP sample we find a correlation coefficient of 0.277 and a false alarm probability of 3.5%. The *Kepler*, TrES and KELT datasets are too small to perform a robust test for correlation, but they each show a similar trend. When all of the data are combined, we find a correlation coefficient of 0.347 and a false alarm probability of only 0.0041%. While the correlation is relatively weak, explaining only a modest amount of the overall scatter in the data, it has a high statistical significance, and is extremely unlikely to be due to random chance.

Figure 13 is similar to Figure 12, except that here we restrict the analysis to planets with $0.4\,M_{\rm J} < M_p < 2.0\,M_{\rm J}$, which is roughly the range over which the most highly inflated planets have been discovered (e.g., Figure 9). In this case we still find a statistically significant difference between the fractional ages of stars hosting large radius planets and those hosting small radius planets, though, due to the smaller sample size, the overall significance is somewhat reduced compared to the sample when no restriction is placed on planet mass (the correlation coefficient itself is somewhat higher). Quantitatively we find that the HAT sample has a Spearman correlation coefficient of 0.428 and a false alarm probability of 0.84%, the WASP sample has a correlation coefficient of 0.273 and a false alarm probability of 7.7%, and the combined sample has a correlation coefficient of 0.398 and a false alarm probability of 0.0068%.

In order to compare planets with similar evolutionary histories, and in analogy to Figure 11, in Figure 14 we plot the fractional age against planet radius gridded by host star mass and orbital semimajor axis. Here we combine all of the data, but restrict the sample to only planets with $0.4\,M_{\rm J} < M_P < 2.0\,M_{\rm J}$ around stars with $t_{tot} < 10$ Gyr. We see the correlation again in several grid cells, so long as there is a sufficiently large sample.

Of course these correlations are likely biased due to observational selection effects. We estimate the effect of observational selections on the measured correlation below in Section 4.1.2, where we conclude that the correlation is reduced, but still significant, after accounting for selections.

We conclude that there is a statistically significant positive correlation between R_p and the fractional age of the system. This correlation is seen in samples of transiting

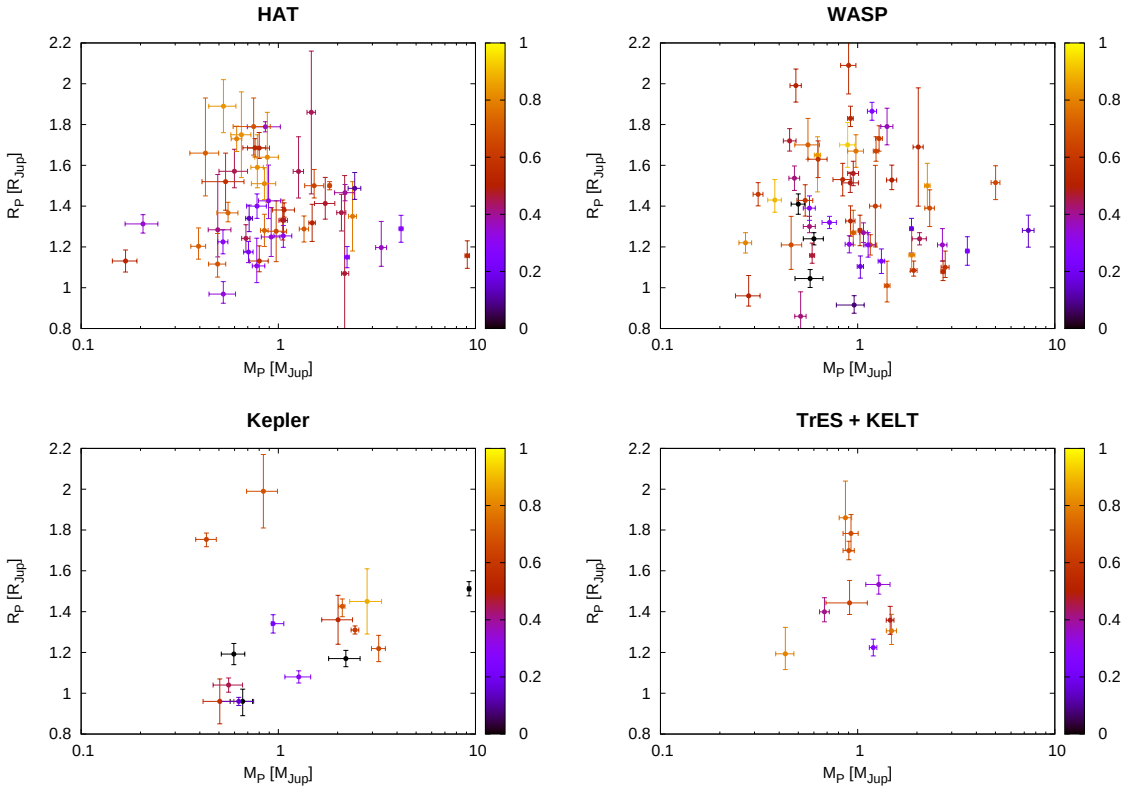

Figure 9. Mass–radius relation for TEPs from HAT (top left), WASP (top right), *Kepler* (bottom left) and TrES and KELT (bottom right) with $R > 0.5\,R_{\rm J}$ and $P < 10$ days around stars with total lifetimes $t_{\rm tot} < 10$ Gyr. The color-scale for each point indicates the fractional age of the system (taken to be $\tau = (t - 200\,{\rm Myr})/(t_{\rm tot} - 200\,{\rm Myr})$, where t is the age determined from the YY isochrones using $T_{\rm eff\star}$, $\rho_\star$ and [Fe/H] and $t_{\rm tot}$ is the maximum age in the YY models for a star with the same mass and [Fe/H]). A handful of stars with bulk densities indicating very young ages show up as black points in the figure. The largest planets are found almost exclusively around moderately evolved ($\tau \gtrsim 0.5$) stars.

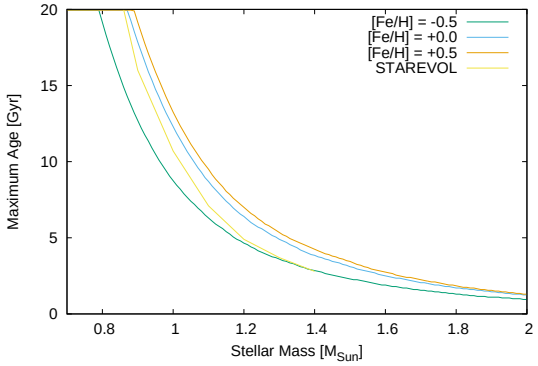

Figure 10. The maximum age of a star as a function of its mass based on interpolating within the YY isochrones. These are shown for three representative metallicities. The maximum age is artificially capped at 19.95 Gyr which is the largest age at which the models are tabulated. For stars with $M \gtrsim 0.85\,M_\odot$, which have maximum ages below this artificial cap, there is a smooth power-law dependence between the maximum age and mass. We use this relation to estimate the fractional age τ of a planetary system. For comparison we also show the terminal main sequence age as a function of stellar mass from the STAREVOL evolution tracks (Charbonnel & Palacios 2004; Lagarde et al. 2012), taken from Table B.6 of Santerne et al. (2016).

planets found by multiple surveys, with strikingly similar results found for the largest two samples (from WASP and HAT). The largest radius planets have generally been found around more evolved stars.

4.1.1. *Relation to the Correlation Between Radius and Equilibrium Temperature*

It is important to note that the correlation between radius and equilibrium temperature (or flux) is much stronger than the apparent correlation between planet radius and the fractional age of the host star. In fact the data are consistent with the latter correlation being entirely a by-product of the former correlation. However, the data also indicate that the radii of planets dynamically increase in time as their host stars become more luminous and the planetary equilibrium temperatures increase.

To demonstrate this we perform a Bayesian linear regression model comparison using the **BayesFactor** package in R[19] which follows the approach of Liang et al. (2008) and Rouder & Morey (2012). We test models of the form:

$$\ln R_p = c_0 + c_1 \ln T_{\rm eq,now} + c_2 \ln T_{\rm eq,ZAMS} + c_3 \ln a + c_4 \tau \quad (1)$$

where c_0–c_4 are varied linear parameters, and we compare all combinations of models where parameters other than c_0 are fixed to 0. This particular parameterization is motivated by Enoch et al. (2012) who found that the radii of close-in Jupiter-mass planets are best modelled by a function of the form given above with $c_2 \equiv c_4 \equiv 0$, and we now include the $T_{\rm eq,ZAMS}$ and τ parameters to

[19] `http://bayesfactorpcl.r-forge.r-project.org/`

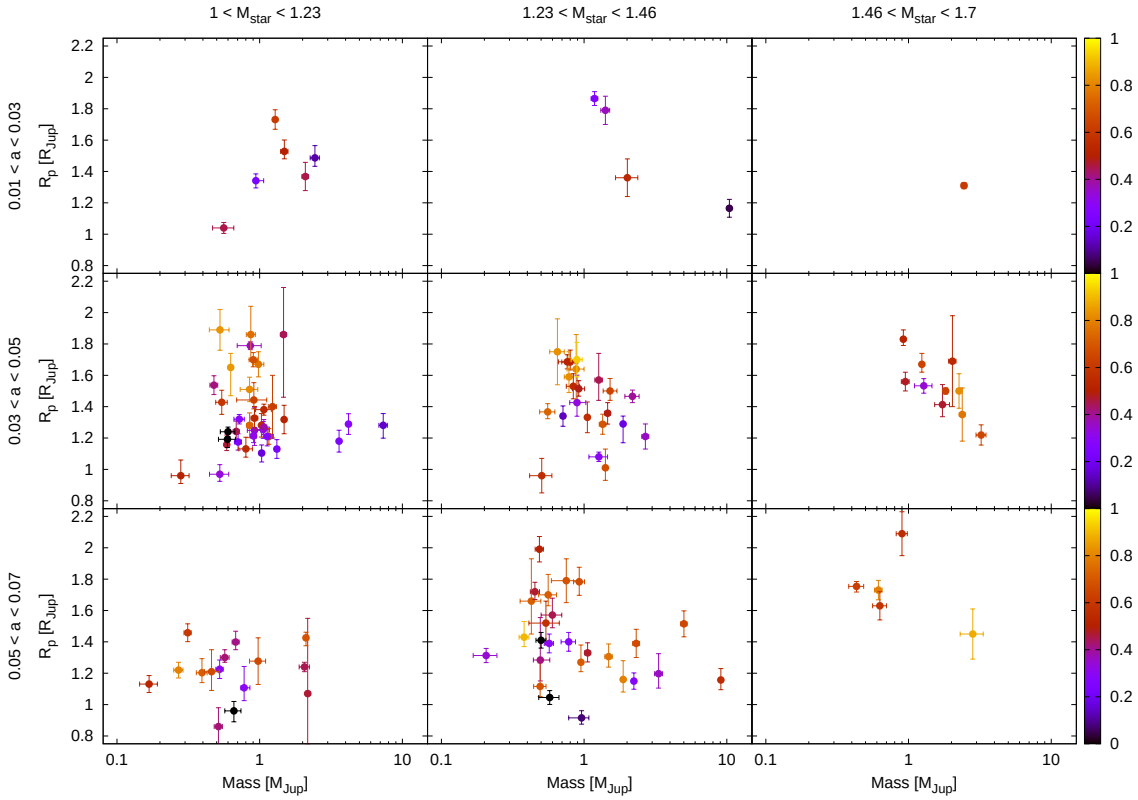

Figure 11. Similar to Figure 9, here we combine all of the data from the different surveys, and show the mass–radius relation for different host star mass ranges (the selections are shown at the top of each column in solar mass units) and orbital semi-major axes (the selections are shown to the left of each row in AU). The overall range of semi-major axis and stellar mass shown here is chosen to encompass the sample of well-characterized highly inflated planets with $R > 1.5\,R_{\rm J}$ around stars with total lifetimes $t_{\rm tot} < 10\,$Gyr. Within a given panel the largest planets tend to be found around more evolved stars. This is the opposite of what one would expect if high irradiation slows a planet's contraction, but does not supply energy deep enough into the interior of the planet to re-inflate as the luminosity of its host star increases.

test whether age is an important additional variable, and/or whether the data could be equally well described if we used the initial equilibrium temperature of the planet (which does not change in time) rather than the present-day equilibrium temperature (which increases in time due to the evolution of the host). Here we consider the full sample of well-characterized planets with $P < 10\,$days, $R_p > 0.5\,R_{\rm J}$, $0.4\,M_{\rm J} < M_p < 2.0\,M_{\rm J}$, and $t_{\rm tot} < 10\,$Gyr. Table 6 lists the linear coefficient estimates and the Bayesian evidences, sorting from highest to lowest, for each of the 15 models under comparison.

We find that the model with the highest Bayesian evidence has the form:

$$\ln R_p = c_0 + c_1 \ln T_{\rm eq,now} + c_3 \ln a \qquad (2)$$

with an evidence that is 2.7×10^9 times higher than the evidence for a model where $c_1 \equiv c_2 \equiv c_3 \equiv c_4 \equiv 0$. This finding is consistent with that of Enoch et al. (2012). The next highest evidence model has the form:

$$\ln R_p = c_0 + c_1 \ln T_{\rm eq,now} + c_3 \ln a + c_4 \tau \qquad (3)$$

with an evidence that 0.37 times that of the highest evidence model. So indeed including τ provides no additional explanatory power beyond what is already provided by $T_{\rm eq,now}$ and a.

At the same time, we also find that models with $\ln T_{\rm eq,now}$ have substantially higher evidence than models using $\ln T_{\rm eq,ZAMS}$ in place of $\ln T_{\rm eq,now}$, while the model using both $\ln T_{\rm eq,ZAMS}$ and τ has higher evidence than the model using $\ln T_{\rm eq,ZAMS}$ alone. Moreover, we find that the maximum posterior value for c_4 is greater than zero in all cases where it is allowed to vary. In other words, planet radii are more strongly correlated with the present day equilibrium temperature than they are with the ZAMS equilibrium temperature, and if the latter is used in place of the former then a significant positive correlation between radius and host star fractional age remains.

Based on this we conclude that the radii of close-in Jupiter-mass giant planets are determined by their present-day equilibrium temperature and semi-major axis, and that the radii of planets increase over time as their equilibrium temperatures increase.

4.1.2. *Selection Effects*

The Effect of Stellar Evolution on the Detectability of Planets:— The sample of known TEPs suffers from a broad range of observational selection effects which in principle might explain a preference for finding large planets around evolved stars. As stars evolve their radii increase, which, for fixed R_p, a and $M_\star$, reduces the transit depth by a factor of $R_\star^{-2}$ (reducing their detectability), but increases the duration of the transits by a factor of $R_\star$ (increasing their detectability). It also increases the geometrical probability of a planet being seen to transit by a factor of $R_\star$ (increasing planet detectability). As stars

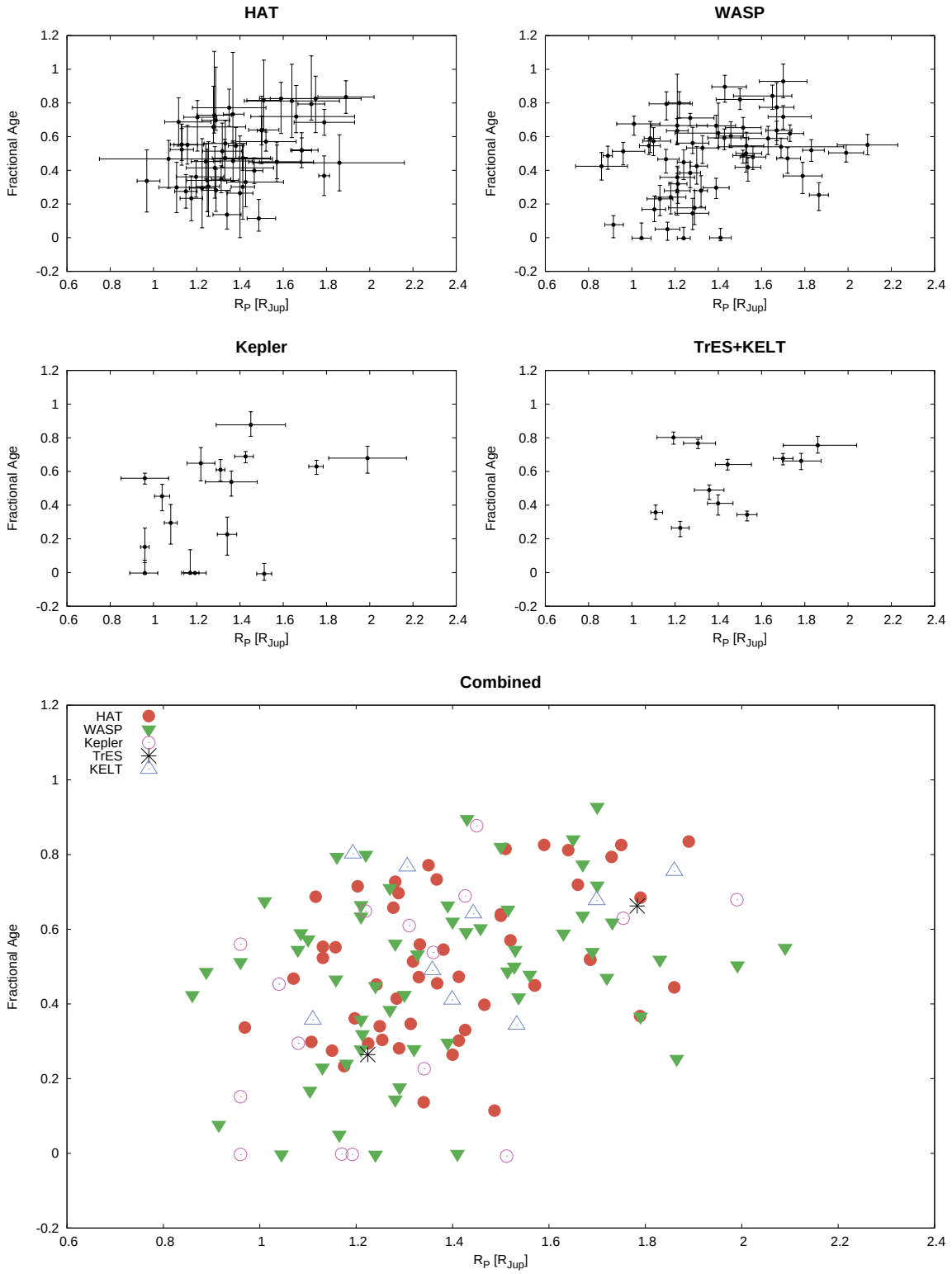

Figure 12. *Top:* The fractional isochrone-based age of the system (see Figure 9) vs. the planetary radius, shown separately for TEP systems discovered by HAT (left) and WASP (right). We only show systems with $P < 10$ days and $t_{\rm tot} < 10$ Gyr. Both the HAT and WASP samples have positive correlations between R_P and τ. For HAT a Spearman non-parametric rank-order correlation test gives a correlation coefficient of 0.344 with a 1.4% false alarm probability. For the WASP sample we find a correlation coefficient of 0.277 and a false alarm probability of 3.5%. *Middle:* Same as the top, here we show planets from *Kepler*, TrES and KELT, with the same selections applied. *Bottom:* Same as top, here we combine data from all of the surveys. The combined data set has a correlation coefficient of 0.347 and a false alarm probability 0.0041%.

evolve they also become more luminous, meaning that at fixed distance they may be monitored with greater photo-

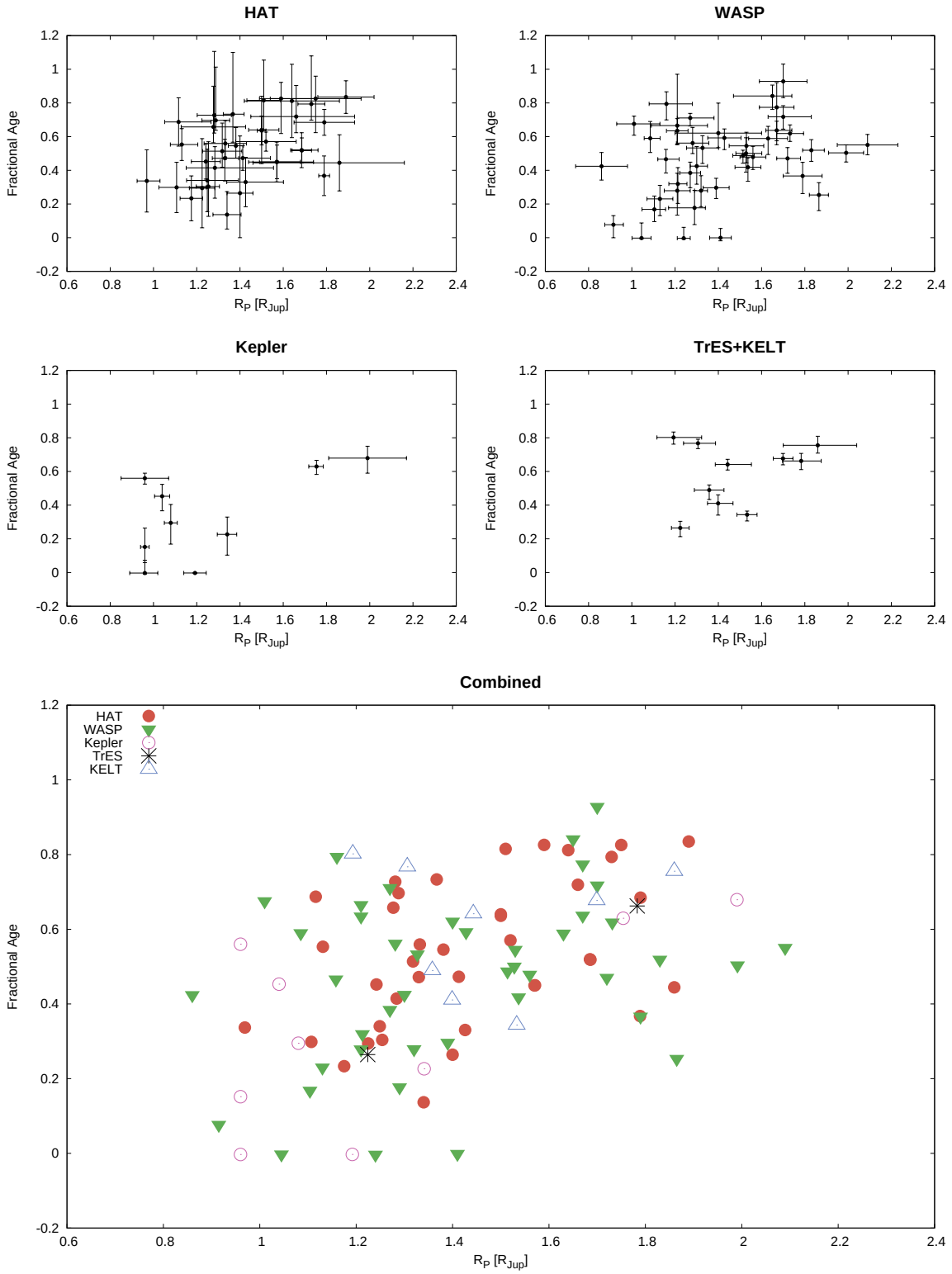

Figure 13. Same as Figure 12, here we only consider systems with planets having masses in the range $0.4\,M_{\rm J} < M_p < 2.0\,M_{\rm J}$, which is roughly the radius range over which highly inflated planets have been discovered. In this case the Spearman non-parametric rank-order correlation test gives a correlation coefficient of 0.428 with a 0.84% false alarm probability. For the WASP sample we find a correlation coefficient of 0.273 and a false alarm probability of 7.7%. The combined sample has a correlation coefficient of 0.398 and a false alarm probability of 0.0068%.

metric precision (further increasing planet detectability).

To determine the relative balance of these competing factors for the HAT surveys, for each TEP system discovered by HAT we estimate the relative number of ZAMS stars with the same stellar mass and metallicity around which one could expect to find a planet with the same ra-

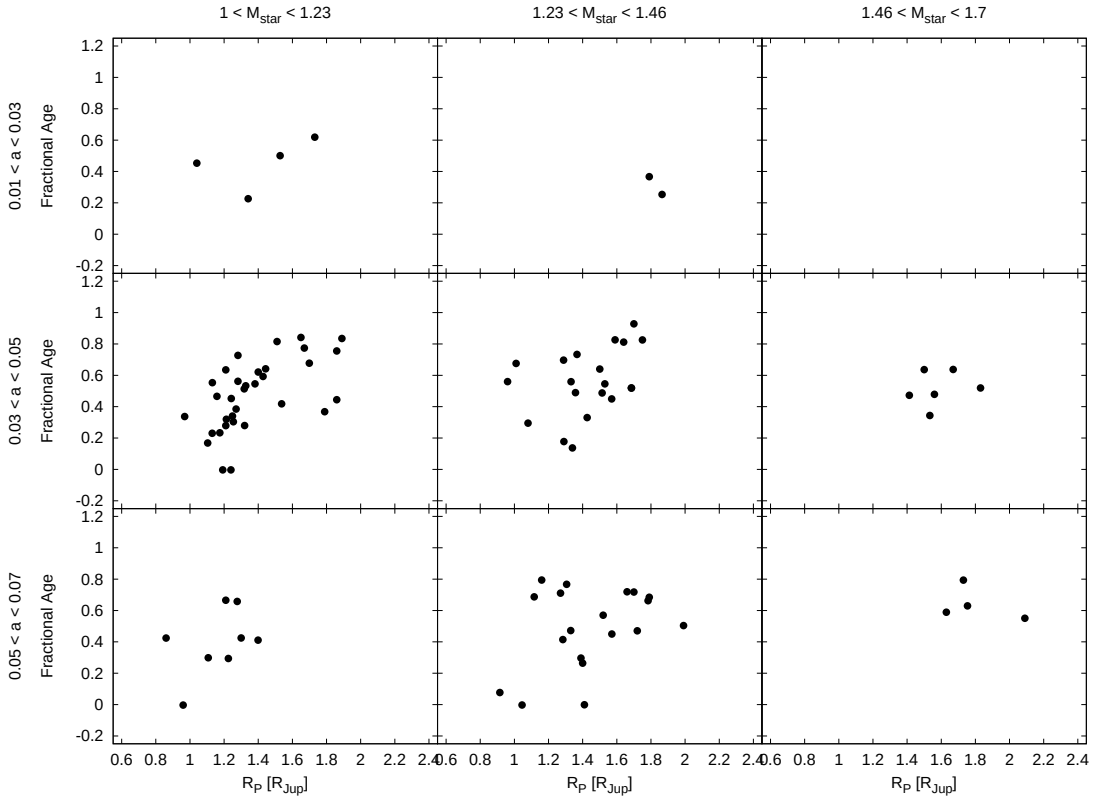

Figure 14. Similar to Figures 13 and 11, here we combine all of the data from the different surveys, and show the fractional isochrone-based age vs. planet radius for different host star mass ranges (the selections are shown at the top of each column in solar mass units) and orbital semi-major axes (the selections are shown to the left of each row in AU). The overall range of semi-major axis and stellar mass shown here is chosen to encompass the sample of well-characterized highly inflated planets with $R > 1.5\,R_{\rm J}$ around stars with total lifetimes $t_{\rm tot} < 10\,{\rm Gyr}$. We also restrict the sample to planets with $0.4\,M_{\rm J} < M_P < 2.0\,M_{\rm J}$.

dius and orbital period and with the same signal-to-noise ratio. To do this we use the following expression:

$$N_{\rm ZAMS}/N_t = \frac{V_{\rm ZAMS}}{V_t}\frac{{\rm Prob}_{\rm ZAMS}}{{\rm Prob}_t} \qquad (4)$$

where $N_{\rm ZAMS}/N_t$ is the relative number of ZAMS planet hosts expected compared to those with age t, $V_{\rm ZAMS}/V_t$ is the relative volume surveyed for ZAMS-equivalent versions of the TEP system (for simplicity we assume a uniform space density of stars), and ${\rm Prob}_{\rm ZAMS}/{\rm Prob}_t = R_{\star,ZAMS}/R_{\star,t}$ is the relative transit probability, which is equal to the ratio of the stellar radii. To estimate $V_{\rm ZAMS}/V_t$ we note that for fixed photometric precision, and assuming white noise-dominated observations, the transit S/N of a given TEP scales as the transit depth times the square root of the number of points in transit, or as $(R_{\star,ZAMS}/R_{\star,t})^{-3/2}$. If the data are red-noise dominated, then the S/N scales simply as the transit depth, which would increase $V_{\rm ZAMS}/V_t$. We then determine the r magnitude of stars in the HAT field containing the TEP in question for which the per-point RMS is larger than the RMS of the observed TEP light curve by $(R_{\star,ZAMS}/R_{\star,t})^{-3/2}$. Accounting for the change in absolute r magnitude between the ZAMS and the present day for the system, this gives us the relative distance of a ZAMS-equivalent system for which the transits would be detected with the same S/N. The cube of this distance is equal to $V_{\rm ZAMS}/V_t$.

In Figure 15 we show $N_{\rm ZAMS}/N_t$ vs R_p for HAT planets. For most TEP systems discovered by HAT, including most of the systems with $R_p > 1.5\,R_{\rm J}$, we have $N_{\rm ZAMS}/N_t > 1$. In other words, the greater transit depths expected for ZAMS systems more than compensates for the lower luminosities, shorter duration transits, and lower transit probabilities. Thus, from a pure transit-detection point-of-view, we should expect to be *more* sensitive to TEPs around ZAMS stars than to TEPs around stars with the measured host star ages.

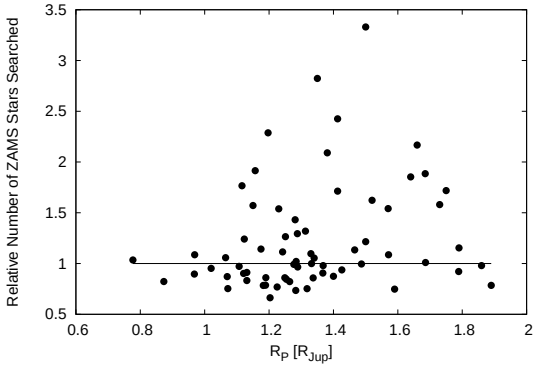

Figure 15. The relative number of ZAMS-equivalent stars searched for a given TEP discovered by HAT to the same transit S/N as the observed TEP system (equation 4) computed as described in Section 4.1.2. This is shown as a function of planet radius. For the largest planets with $R_P > 1.5\,R_{\rm J}$ the HAT survey is more sensitive to finding the same planet around a ZAMS star than it is to finding the planet around the moderately evolved star where it was discovered.

Table 6
Parameter Estimates and Bayesian Evidence For Models of the Form Eq. 1

$\ln T_{\rm eq,now}$ c_1	$\ln T_{\rm eq,ZAMS}$ c_2	$\ln a$ c_3	τ c_4	Bayesian Evidence
0.92 ± 0.12	0	0.273 ± 0.075	0	2.66×10^{9}
0.81 ± 0.14	0	0.216 ± 0.086	0.107 ± 0.088	9.99×10^{8}
0.96 ± 0.20	-0.07 ± 0.21	0.263 ± 0.079	0	5.01×10^{8}
0.558 ± 0.099	0	0	0.223 ± 0.077	2.53×10^{8}
0.77 ± 0.25	0.03 ± 0.23	0.216 ± 0.086	0.111 ± 0.096	2.09×10^{8}
0.57 ± 0.25	-0.01 ± 0.24	0	0.217 ± 0.088	4.75×10^{7}
0.658 ± 0.099	0	0	0	2.93×10^{7}
0	0.492 ± 0.098	0	0.332 ± 0.077	1.73×10^{7}
0.90 ± 0.22	-0.29 ± 0.21	0	0	1.17×10^{7}
0	0.62 ± 0.14	0.123 ± 0.084	0.291 ± 0.080	9.95×10^{6}
0	0.76 ± 0.14	0.224 ± 0.086	0	7.84×10^{4}
0	0.53 ± 0.11	0	0	1.44×10^{4}
0	0	-0.153 ± 0.067	0.392 ± 0.086	2.37×10^{3}
0	0	0	0.364 ± 0.087	9.04×10^{2}
0	0	-0.094 ± 0.074	0	4.87×10^{-1}

Note. — The models tested are sorted from highest to lowest evidence. The Bayesian evidence is reported relative to that for a model with only a freely varying mean for the $\ln R_p$ values. For each parameter we report the mean and standard deviation of its posterior probability distribution.

Put another way, while selection effects may lead to fewer small planets being found around older stars (missing planets in the upper left corner of Figure 12), based on the estimate in Figure 15, selection effects due to transit detectability do not explain why we find fewer large planets around unevolved stars (missing planets in the lower right corner of Figure 12). If the occurrence rate of large radius planets is independent of host star age, or if it is larger for unevolved stars than for evolved stars, we would expect to have found *more* large planets around unevolved stars than evolved stars.

The Effect of Stellar Evolution on the Ability to Confirm Planets:— Other observational selection effects may still be at play. If the orbits of these planets shrink over time due to tidal evolution, then the transit probability and the fraction of points in transit both increase in time by more that what we estimated. Beyond simply detecting the transits, further selections are imposed in the follow-up program carried out to confirm the planets. Figure 16 compares the present day effective temperature and $v \sin i$ for HAT TEPs to the expected values on the ZAMS (estimated as discussed below). For all of the $R_p > 1.5\,R_{\rm J}$ planets found by HAT the host star had a higher $T_{\rm eff\star}$ on the ZAMS than at the present day. The most extreme case is HAT-P-7 which had an estimated ZAMS effective temperature of 6860 K compared to its present-day temperature of 6350 ± 100 K. While precision RVs are more challenging for early F dwarfs than for later F dwarfs, the ZAMS temperatures of the hosts of the largest TEPs found by HAT are still within the range where we carry out follow-up observations (we do not follow-up hosts of spectral type A or earlier if they are faint stars with $V \gtrsim 13$).

An additional potential selection effect relates to the stellar rotation. Neglecting tidal interactions between the stars and planets, the host stars would have had higher projected rotation velocities at ZAMS, primarily resulting from their lower moments of inertia (most of the hosts of the largest planets found by HAT have radiative envelopes, or would have had them for much of their main sequence lifetimes, and thus would not lose substantial angular momentum from magnetized stellar winds). Roughly speaking we expect $v \sin i \propto R_\star^{-1}$ (assuming $I \propto R_\star^2$). The most rapidly rotating ZAMS host is HAT-P-41 for which we estimate a ZAMS rotation velocity of $24\,{\rm km\,s^{-1}}$, which is still well within the range where we continue follow-up (we do not follow-up hosts with $v \sin i \gtrsim 50\,{\rm km\,s^{-1}}$ if they are around faint stars with $V \gtrsim 13$). Thus while precise RVs would be somewhat more challenging for ZAMS planet hosts than for moderately evolved hosts, these factors are unlikely to be responsible for the lack of highly inflated planets discovered to date around stars close to ZAMS.

Correcting the Correlation Coefficient for Observational Selections:— In order to determine quantitatively how selection effects impact the correlation measured between R_p and τ, we follow Efron & Petrosian (1999) in calculating a modified Kendall correlation coefficient that is applicable to data suffering a non-trivial truncation. The procedure is as follows. We will call the observed data points $(R_{P,i}, \tau_i)$ and $(R_{P,j}, \tau_j)$, with $i \neq j$, comparable if each point falls within the other point's selection range. Here point j is within the selection range for point i if, holding everything else constant, we could still have discovered the planet around star i if the system had values of $(R_{P,i}, \tau_j)$, $(R_{P,j}, \tau_i)$ or $(R_{P,j}, \tau_j)$ instead of $(R_{P,i}, \tau_i)$. Letting $\mathcal{J}$ be the set of all comparable pairs, and N_p be the total number of such pairs, the modified Kendall correlation coefficient is then given by

$$r_K = \frac{1}{N_p} \sum_{(i,j)\in\mathcal{J}} {\rm sign}\left((R_{P,i} - R_{P,j})(\tau_i - \tau_j)\right). \qquad (5)$$

For uncorrelated data r_K has an expected value of 0, whereas perfectly correlated data has $r_K = 1$ and perfectly anti-correlated data has $r_K = -1$. To determine the probability of finding $|r_K| > |r_{K,\rm observed}|$ it is necessary to carry out bootstrap simulations. To do this we

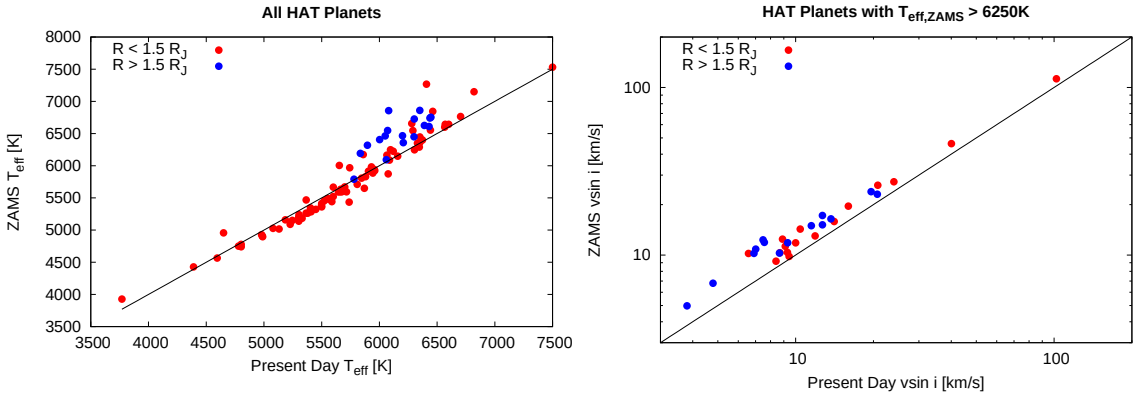

Figure 16. Left: The estimated TEP host-star effective temperature on the ZAMS vs. its present day measured effective temperature for all TEP systems discovered to date by HAT. While stars hosting planets with $R_P > 1.5\,R_{\rm J}$ had higher effective temperatures on the ZAMS, none of them would have been too hot for us to proceed with confirmation follow-up observations. Right: The estimated projected rotation velocity on the ZAMS vs. present day measured rotation velocity for HAT TEP hosts with $T_{\rm eff,ZAMS} > 6250\,{\rm K}$. The estimated ZAMS $v \sin i$ is calculated by scaling the measured $v \sin i$ by $R_\star/R_{\star,ZAMS}$ assuming the spin-down for these radiative-envelope stars is due entirely to changes in the moment of inertia, and assuming the latter scales as $R_\star^2$. While stars hosting planets with $R_P > 1.5\,R_{\rm J}$ would have been rotating more rapidly on the ZAMS than at the present day, none of them would have been rotating too rapidly for us to proceed with confirmation follow-up observations.

calculate r_K for $N_{\rm sim}$ simulated data sets, and for each simulated data set we randomly select N values of i, with replacement, from the observed samples, adopt $R_{P,i}$ for each simulated point, and associate with it a value of τ drawn at random from the set of points that are comparable to i (including i itself in this case).

The primary challenge in calculating equation 5 for the observed sample of close-in giant planets is to determine the set of comparable pairs. We do this for the HAT planets by subtracting the observed transit signal from the survey light curve, rescaling the scatter to match the expected change in r.m.s. due to the change in the stellar luminosity with age, adding the expected transit signal given the new trial planetary and stellar radii, but assuming the original ephemeris and orbital inclination, and using BLS to determine whether or not the transit could be recovered. Using the set of comparable pairs determined in this fashion, we find $r_K = 0.228$, with a 2.88% false alarm probability, based on the bootstrap simulations (or $r_K = 0.284$ with a 2.92% false alarm probability when restricted to planets with $0.4\,M_{\rm J} < M_p < 2.0\,M_{\rm J}$). For comparison, if we ignore the selection effects and assume all points are comparable, we find $r_K = 0.235$ with a false alarm probability of 1.52% (or $r_K = 0.297$ with a 0.87% false alarm probability when restricted to planets with $0.4\,M_{\rm J} < M_p < 2.0\,M_{\rm J}$). The false alarm probabilities in the latter case are essentially the same as what was reported above using the Spearman rank-order correlation test instead of the Kendall test, demonstrating the consistency of the two methods.

We conclude that while observational selections do slightly bias the measured correlation between R_p and τ for HAT, the effect is small. While we cannot determine the set of comparable pairs for WASP, the selections are likely very similar to HAT, and we expect the effect on the measured correlation of accounting for observational selections to be similarly small. We therefore expect that the full combined set of planets would still exhibit a highly significant correlation between R_p and τ, even after accounting for observational selections.

4.1.3. *Systematic Errors in Stellar Parameters*

The radii of TEPs are not measured directly, but rather are measured relative to the stellar radii, which in turn are determined by matching the effective temperatures, stellar densities, and stellar metallicities to models (either theoretical stellar evolution models, as done for example for most HAT systems, or by utilizing empirical models calibrated with stellar eclipsing binary systems, as has been done for many WASP systems). Any systematic error in the stellar radius would lead to a proportional error in the planet radius, and the fact that the largest planets are more commonly found around the most evolved (and largest) stars is what one would expect to see if there were significant unaccounted-for systematic errors. Here we consider a variety of potential systematic errors, and argue that none of these are responsible for the observed correlation.

Eccentricity:— One potentially important source of systematic errors in this respect is the planetary eccentricity, which is constrained primarily by the RV data, and which is needed to determine the stellar density from the measured transit duration, impact parameter, and radius ratio. The host stars of the largest radius planets are among the hottest, fastest rotating, and highest jitter stars around which transiting planets have been found (e.g., Figure 16, and Hartman et al. 2011c). For these systems the eccentricity is typically poorly constrained, and circular orbits have often been adopted.[20] If the systems were actually highly eccentric, with transits near apastron, then the stellar densities would be higher than what was inferred assuming circular orbits, and the stellar and planetary radii would be smaller than what has been estimated. There are, however, several large planets transiting moderately evolved stars for which secondary eclipses have been observed, providing tight constraints on the eccentricity (e.g., TrES-4b Knutson et al. 2009, WASP-12b Campo et al. 2011, HAT-P-32b Zhao et al. 2014, and WASP-48b O'Rourke et al. 2014). Moreover,

[20] If circular orbits are not adopted, then there is a bias toward overestimating the eccentricity as shown by Lucy & Sweeney (1971). This bias may affect some of the earliest discovered planets especially.

the most inflated planets are on short period orbits, where we expect circularization. This expectation has been observationally verified in cases where sufficiently high precision RVs have been possible, or when secondary eclipse follow-up observations have been made. We also note that at least for the majority of the very large radius HAT planets, when the eccentricity is allowed to vary, the planet and stellar radii determined from the median of the posterior distributions are found to be larger than when the eccentricity is fixed to zero.

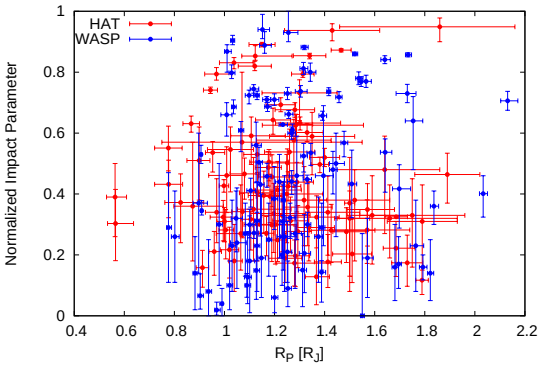

Figure 17. Normalized impact parameter vs. planetary radius for TEPs found by HAT and WASP. The impact parameters of WASP TEPs appear to be uniformly distributed between 0 and 1, as expected for random orientations in space. The largest HAT planets have, if anything, a bias toward low impact parameters. If these suffer from a systematic error, the stellar and planetary radii would be underestimated.

Impact Parameter:— Another potential source of systematic error is if the impact parameter is in error, perhaps due to an incorrect treatment of limb darkening (e.g., Espinoza & Jordán 2015). Errors in the impact parameter will translate into concomitant errors in the stellar density, and in the stellar radius and age. In order to over-estimate the size of the planets, the impact parameter would need to have been overestimated. Looking at the distribution of measured planetary impact parameters, however, shows no evidence for this being the case (Figure 17). The impact parameter for the WASP planets appears to be uniformly distributed between 0 and 1, as expected for random orbital orientations, whereas the HAT planets are, if anything, biased toward low impact parameters (if these are in error, the stars and planets would be even larger than currently estimated).

Stellar Atmospheric Parameters:— Other potential sources of systematic errors include errors in the stellar effective temperatures (if the stars are hotter than measured, they would be closer to the ZAMS) or metallicities, or an error in the assumed stellar abundance pattern (generally stars are modelled assuming solar-scaled abundances). A check on the spectroscopic temperature estimates can be performed by comparing the broad-band photometric colors to the spectroscopically determined temperatures. We show this comparison in Figure 18 where we use the color of the points to show the planet radius. While there is perhaps a slight systematic difference in the $V-K$ vs. $T_{\rm eff\star}$ relation between large and small radius planets, with large radius planets being found, on average, around slightly

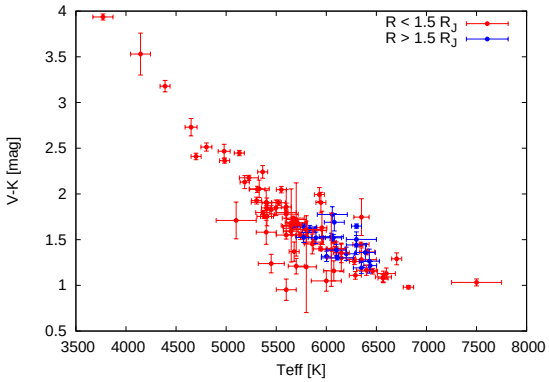

Figure 18. Photometric $V-K$ color (not corrected for reddening) vs. effective temperature for TEP host stars from HAT and WASP with $R_P > 0.5\,R_{\rm J}$ and $P < 10$ days. The blue and red colors are used to distinguish between stars hosting planets with $R_P > 1.5\,R_{\rm J}$ and $R_P < 1.5\,R_{\rm J}$, respectively. No systematic difference in the color-temperature relation is seen between these two classes of planets. Such a difference might have indicated a systematic error in the stellar effective temperature measurements of the stars hosting large planets.

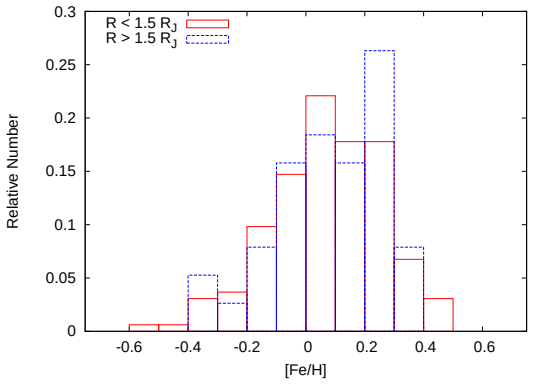

Figure 19. Normalized histograms of [Fe/H] for transiting planet host stars from HAT and WASP, separated by planetary radius. No significant difference is seen between metallicities of large planet radius host stars, and small planet radius host stars.

redder stars at fixed $T_{\rm eff\star}$ than small radius planets, the difference is too small to be responsible for the detected trend between planet radius and fractional host age. Moreover, the difference is also consistent with more evolved/luminous stars generally being more distant from the Solar System than less evolved stars, and thus exhibiting greater reddening. No systematic difference is seen in the host star metallicity distributions of small and large radius planets (Figure 19).

Priors Used In Stellar Modelling:— Stars evolve faster as they age such that a large area on the Hertzsprung-Russell diagram is covered by stellar models spanning a small range of ages near the end of a star's life. As a result, when observed stellar properties are compared to models there can be a bias toward matching to late-ages. This well-known effect, dubbed the stellar terminal age bias by Pont & Eyer (2004), can be corrected by adopting appropriate priors on the model parameters (e.g., adopting a uniform prior on the age). Similarly, failing to account for the greater prevalence of low-mass stars in the Galaxy relative to high-mass stars can lead to overpredicting stellar masses (e.g., Lloyd 2011). For most transiting planets in the literature, these possible

biases have not been accounted for in performing this comparison (i.e., generally the analyses have adopted uniform priors on the relevant observables, namely the effective temperature, density and metallicity). While these effects could lead to over-estimated stellar radii, potentially explaining the preference for large radius planets around evolved stars, in practice we only expect such biases to be significant if the observed parameters are not well constrained relative to the scale over which the astrophysically-motivated priors change substantially. To estimate the importance of this effect, we calculate new stellar parameters for each of the HAT TEP systems with $R > 1.5\,R_{\rm J}$. Here we place a uniform prior on the stellar age between the minimum age of the isochrones and 14 Gyr (this amounts to assuming a constant star formation rate over this period), we use the Chabrier (2003) initial mass function to place a prior on the stellar mass, and we assume a Gaussian prior on the metallicity with a mean of [Fe/H]$= 0$ dex, and a standard deviation of 0.5 dex. The details of how we implement this are described in Appendix A.

We find that for all 17 systems the changes to the parameters are much smaller than the uncertainties (the changes are all well below 0.1%, and in most cases below 0.01%). We also find that the prior on the stellar mass, which increases toward smaller mass stars, generally has a larger impact than the priors on the age or metallicity. The result is that in most cases the stellar masses and radii are very slightly lower when priors are placed on the stellar properties, while the ages are very slightly higher. The latter is due to the prior on stellar mass pulling the solution toward lower effective temperatures, which at the measured stellar densities requires higher ages. We conclude that since the changes in the stellar parameters are insignificant, the correlation between the planetary radii and host star fractional age is not due to biases in the stellar parameters stemming from using incorrect priors.

4.1.4. *Theoretical Significance*

As we have shown, there is a significant correlation between the radii of close-in giant planets and the fractional ages of their host stars. This correlation is apparently a by-product of the more fundamental correlation between planet radius and equilibrium temperature, but the data also indicate that planetary radii increase over time as their host stars evolve and become more luminous.

Such an effect is contrary to models of planet evolution where excess energy associated with a planet's proximity to its host star does not penetrate deep into the planet interior, but only acts to slow the planet's contraction. Burrows et al. (2000) and Baraffe et al. (2008) are examples of such "default" models. Other examples of such models include Burrows et al. (2007), who showed, among other things, how additional opacity which further slows the contraction could explain the radii of inflated planets known at that time, and Ibgui et al. (2010) who showed how extended tidal heating of the planet atmosphere can increase the final "equilibrium" radius of a planet. More generally, Spiegel & Burrows (2013) explored a variety of effects related to planet inflation, including the effect on planetary evolution of varying the depth at which additional energy is deposited in the interior (see also Lopez & Fortney 2016 for a recent discussion). If the inflation mechanism only slows, but does not reverse, the contraction, one would expect that at fixed semimajor axis, older planets should be smaller than younger planets, despite the increase in equilibrium temperature as the host stars evolve. This is not what we see (Figure 11, also Section 4.1.1).

On the other hand theories in which the energy is deposited deep in the core of the planet may allow planets to become more inflated as the energy source increases over time (Spiegel & Burrows 2013). Examples of such models include tidal heating of an eccentric planet's core as considered by Bodenheimer et al. (2001), Liu et al. (2008) and Ibgui et al. (2011), or the Ohmic heating model proposed by Batygin & Stevenson (2010); Batygin et al. (2011) (though see Huang & Cumming 2012 and Wu & Lithwick 2013 who argue that this mechanism cannot heat the deep interior). Our finding that planets apparently re-inflate over time is evidence that some mechanism of this type is in operation.

5. SUMMARY

The existence of highly inflated close-in giant planets is one of the long-standing mysteries that has emerged in the field of exoplanets. By continuing to build up the sample of inflated planets we are beginning to see patterns in their properties, allowing us to narrow down on the physical processes responsible for the inflation. Here we presented the discovery of two transiting highly inflated planets HAT-P-65b and HAT-P-66b. The planets are both around moderately evolved stars, which we find to be a general trend—highly inflated planets with $R \gtrsim 1.5\,R_{\rm J}$ have been preferentially found around moderately evolved stars compared to smaller radius planets. This effect is independently seen in the samples of planets found by HAT, WASP, *Kepler*, TrES and KELT. We argue that this is not due to observational selection effects, which tend to favor the discovery of large planets around younger stars, nor is it likely to be the result of systematic errors in the planetary or stellar parameters. We find that the correlation can be explained as a by-product of the more fundamental, and well known, correlation between planet radius and equilibrium temperature, and that the present day equilibrium temperature of close-in giant planets, which increases with time as host stars evolve, provides a significantly better predictor of planet radii than does the initial equilibrium temperature at the zero age main sequence.

We conclude that, after contracting during the pre-main-sequence, close-in giant planets are re-inflated over time as their host stars evolve. This provides evidence that the mechanism responsible for this inflation deposits energy deep within the planetary interiors.

The result presented in this paper motivates further observational work to discover and characterize highly inflated planets. In particular more work is needed to determine the time-scale for planet re-inflation. The expected release of accurate parallaxes for these systems from Gaia should enable more precise ages for all of these systems. Many more systems are needed to trace the evolution of planet radius with age as a function of planetary mass, host star mass, orbital separation, and other potentially important parameters. Furthermore, the evidence for planetary re-inflation presented here provides additional motivation to search for highly inflated long-

period planets transiting giant stars.

HATNet operations have been funded by NASA grants NNG04GN74G and NNX13AJ15G. Follow-up of HATNet targets has been partially supported through NSF grant AST-1108686. G.Á.B., Z.C., and K.P. acknowledge partial support from NASA grant NNX09AB29G. J.H. acknowledges support from NASA grant NNX14AE87G. K.P. acknowledges support from NASA grant NNX13AQ62G. We acknowledge partial support also from the *Kepler* Mission under NASA Cooperative Agreement NCC2-1390 (D.W.L., PI). A.S. is supported by the European Union under a Marie Curie Intra-European Fellowship for Career Development with reference FP7-PEOPLE-2013-IEF, number 627202. Part of this work was supported by Fundação para a Ciência e a Tecnologia (FCT, Portugal, ref. UID/FIS/04434/2013) through national funds and by FEDER through COMPETE2020 (ref. POCI-01-0145-FEDER-007672). Data presented in this paper are based on observations obtained at the HAT station at the Submillimeter Array of SAO, and the HAT station at the Fred Lawrence Whipple Observatory of SAO. This research has made use of the NASA Exoplanet Archive, which is operated by the California Institute of Technology, under contract with the National Aeronautics and Space Administration under the Exoplanet Exploration Program. Data presented herein were obtained at the WIYN Observatory from telescope time allocated to NN-EXPLORE through the scientific partnership of the National Aeronautics and Space Administration, the National Science Foundation, and the National Optical Astronomy Observatory. This work was supported by a NASA WIYN PI Data Award, administered by the NASA Exoplanet Science Institute. We gratefully acknowledge R. W. Noyes for his many contributions to the HATNet transit survey, and we also gratefully acknowledge contributions from J. Johnson, and from G. Marcy to the collection and reduction of the Keck/HIRES observations presented here. The authors wish to recognize and acknowledge the very significant cultural role and reverence that the summit of Mauna Kea has always had within the indigenous Hawaiian community. We are most fortunate to have the opportunity to conduct observations from this mountain.

REFERENCES

Albrecht, S., Winn, J. N., Johnson, J. A., et al. 2011, ApJ, 738, 50
Ammler-von Eiff, M., Santos, N. C., Sousa, S. G., et al. 2009, A&A, 507, 523
Anderson, D. R., Collier Cameron, A., Gillon, M., et al. 2011a, A&A, 534, A16
Anderson, D. R., Smith, A. M. S., Lanotte, A. A., et al. 2011b, MNRAS, 416, 2108
Anderson, D. R., Collier Cameron, A., Hellier, C., et al. 2011c, ApJ, 726, L19
—. 2011d, A&A, 531, A60
Anderson, D. R., Collier Cameron, A., Gillon, M., et al. 2012, MNRAS, 422, 1988
Anderson, D. R., Collier Cameron, A., Delrez, L., et al. 2014, MNRAS, 445, 1114
Anderson, D. R., Collier Cameron, A., Hellier, C., et al. 2015, A&A, 575, A61
Bakos, G., Noyes, R. W., Kovács, G., et al. 2004, PASP, 116, 266
Bakos, G. Á., Shporer, A., Pál, A., et al. 2007, ApJ, 671, L173
Bakos, G. Á., Pál, A., Torres, G., et al. 2009a, ApJ, 696, 1950
Bakos, G. Á., Howard, A. W., Noyes, R. W., et al. 2009b, ApJ, 707, 446
Bakos, G. Á., Torres, G., Pál, A., et al. 2010, ApJ, 710, 1724
Bakos, G. Á., Hartman, J., Torres, G., et al. 2011, ApJ, 742, 116
Bakos, G. Á., Hartman, J. D., Torres, G., et al. 2012, AJ, 144, 19
Bakos, G. Á., Csubry, Z., Penev, K., et al. 2013, PASP, 125, 154
Bakos, G. Á., Hartman, J. D., Bhatti, W., et al. 2015a, AJ, 149, 149
Bakos, G. Á., Penev, K., Bayliss, D., et al. 2015b, ApJ, 813, 111
Bakos, G. Á., Hartman, J. D., Torres, G., et al. 2016, ArXiv e-prints, 1606.04556
Baraffe, I., Chabrier, G., & Barman, T. 2008, A&A, 482, 315
Barros, S. C. C., Pollacco, D. L., Gibson, N. P., et al. 2011a, MNRAS, 416, 2593
—. 2012, MNRAS, 419, 1248
Barros, S. C. C., Faedi, F., Collier Cameron, A., et al. 2011b, A&A, 525, A54
Batygin, K., & Stevenson, D. J. 2010, ApJ, 714, L238
Batygin, K., Stevenson, D. J., & Bodenheimer, P. H. 2011, ApJ, 738, 1
Bayliss, D., Zhou, G., Penev, K., et al. 2013, AJ, 146, 113
Bayliss, D., Hartman, J. D., Bakos, G. Á., et al. 2015, AJ, 150, 49
Beatty, T. G., Pepper, J., Siverd, R. J., et al. 2012, ApJ, 756, L39
Becker, J. C., Vanderburg, A., Adams, F. C., Rappaport, S. A., & Schwengeler, H. M. 2015, ApJ, 812, L18
Béky, B., Bakos, G. Á., Hartman, J., et al. 2011, ApJ, 734, 109
Bento, J., Schmidt, B., Hartman, J., et al. 2016, ArXiv e-prints, 1607.00688
Bhatti, W., Bakos, G. Á., Hartman, J. D., et al. 2016, ArXiv e-prints, 1607.00322
Bieryla, A., Hartman, J. D., Bakos, G. Á., et al. 2014, AJ, 147, 84
Bieryla, A., Collins, K., Beatty, T. G., et al. 2015, AJ, 150, 12
Bodenheimer, P., Lin, D. N. C., & Mardling, R. A. 2001, ApJ, 548, 466
Boisse, I., Hartman, J. D., Bakos, G. Á., et al. 2013, A&A, 558, A86
Borucki, W. J., Koch, D., Basri, G., et al. 2010, Science, 327, 977
Bouchy, F., Hébrard, G., Udry, S., et al. 2009, A&A, 505, 853
Bouchy, F., Hebb, L., Skillen, I., et al. 2010, A&A, 519, A98
Brahm, R., Jordán, A., Hartman, J. D., et al. 2015, AJ, 150, 33
Brahm, R., Jordán, A., Bakos, G. Á., et al. 2016, AJ, 151, 89
Buchhave, L. A., Bakos, G. Á., Hartman, J. D., et al. 2010, ApJ, 720, 1118
—. 2011, ApJ, 733, 116
Buchhave, L. A., Latham, D. W., Johansen, A., et al. 2012, Nature, 486, 375
Burrows, A., Guillot, T., Hubbard, W. B., et al. 2000, ApJ, 534, L97
Burrows, A., Hubeny, I., Budaj, J., & Hubbard, W. B. 2007, ApJ, 661, 502
Butler, R. P., Marcy, G. W., Williams, E., et al. 1996, PASP, 108, 500
Campo, C. J., Harrington, J., Hardy, R. A., et al. 2011, ApJ, 727, 125
Cardelli, J. A., Clayton, G. C., & Mathis, J. S. 1989, ApJ, 345, 245
Chabrier, G. 2003, PASP, 115, 763
Charbonneau, D., Brown, T. M., Latham, D. W., & Mayor, M. 2000, ApJ, 529, L45
Charbonnel, C., & Palacios, A. 2004, in IAU Symposium, Vol. 215, Stellar Rotation, ed. A. Maeder & P. Eenens, 440
Christensen-Dalsgaard, J., Kjeldsen, H., Brown, T. M., et al. 2010, ApJ, 713, L164
Christian, D. J., Gibson, N. P., Simpson, E. K., et al. 2009, MNRAS, 392, 1585
Christiansen, J. L., Ballard, S., Charbonneau, D., et al. 2010, ApJ, 710, 97
Ciceri, S., Mancini, L., Henning, T., et al. 2015, ArXiv e-prints, 1511.06305
Claret, A. 2004, A&A, 428, 1001
Collier Cameron, A., Bouchy, F., Hébrard, G., et al. 2007, MNRAS, 375, 951
Collier Cameron, A., Guenther, E., Smalley, B., et al. 2010, MNRAS, 407, 507
Collins, K. A., Eastman, J. D., Beatty, T. G., et al. 2014, AJ, 147, 39
Dai, F., Winn, J. N., Arriagada, P., et al. 2015, ApJ, 813, L9
de Val-Borro, M., Bakos, G. Á., Brahm, R., et al. 2016, ArXiv e-prints, 1607.00006
Delrez, L., Van Grootel, V., Anderson, D. R., et al. 2014, A&A, 563, A143
Delrez, L., Santerne, A., Almenara, J.-M., et al. 2015, ArXiv e-prints, 1506.02471
Demory, B.-O., & Seager, S. 2011, ApJS, 197, 12
Dittmann, J. A., Close, L. M., Scuderi, L. J., Turner, J., & Stephenson, P. C. 2012, New Astronomy, 17, 438
Djupvik, A. A., & Andersen, J. 2010, in Highlights of Spanish Astrophysics V, ed. J. M. Diego, L. J. Goicoechea, J. I. González-Serrano, & J. Gorgas, 211
Droege, T. F., Richmond, M. W., Sallman, M. P., & Creager, R. P. 2006, PASP, 118, 1666
Eastman, J. D., Beatty, T. G., Siverd, R. J., et al. 2016, AJ, 151, 45
Efron, B., & Petrosian, V. 1999, Journal of the American Statistical Association, 94, 824
Enoch, B., Collier Cameron, A., & Horne, K. 2012, A&A, 540, A99
Enoch, B., Cameron, A. C., Anderson, D. R., et al. 2011a, MNRAS, 410, 1631
Enoch, B., Anderson, D. R., Barros, S. C. C., et al. 2011b, AJ, 142, 86
Espinoza, N., & Jordán, A. 2015, MNRAS, 450, 1879
Espinoza, N., Bayliss, D., Hartman, J. D., et al. 2016, ArXiv e-prints, 1606.00023
Faedi, F., Barros, S. C. C., Anderson, D. R., et al. 2011, A&A, 531, A40
Faedi, F., Pollacco, D., Barros, S. C. C., et al. 2013, A&A, 551, A73
Fűresz, G. 2008, PhD thesis, Univ. of Szeged, Hungary
Fortney, J. J., Marley, M. S., & Barnes, J. W. 2007, ApJ, 659, 1661
Fukui, A., Narita, N., Tristram, P. J., et al. 2011, PASJ, 63, 287
Fulton, B. J., Collins, K. A., Gaudi, B. S., et al. 2015, ApJ, 810, 30
Geweke, J. 1992, in BAYESIAN STATISTICS 4, ed. J. M. Bernardo, J. Berger, A. P. Dawid, & J. F. M. Smith (Oxford University Press), 169–193
Gibson, N. P., Pollacco, D., Simpson, E. K., et al. 2008, A&A, 492, 603
—. 2009, ApJ, 700, 1078
Gibson, N. P., Pollacco, D. L., Barros, S., et al. 2010, MNRAS, 401, 1917
Gillon, M., Anderson, D. R., Triaud, A. H. M. J., et al. 2009a, A&A, 501, 785
Gillon, M., Smalley, B., Hebb, L., et al. 2009b, A&A, 496, 259
Gillon, M., Doyle, A. P., Lendl, M., et al. 2011, A&A, 533, A88
Gillon, M., Anderson, D. R., Collier-Cameron, A., et al. 2013, A&A, 552, A82

—. 2014, A&A, 562, L3
Girardi, L., Bertelli, G., Bressan, A., et al. 2002, A&A, 391, 195
Gómez Maqueo Chew, Y., Faedi, F., Pollacco, D., et al. 2013, A&A, 559, A36
Grunblatt, S. K., Huber, D., Gaidos, E. J., et al. 2016, ArXiv e-prints, 1606.05818
Hansen, B. M. S., & Barman, T. 2007, ApJ, 671, 861
Hartman, J. D., Bakos, G. Á., Torres, G., et al. 2009, ApJ, 706, 785
Hartman, J. D., Bakos, G. Á., Sato, B., et al. 2011a, ApJ, 726, 52
Hartman, J. D., Bakos, G. Á., Kipping, D. M., et al. 2011b, ApJ, 728, 138
Hartman, J. D., Bakos, G. Á., Torres, G., et al. 2011c, ApJ, 742, 59
Hartman, J. D., Bakos, G. Á., Béky, B., et al. 2012, AJ, 144, 139
Hartman, J. D., Bakos, G. Á., Torres, G., et al. 2014, AJ, 147, 128
Hartman, J. D., Bhatti, W., Bakos, G. Á., et al. 2015a, AJ, 150, 168
Hartman, J. D., Bakos, G. Á., Buchhave, L. A., et al. 2015b, AJ, 150, 197
Hartman, J. D., Bayliss, D., Brahm, R., et al. 2015c, AJ, 149, 166
Hebb, L., Collier-Cameron, A., Loeillet, B., et al. 2009, ApJ, 693, 1920
Hebb, L., Collier-Cameron, A., Triaud, A. H. M. J., et al. 2010, ApJ, 708, 224
Hébrard, G., Collier Cameron, A., Brown, D. J. A., et al. 2013, A&A, 549, A134
Hellier, C., Anderson, D. R., Collier-Cameron, A., et al. 2011a, ApJ, 730, L31
Hellier, C., Anderson, D. R., Collier Cameron, A., et al. 2009a, Nature, 460, 1098
Hellier, C., Anderson, D. R., Gillon, M., et al. 2009b, ApJ, 690, L89
Hellier, C., Anderson, D. R., Collier Cameron, A., et al. 2010, ApJ, 723, L60
—. 2011b, A&A, 535, L7
—. 2012, MNRAS, 426, 739
Hellier, C., Anderson, D. R., Cameron, A. C., et al. 2014, MNRAS, 440, 1982
Hellier, C., Anderson, D. R., Collier Cameron, A., et al. 2015, AJ, 150, 18
—. 2016, ArXiv e-prints, 1604.04195
Henry, G. W., Marcy, G. W., Butler, R. P., & Vogt, S. S. 2000, ApJ, 529, L41
Howard, A. W., Bakos, G. Á., Hartman, J., et al. 2012, ApJ, 749, 134
Huang, C. X., Hartman, J. D., Bakos, G. Á., et al. 2015, AJ, 150, 85
Huang, X., & Cumming, A. 2012, ApJ, 757, 47
Ibgui, L., Burrows, A., & Spiegel, D. S. 2010, ApJ, 713, 751
Ibgui, L., Spiegel, D. S., & Burrows, A. 2011, ApJ, 727, 75
Isaacson, H., & Fischer, D. 2010, ApJ, 725, 875
Johnson, J. A., Winn, J. N., Albrecht, S., et al. 2009a, PASP, 121, 1104
Johnson, J. A., Winn, J. N., Cabrera, N. E., & Carter, J. A. 2009b, ApJ, 692, L100
Johnson, J. A., Winn, J. N., Narita, N., et al. 2008, ApJ, 686, 649
Johnson, J. A., Winn, J. N., Bakos, G. Á., et al. 2011, ApJ, 735, 24
Jordán, A., Brahm, R., Bakos, G. Á., et al. 2014, AJ, 148, 29
Joshi, Y. C., Pollacco, D., Collier Cameron, A., et al. 2009, MNRAS, 392, 1532
Juncher, D., Buchhave, L. A., Hartman, J. D., et al. 2015, PASP, 127, 851
Kipping, D. M., Bakos, G. Á., Hartman, J., et al. 2010, ApJ, 725, 2017
Kipping, D. M., Hartman, J., Bakos, G. Á., et al. 2011, AJ, 142, 95
Knutson, H. A., Charbonneau, D., Burrows, A., O'Donovan, F. T., & Mandushev, G. 2009, ApJ, 691, 866
Kovács, G., Bakos, G., & Noyes, R. W. 2005, MNRAS, 356, 557
Kovács, G., Zucker, S., & Mazeh, T. 2002, A&A, 391, 369
Kovács, G., Bakos, G. Á., Torres, G., et al. 2007, ApJ, 670, L41
Kovács, G., Bakos, G. Á., Hartman, J. D., et al. 2010, ApJ, 724, 866
Krejčová, T., Budaj, J., & Krushevska, V. 2010, Contributions of the Astronomical Observatory Skalnate Pleso, 40, 77
Kuhn, R. B., Rodriguez, J. E., Collins, K. A., et al. 2015, ArXiv e-prints, 1509.02323
Lagarde, N., Decressin, T., Charbonnel, C., et al. 2012, A&A, 543, A108
Latham, D. W., Bakos, G. Á., Torres, G., et al. 2009, ApJ, 704, 1107
Lendl, M., Anderson, D. R., Collier-Cameron, A., et al. 2012, A&A, 544, A72
Lendl, M., Triaud, A. H. M. J., Anderson, D. R., et al. 2014, A&A, 568, A81
Liang, F., Paulo, R., Molina, G., Clyde, M. A., & Berger, J. O. 2008, Journal of the American Statistical Association, 103, 410
Lister, T. A., Anderson, D. R., Gillon, M., et al. 2009, ApJ, 703, 752
Liu, X., Burrows, A., & Ibgui, L. 2008, ApJ, 687, 1191
Lloyd, J. P. 2011, ApJ, 739, L49
Lopez, E. D., & Fortney, J. J. 2016, ApJ, 818, 4
Lucy, L. B., & Sweeney, M. A. 1971, AJ, 76, 544
Mancini, L., Hartman, J. D., Penev, K., et al. 2015, A&A, 580, A63
Mandel, K., & Agol, E. 2002, ApJ, 580, L171
Mandushev, G., O'Donovan, F. T., Charbonneau, D., et al. 2007, ApJ, 667, L195
Mandushev, G., Quinn, S. N., Buchhave, L. A., et al. 2011, ApJ, 741, 114
Maxted, P. F. L., Anderson, D. R., Gillon, M., et al. 2010a, AJ, 140, 2007
Maxted, P. F. L., Anderson, D. R., Collier Cameron, A., et al. 2010b, PASP, 122, 1465
—. 2011, PASP, 123, 547
—. 2013, PASP, 125, 48
—. 2016, ArXiv e-prints, 1602.01740
Mohler-Fischer, M., Mancini, L., Hartman, J. D., et al. 2013, A&A, 558, A55
Močnik, T., Anderson, D. R., Brown, D. J. A., et al. 2016, ArXiv e-prints, 1603.05638
Neveu-VanMalle, M., Queloz, D., Anderson, D. R., et al. 2014, A&A, 572, A49
Noyes, R. W., Hartmann, L. W., Baliunas, S. L., Duncan, D. K., & Vaughan, A. H. 1984, ApJ, 279, 763
Noyes, R. W., Bakos, G. Á., Torres, G., et al. 2008, ApJ, 673, L79
O'Donovan, F. T., Charbonneau, D., Mandushev, G., et al. 2006, ApJ, 651, L61
O'Rourke, J. G., Knutson, H. A., Zhao, M., et al. 2014, ApJ, 781, 109
Pál, A. 2012, MNRAS, 421, 1825
Pál, A., Bakos, G. Á., Torres, G., et al. 2008, ApJ, 680, 1450
—. 2010, MNRAS, 401, 2665
Penev, K., Bakos, G. Á., Bayliss, D., et al. 2013, AJ, 145, 5
Penev, Dr., K. M., Hartman, Dr., J. D., Bakos, Dr., G. A., et al. 2016, ArXiv e-prints, 1606.00848
Pepper, J., Siverd, R. J., Beatty, T. G., et al. 2013, ApJ, 773, 64
Pollacco, D., Skillen, I., Collier Cameron, A., et al. 2008, MNRAS, 385, 1576
Pollacco, D. L., Skillen, I., Collier Cameron, A., et al. 2006, PASP, 118, 1407
Pont, F., & Eyer, L. 2004, MNRAS, 351, 487
Prša, A., Harmanec, P., Torres, G., et al. 2016, AJ, 152, 41
Queloz, D., Anderson, D. R., Collier Cameron, A., et al. 2010, A&A, 517, L1
Quinn, S. N., Bakos, G. Á., Hartman, J., et al. 2012, ApJ, 745, 80
Rabus, M., Deeg, H. J., Alonso, R., Belmonte, J. A., & Almenara, J. M. 2009, A&A, 508, 1011
Rabus, M., Jordán, A., Hartman, J. D., et al. 2016, ArXiv e-prints, 1603.02894
Raetz, S., Mugrauer, M., Schmidt, T. O. B., et al. 2009, Astronomische Nachrichten, 330, 475
Rodriguez, J. E., Colon, K. D., Stassun, K. G., et al. 2015, ArXiv e-prints, 1509.08953
Rouder, J. N., & Morey, R. D. 2012, Multivariate Behavioral Research, 47, 877, pMID: 26735007
Santerne, A., Hébrard, G., Deleuil, M., et al. 2014, A&A, 571, A37

Santerne, A., Moutou, C., Tsantaki, M., et al. 2016, A&A, 587, A64
Santos, N. C., Sousa, S. G., Mortier, A., et al. 2013, A&A, 556, A150
Sato, B., Hartman, J. D., Bakos, G. Á., et al. 2012, PASJ, 64
Shporer, A., Bakos, G. Á., Bouchy, F., et al. 2009, ApJ, 690, 1393
Simpson, E. K., Faedi, F., Barros, S. C. C., et al. 2011, AJ, 141, 8
Siverd, R. J., Beatty, T. G., Pepper, J., et al. 2012, ApJ, 761, 123
Skillen, I., Pollacco, D., Collier Cameron, A., et al. 2009, A&A, 502, 391
Smalley, B., Anderson, D. R., Collier Cameron, A., et al. 2010, A&A, 520, A56
—. 2011, A&A, 526, A130
Smalley, B., Anderson, D. R., Collier-Cameron, A., et al. 2012, A&A, 547, A61
Smith, A. M. S., Anderson, D. R., Collier Cameron, A., et al. 2012, AJ, 143, 81
Smith, A. M. S., Anderson, D. R., Bouchy, F., et al. 2013, A&A, 552, A120
Smith, A. M. S., Anderson, D. R., Armstrong, D. J., et al. 2014, A&A, 570, A64
Snaith, O., Haywood, M., Di Matteo, P., et al. 2015, A&A, 578, A87
Southworth, J., Hinse, T. C., Jørgensen, U. G., et al. 2009a, MNRAS, 396, 1023
Southworth, J., Hinse, T. C., Dominik, M., et al. 2009b, ApJ, 707, 167
Sozzetti, A., Torres, G., Charbonneau, D., et al. 2007, ApJ, 664, 1190
—. 2009, ApJ, 691, 1145
Spake, J. J., Brown, D. J. A., Doyle, A. P., et al. 2016, PASP, 128, 024401
Spiegel, D. S., & Burrows, A. 2013, ApJ, 772, 76
Stempels, H. C., Collier Cameron, A., Hebb, L., Smalley, B., & Frandsen, S. 2007, MNRAS, 379, 773
Street, R. A., Simpson, E., Barros, S. C. C., et al. 2010, ApJ, 720, 337
Szabo, G. M., Haja, O., Szatmary, K., Pal, A., & Kiss, L. L. 2010, Information Bulletin on Variable Stars, 5919
ter Braak, C. J. F. 2006, Statistics and Computing, 16, 239
Torres, G., Fischer, D. A., Sozzetti, A., et al. 2012, ApJ, 757, 161
Torres, G., Winn, J. N., & Holman, M. J. 2008, ApJ, 677, 1324
Torres, G., Bakos, G. Á., Kovács, G., et al. 2007, ApJ, 666, L121
Torres, G., Bakos, G. Á., Hartman, J., et al. 2010, ApJ, 715, 458
Triaud, A. H. M. J., Queloz, D., Hellier, C., et al. 2011, A&A, 531, A24
Triaud, A. H. M. J., Anderson, D. R., Collier Cameron, A., et al. 2013, A&A, 551, A80
Tripathi, A., Winn, J. N., Johnson, J. A., et al. 2010, ApJ, 715, 421
Turner, O. D., Anderson, D. R., Collier Cameron, A., et al. 2015, ArXiv e-prints, 1509.02210
Van Eylen, V., Albrecht, S., Gandolfi, D., et al. 2016, ArXiv e-prints, 1605.09180
Vogt, S. S., Allen, S. L., Bigelow, B. C., et al. 1994, in Society of Photo-Optical Instrumentation Engineers (SPIE) Conference Series, Vol. 2198, Society of Photo-Optical Instrumentation Engineers (SPIE) Conference Series, ed. D. L. Crawford & E. R. Craine, 362
Weinberg, M. D., Yoon, I., & Katz, N. 2013, ArXiv e-prints, 1301.3156
Welsh, W. F., Orosz, J. A., Seager, S., et al. 2010, ApJ, 713, L145
West, R. G., Anderson, D. R., Gillon, M., et al. 2009, AJ, 137, 4834
West, R. G., Hellier, C., Almenara, J.-M., et al. 2016, A&A, 585, A126
Winn, J. N., Holman, M. J., Carter, J. A., et al. 2009, AJ, 137, 3826
Winn, J. N., Johnson, J. A., Howard, A. W., et al. 2010, ApJ, 718, 575
Winn, J. N., Howard, A. W., Johnson, J. A., et al. 2011, AJ, 141, 63
Wu, Y., & Lithwick, Y. 2013, ApJ, 763, 13
Yi, S., Demarque, P., Kim, Y.-C., et al. 2001, ApJS, 136, 417
Zacharias, N., Finch, C. T., Girard, T. M., et al. 2013, AJ, 145, 44
Zechmeister, M., & Kürster, M. 2009, A&A, 496, 577
Zhao, M., O'Rourke, J. G., Wright, J. T., et al. 2014, ApJ, 796, 115
Zhou, G., Bayliss, D., Penev, K., et al. 2014, AJ, 147, 144
Zhou, G., Bayliss, D., Hartman, J. D., et al. 2015, ApJ, 814, L16

APPENDIX

ESTIMATING TRANSITING PLANET HOST STAR PARAMETERS WITH PRIORS ON THE STELLAR MASS, AGE, AND METALLICITY

The physical parameters of transiting planet host stars are determined by comparing the observed parameters $T_{\rm eff\star}$, $\rho_\star$ and [Fe/H] to theoretical stellar evolution models. In practice the light curve analysis produces a Markov Chain of $\rho_\star$ values, which we combine with simulated chains of $T_{\rm eff\star}$ and [Fe/H] values (we assume the three parameters are uncorrelated, and that $T_{\rm eff\star}$ and [Fe/H] have Gaussian uncertainties). For a given $(\rho_\star, T_{\rm eff\star}, [{\rm Fe/H}])$ link in the chain, we perform a trilinear interpolation within a grid of isochrones from the YY models to get the corresponding stellar mass, age, radius, luminosity, and absolute magnitudes in various pass-bands. Our interpolation routine can use any combination of three parameters as the independent variables, below we make use of this feature using the mass, age and metallicity as the independent variables. The resulting chain of stellar physical parameters is then used to provide best estimates and uncertainties for each of these parameters.

As discussed in Section 4.1.3 this process may lead to systematic errors in the stellar parameters if priors are not adopted to account for the intrinsic distribution of stars in the Galaxy. The prior is applied as a multiplicative weight that is associated with each link in the Markov Chain. The weights are calculated as follows.

Let $P_m(m)$, $P_t(t)$, and $P_{[{\rm Fe/H}]}([{\rm Fe/H}])$ be prior probability densities to be placed on the stellar mass, age and metallicity, respectively. Here we use the Chabrier (2003) initial mass function for the prior on the stellar mass, a uniform distribution for the prior on the stellar age, and a Gaussian distribution with mean 0 dex and standard deviation 0.5 dex for the prior on the metallicity. Further, let $C_m(m)$, $C_t(t)$, and $C_{[{\rm Fe/H}]}([{\rm Fe/H}])$ be the corresponding cumulative distributions of these prior probability densities.

For a given $(m, t, [{\rm Fe/H}])$ link generated from an input set of $(\rho_\star, T_{\rm eff\star}, [{\rm Fe/H}])$, we find $m^+ = C_m^{-1}(C_m(m) + \Delta u_m)$, $t^+ = C_t^{-1}(C_t(t) + \Delta u_t)$ and $[{\rm Fe/H}]^+ = {\rm C}^{-1}_{[{\rm Fe/H}]}({\rm C}_{[{\rm Fe/H}]}([{\rm Fe/H}]) + \Delta {\rm u}_{[{\rm Fe/H}]})$ for some small probability steps $\Delta u_m \ll 1$, $\Delta u_t \ll 1$ and $\Delta u_{[{\rm Fe/H}]} \ll 1$. Likewise we calculate m^-, t^- and $[{\rm Fe/H}]^-$ for a negative Δu. We then perform trilinear interpolation within the isochrones to find $(\rho_{m+}, T_{{\rm eff},m+}, [{\rm Fe/H}]_{\rm m+})$ associated with the point $(m^+, t, [{\rm Fe/H}])$, and similarly for m^-, t^+, etc.

Letting

$$\mathbf{v_m} = (\rho_{m+} - \rho_{m-}, T_{{\rm eff},m+} - T_{{\rm eff},m-}, [{\rm Fe/H}]_{\rm m+} - [{\rm Fe/H}]_{\rm m-}) \quad \text{(A1)}$$

be the vector running from the m^- point to the m^+ point, and similarly for $\mathbf{v_t}$ and $\mathbf{v}_{[\mathrm{Fe/H}]}$, the weight w is then calculated as

$$w = \frac{\Delta u_m \Delta u_t \Delta u_{[\mathrm{Fe/H}]}}{\mathbf{v_m} \cdot (\mathbf{v_t} \times \mathbf{v}_{[\mathrm{Fe/H}]})} \tag{A2}$$

where the denominator is the volume of the parallelepiped spanned by the three vectors. We use these weights in calculating the weighted median and 1σ confidence regions of each parameter chain.

Table 7
Relative radial velocities and bisector spans for HAT-P-65 and HAT-P-66.

Star	BJD (2,450,000+)	RV[a] ($m\,s^{-1}$)	σ_{RV}[b] ($m\,s^{-1}$)	BS ($m\,s^{-1}$)	σ_{BS} ($m\,s^{-1}$)	Phase	Instrument
HAT-P-65							
HAT-P-65	5544.74169	...	...	19.6	29.8	0.161	HIRES
HAT-P-65	5544.75713	−27.18	7.33	59.9	26.9	0.167	HIRES
HAT-P-65	5545.73503	65.09	6.31	20.1	10.9	0.542	HIRES
HAT-P-65	5814.97581	54.96	5.43	−23.6	7.4	0.880	HIRES
HAT-P-65	5850.91750	39.48	5.64	43.7	11.2	0.675	HIRES
HAT-P-65	5853.90364	67.84	5.18	−0.2	6.9	0.821	HIRES
HAT-P-65	5878.76104	−74.79	5.32	−1.6	4.4	0.361	HIRES
HAT-P-65	5879.78830	79.69	5.53	−1.7	5.2	0.756	HIRES
HAT-P-65	5880.82088	−70.82	5.50	0.2	6.5	0.152	HIRES
HAT-P-65	5881.83486	−15.35	6.61	−21.2	8.1	0.541	HIRES
HAT-P-65	5904.71775	−81.04	4.62	2.2	7.0	0.324	HIRES
HAT-P-65	6193.91043	−34.59	5.57	5.4	5.3	0.319	HIRES
HAT-P-65	6534.99676	−65.37	5.92	5.5	12.5	0.231	HIRES
HAT-P-66							
HAT-P-66	6991.98631	−26.96	45.68	...	...	0.227	TRES
HAT-P-66	7061.78904	85.42	58.94	...	...	0.713	TRES
HAT-P-66	7064.81417	132.13	59.20	...	...	0.731	TRES
HAT-P-66	7079.67198	54.56	57.38	...	...	0.730	TRES
HAT-P-66	7110.88787	−60.24	49.59	...	...	0.233	TRES
HAT-P-66	7112.39413	74.38	17.40	4.6	31.3	0.740	Sophie
HAT-P-66	7136.46148	84.58	12.70	0.8	22.9	0.838	Sophie
HAT-P-66	7146.66832	−108.08	42.72	...	...	0.272	TRES
HAT-P-66	7166.67684[d]	170.19	73.39	...	...	0.004	TRES
HAT-P-66	7167.68267	−22.39	54.73	...	...	0.343	TRES
HAT-P-66	7168.70209	116.29	42.72	...	...	0.686	TRES
HAT-P-66	7180.66291	190.92	75.28	...	...	0.710	TRES
HAT-P-66	7191.40443	−132.24	20.50	−42.1	36.9	0.324	Sophie
HAT-P-66	7193.37858[d]	137.63	47.00	−204.0	84.6	0.989	Sophie
HAT-P-66	7195.40734	71.00	16.30	61.3	29.3	0.671	Sophie
HAT-P-66	7331.65788	−22.35	16.10	30.7	29.0	0.515	Sophie
HAT-P-66	7333.68313	−89.69	13.40	33.6	24.1	0.196	Sophie
HAT-P-66	7334.67374	9.77	10.60	17.4	19.1	0.529	Sophie
HAT-P-66	7335.68108	94.91	11.70	57.0	21.1	0.868	Sophie
HAT-P-66	7379.14314	−17.16	4.52	5.2	5.5	0.492	HIRES
HAT-P-66	7400.62823	92.74	13.00	48.4	23.4	0.721	Sophie
HAT-P-66	7402.71917	−53.77	17.00	−29.5	30.6	0.424	Sophie
HAT-P-66	7403.52312	91.28	18.30	−6.8	32.9	0.695	Sophie
HAT-P-66	7404.61059	−18.72	17.00	−3.1	30.6	0.061	Sophie
HAT-P-66	7405.56638	−60.84	14.00	25.1	25.2	0.382	Sophie
HAT-P-66	7412.16895	51.53	3.81	4.8	8.7	0.604	HIRES
HAT-P-66	7413.08806	61.91	3.34	−3.3	4.6	0.913	HIRES
HAT-P-66	7413.94835	−67.66	2.93	5.4	3.0	0.202	HIRES
HAT-P-66	7415.04674	37.83	3.20	−14.4	5.7	0.572	HIRES
HAT-P-66	7422.94521	...	...	2.3	2.2	0.230	HIRES

[a] The zero-point of these velocities is arbitrary. An overall offset γ_{rel} fitted independently to the velocities from each instrument has been subtracted. RVs are not measured for the I_2-free HIRES template spectra, but spectral line BSs are measured for these spectra.
[b] Internal errors excluding the component of astrophysical jitter considered in Section 3.3.
[c] Ca II HK line core emission index measured from the Keck-I/HIRES spectra following Isaacson & Fischer (2010).
[d] These observations were excluded from the analysis because they were obtained during transit and the RVs may be affected by the Rossiter-McLaughlin effect.

Table 8
Adopted Parameters for Transiting Planet Systems Discovered by HAT, KELT, TrES and WASP.

Planet	Period (d)	M_p (M_J)	R_p (R_J)	T_{eq} (K)	$T_{eff\star}$ (K)	$\rho_\star$ ($g\,cm^{-3}$)	[Fe/H]	$M_\star$ ($M_\odot$)	Age (Gyr)	t_{tot} (Gyr)	Refs.
HAT-P-10/ WASP-11b	3.722	0.487 ± 0.018	$1.005^{+0.032}_{-0.027}$	1020 ± 17	4980 ± 60	$2.374^{+0.208}_{-0.189}$	0.13 ± 0.08	0.830 ± 0.030	7.90 ± 3.80	19.95	28
HAT-P-11b	4.888	0.081 ± 0.009	0.422 ± 0.014	878 ± 15	4780 ± 50	$2.699^{+0.242}_{-0.222}$	0.31 ± 0.05	$0.810^{+0.020}_{-0.030}$	$6.50^{+5.90}_{-4.10}$	19.95	45
HAT-P-12b	3.213	0.211 ± 0.012	$0.959^{+0.029}_{-0.021}$	963 ± 16	4650 ± 60	$2.999^{+0.175}_{-0.214}$	-0.29 ± 0.05	0.733 ± 0.018	2.50 ± 2.00	19.95	32
HAT-P-13b	2.916	0.850 ± 0.038	1.281 ± 0.079	1656^{+46}_{-43}	5653 ± 90	$0.448^{+0.082}_{-0.071}$	0.41 ± 0.08	$1.220^{+0.050}_{-0.100}$	$5.00^{+2.50}_{-0.70}$	6.80	34,51
HAT-P-14b	4.628	2.232 ± 0.059	1.150 ± 0.052	1570 ± 34	6600 ± 90	$0.618^{+0.078}_{-0.066}$	0.11 ± 0.08	1.386 ± 0.045	1.30 ± 0.40	4.20	50
HAT-P-15b	10.864	1.946 ± 0.066	1.072 ± 0.043	904 ± 20	5568 ± 90	$1.137^{+0.142}_{-0.122}$	0.22 ± 0.08	1.013 ± 0.043	$6.80^{+2.50}_{-1.60}$	13.10	55
HAT-P-16b	2.776	4.193 ± 0.094	1.289 ± 0.066	1626 ± 40	6158 ± 80	$0.908^{+0.134}_{-0.113}$	0.17 ± 0.08	1.218 ± 0.039	2.00 ± 0.80	6.60	52
HAT-P-17b	10.339	0.530 ± 0.019	1.000 ± 0.030	787 ± 15	5246 ± 80	$2.123^{+0.207}_{-0.188}$	0.00 ± 0.08	0.861 ± 0.039	6.90 ± 3.30	19.95	97
HAT-P-18b	5.508	0.197 ± 0.013	0.995 ± 0.052	852 ± 28	4803 ± 80	$2.589^{+0.432}_{-0.359}$	0.10 ± 0.08	0.770 ± 0.031	$12.40^{+4.40}_{-6.40}$	19.95	75
HAT-P-19b	4.009	0.292 ± 0.018	1.132 ± 0.072	1010 ± 42	4989 ± 126	$2.169^{+0.438}_{-0.353}$	0.23 ± 0.08	0.842 ± 0.042	8.80 ± 5.20	19.95	75
HAT-P-1b	4.465	0.524 ± 0.031	1.225 ± 0.059	1306 ± 30	6076 ± 27	$1.150^{+0.188}_{-0.161}$	0.21 ± 0.03	$1.133^{+0.075}_{-0.079}$	$2.70^{+2.50}_{-2.00}$	8.70	11,13,18

Table 8 — *Continued*

Planet	Period (d)	M_p (M_J)	R_p (R_J)	T_{eq} (K)	$T_{eff\star}$ (K)	$\rho_\star$ (g cm^{-3})	[Fe/H]	$M_\star$ ($M_\odot$)	Age (Gyr)	t_{tot} (Gyr)	Refs.
HAT-P-20b	2.875	7.246 ± 0.187	0.867 ± 0.033	970 ± 23	4595 ± 80	$3.196^{+0.336}_{-0.297}$	0.35 ± 0.08	0.756 ± 0.028	$6.70^{+5.70}_{-3.80}$	19.95	84
HAT-P-21b	4.124	4.063 ± 0.161	1.024 ± 0.092	1283 ± 50	5588 ± 80	$0.992^{+0.260}_{-0.200}$	0.01 ± 0.08	0.947 ± 0.042	10.20 ± 2.50	15.00	84
HAT-P-22b	3.212	2.147 ± 0.061	1.080 ± 0.058	1283 ± 32	5302 ± 80	$1.154^{+0.164}_{-0.140}$	0.24 ± 0.08	0.916 ± 0.035	12.40 ± 2.60	18.85	84
HAT-P-23b	1.213	2.090 ± 0.111	1.368 ± 0.090	2056 ± 66	5905 ± 80	$0.915^{+0.189}_{-0.152}$	0.15 ± 0.04	1.130 ± 0.035	4.00 ± 1.00	8.55	84
HAT-P-24b	3.355	0.685 ± 0.033	1.242 ± 0.067	1637 ± 42	6373 ± 80	$0.737^{+0.129}_{-0.105}$	-0.16 ± 0.08	1.191 ± 0.042	2.80 ± 0.60	5.95	56
HAT-P-25b	3.653	0.567 ± 0.022	$1.190^{+0.081}_{-0.056}$	1202 ± 36	5500 ± 80	$1.616^{+0.213}_{-0.247}$	0.31 ± 0.08	1.010 ± 0.032	3.20 ± 2.30	13.50	96
HAT-P-26b	4.235	0.059 ± 0.007	$0.565^{+0.072}_{-0.032}$	1001^{+66}_{-37}	5079 ± 88	$2.351^{+0.443}_{-0.714}$	-0.04 ± 0.08	0.816 ± 0.033	$9.00^{+3.00}_{-4.90}$	19.95	77
HAT-P-27b	3.040	0.660 ± 0.033	$1.038^{+0.077}_{-0.058}$	1207 ± 41	5302 ± 88	$1.842^{+0.269}_{-0.306}$	0.29 ± 0.10	0.945 ± 0.035	$4.40^{+3.80}_{-2.60}$	17.10	80
HAT-P-28b	3.257	0.636 ± 0.037	$1.189^{+0.102}_{-0.075}$	1371 ± 50	5681 ± 88	$1.143^{+0.233}_{-0.239}$	0.12 ± 0.08	1.024 ± 0.046	5.80 ± 2.30	12.05	79
HAT-P-29b	5.723	$0.778^{+0.076}_{-0.040}$	$1.107^{+0.136}_{-0.082}$	1260^{+64}_{-45}	6087 ± 88	$0.926^{+0.201}_{-0.251}$	0.21 ± 0.08	1.207 ± 0.046	2.20 ± 1.00	6.90	79
HAT-P-2b	5.633	9.090 ± 0.240	$1.157^{+0.073}_{-0.062}$	1540 ± 30	6290 ± 60	$0.435^{+0.073}_{-0.065}$	0.14 ± 0.08	1.360 ± 0.040	2.60 ± 0.50	4.55	60
HAT-P-30b	2.811	0.711 ± 0.028	1.340 ± 0.065	1630 ± 42	6304 ± 88	$0.974^{+0.137}_{-0.113}$	0.13 ± 0.08	1.242 ± 0.041	$1.00^{+0.80}_{-0.50}$	6.05	81
HAT-P-31b	5.005	$2.171^{+0.105}_{-0.077}$	$1.070^{+0.480}_{-0.320}$	1450^{+230}_{-110}	6065 ± 100	$0.690^{+0.340}_{-0.260}$	0.15 ± 0.08	$1.218^{+0.089}_{-0.063}$	$3.17^{+0.70}_{-1.11}$	6.55	74
HAT-P-32b	2.150	0.860 ± 0.164	1.789 ± 0.025	1786 ± 26	6207 ± 88	$0.903^{+0.050}_{-0.047}$	-0.04 ± 0.08	1.160 ± 0.041	2.70 ± 0.80	7.00	85
HAT-P-33b	3.474	0.762 ± 0.101	1.686 ± 0.045	1782 ± 28	6446 ± 88	$0.442^{+0.033}_{-0.030}$	0.07 ± 0.08	1.375 ± 0.040	2.30 ± 0.30	4.25	85
HAT-P-34b	5.453	3.328 ± 0.211	$1.197^{+0.128}_{-0.092}$	1520 ± 60	6442 ± 88	$0.542^{+0.129}_{-0.122}$	0.22 ± 0.04	1.392 ± 0.047	$1.70^{+0.40}_{-0.50}$	4.35	95
HAT-P-35b	3.647	1.054 ± 0.033	1.332 ± 0.098	1581 ± 45	6096 ± 88	$0.590^{+0.120}_{-0.098}$	0.11 ± 0.08	1.236 ± 0.048	$3.50^{+0.80}_{-0.50}$	6.10	95
HAT-P-36b	1.327	1.832 ± 0.099	1.264 ± 0.071	1823 ± 55	5560 ± 100	$1.099^{+0.194}_{-0.159}$	0.26 ± 0.10	1.022 ± 0.049	$6.60^{+2.90}_{-1.80}$	12.80	95
HAT-P-37b	2.797	1.169 ± 0.103	1.178 ± 0.077	1271 ± 47	5500 ± 100	$1.942^{+0.342}_{-0.351}$	0.03 ± 0.10	0.929 ± 0.043	$3.60^{+4.10}_{-2.20}$	16.25	95
HAT-P-38b	4.640	0.267 ± 0.020	$0.825^{+0.092}_{-0.063}$	1082 ± 55	5330 ± 100	$1.588^{+0.413}_{-0.415}$	0.06 ± 0.10	0.886 ± 0.044	10.10 ± 4.80	19.50	104
HAT-P-39b	3.544	0.599 ± 0.099	$1.571^{+0.108}_{-0.081}$	1752 ± 43	6430 ± 100	$0.461^{+0.059}_{-0.063}$	0.19 ± 0.10	1.404 ± 0.051	2.00 ± 0.40	4.20	94
HAT-P-3b	2.900	$0.596^{+0.024}_{-0.026}$	$0.899^{+0.043}_{-0.049}$	1127^{+49}_{-39}	5185 ± 46	$2.254^{+0.423}_{-0.281}$	0.27 ± 0.04	$0.928^{+0.044}_{-0.054}$	$1.50^{+5.40}_{-1.40}$	18.15	3,11,59
HAT-P-40b	4.457	0.615 ± 0.038	1.730 ± 0.062	1770 ± 33	6080 ± 100	$0.196^{+0.020}_{-0.020}$	0.22 ± 0.10	$1.512^{+0.045}_{-0.109}$	$2.70^{+0.90}_{-0.30}$	3.35	94
HAT-P-41b	2.694	0.800 ± 0.102	$1.685^{+0.076}_{-0.051}$	1941 ± 38	6390 ± 100	$0.418^{+0.033}_{-0.042}$	0.21 ± 0.10	1.418 ± 0.047	2.20 ± 0.40	4.05	94
HAT-P-42b	4.642	0.975 ± 0.126	1.277 ± 0.149	1427 ± 58	5743 ± 50	$0.467^{+0.154}_{-0.111}$	0.27 ± 0.08	1.179 ± 0.067	$5.10^{+1.80}_{-0.70}$	7.65	112
HAT-P-43b	3.333	0.660 ± 0.083	$1.283^{+0.057}_{-0.034}$	1361 ± 24	5645 ± 74	$1.091^{+0.083}_{-0.106}$	0.23 ± 0.08	$1.048^{+0.031}_{-0.042}$	$5.70^{+1.90}_{-1.10}$	11.65	112
HAT-P-44b	4.301	0.392 ± 0.031	$1.280^{+0.145}_{-0.074}$	1126^{+67}_{-42}	5295 ± 100	$1.402^{+0.277}_{-0.388}$	0.33 ± 0.10	0.939 ± 0.041	8.90 ± 3.90	17.50	123
HAT-P-45b	3.129	$0.892^{+0.137}_{-0.099}$	$1.426^{+0.175}_{-0.087}$	1652^{+90}_{-52}	6330 ± 100	$0.776^{+0.149}_{-0.220}$	0.07 ± 0.10	1.259 ± 0.058	2.00 ± 0.80	5.65	123
HAT-P-46b	4.463	$0.493^{+0.082}_{-0.052}$	$1.284^{+0.271}_{-0.133}$	1458^{+140}_{-75}	6120 ± 100	$0.676^{+0.249}_{-0.291}$	0.30 ± 0.10	$1.284^{+0.095}_{-0.060}$	$2.50^{+0.70}_{-1.00}$	5.75	123
HAT-P-47b	4.732	0.206 ± 0.039	1.313 ± 0.045	1605 ± 22	6703 ± 50	$0.564^{+0.049}_{-0.045}$	0.00 ± 0.08	1.387 ± 0.038	1.50 ± 0.30	3.95	161
HAT-P-48b	4.409	0.168 ± 0.024	1.131 ± 0.054	1361 ± 25	5946 ± 50	$0.847^{+0.109}_{-0.093}$	0.02 ± 0.08	1.099 ± 0.041	$4.70^{+1.30}_{-0.80}$	8.80	161
HAT-P-49b	2.692	1.730 ± 0.205	$1.413^{+0.128}_{-0.077}$	2131^{+69}_{-42}	6820 ± 52	$0.353^{+0.049}_{-0.069}$	0.07 ± 0.08	1.543 ± 0.051	1.50 ± 0.20	2.95	126
HAT-P-4b	3.057	0.556 ± 0.068	$1.367^{+0.052}_{-0.044}$	1686^{+30}_{-26}	5860 ± 80	$0.427^{+0.073}_{-0.058}$	0.24 ± 0.08	$1.248^{+0.070}_{-0.120}$	$4.60^{+2.20}_{-1.00}$	6.20	5,11,71
HAT-P-50b	3.122	1.350 ± 0.073	1.288 ± 0.064	1862 ± 34	6280 ± 49	0.357 ± 0.037	-0.18 ± 0.08	$1.273^{+0.049}_{-0.115}$	$3.37^{+1.44}_{-0.27}$	4.75	135
HAT-P-51b	4.218	0.309 ± 0.018	1.293 ± 0.054	1192 ± 21	5449 ± 50	$1.223^{+0.100}_{-0.135}$	0.27 ± 0.08	0.976 ± 0.028	8.20 ± 1.70	15.15	135
HAT-P-52b	2.754	0.818 ± 0.029	1.009 ± 0.072	1218 ± 37	5131 ± 50	1.750 ± 0.290	0.28 ± 0.08	0.887 ± 0.027	9.40 ± 4.10	19.95	135
HAT-P-53b	1.962	1.484 ± 0.056	1.318 ± 0.091	1778 ± 48	5956 ± 50	0.870 ± 0.130	0.00 ± 0.08	1.093 ± 0.043	$4.67^{+1.45}_{-0.83}$	8.90	135
HAT-P-54b	3.800	0.760 ± 0.032	0.944 ± 0.028	818 ± 12	4390 ± 50	$3.876^{+0.283}_{-0.253}$	-0.13 ± 0.08	0.645 ± 0.020	$3.90^{+4.30}_{-2.10}$	19.95	132
HAT-P-55b	3.585	0.582 ± 0.056	1.182 ± 0.055	1313 ± 26	5808 ± 50	$1.380^{+0.167}_{-0.143}$	-0.03 ± 0.08	1.013 ± 0.037	4.20 ± 1.70	11.50	151
HAT-P-56b	2.791	2.180 ± 0.250	1.466 ± 0.040	1840 ± 21	6566 ± 50	0.627 ± 0.033	-0.08 ± 0.08	1.296 ± 0.036	2.01 ± 0.35	4.75	140
HAT-P-57b	2.465	$0.000^{+1.850}_{-0.000}$	1.413 ± 0.054	2200 ± 76	7500 ± 250	$0.615^{+0.022}_{-0.036}$	-0.25 ± 0.25	1.470 ± 0.120	$1.00^{+0.67}_{-0.51}$	2.85	137
HAT-P-58b	4.014	0.394 ± 0.034	$1.203^{+0.090}_{-0.063}$	1500^{+49}_{-29}	5931 ± 50	0.564 ± 0.066	0.01 ± 0.08	$1.110^{+0.080}_{-0.042}$	$6.10^{+0.82}_{-1.66}$	8.45	162
HAT-P-59b	4.142	1.624 ± 0.061	1.121 ± 0.066	1273 ± 27	5665 ± 50	1.070 ± 0.130	0.41 ± 0.08	1.089 ± 0.022	4.30 ± 1.00	10.20	162
HAT-P-5b	2.788	1.060 ± 0.110	$1.254^{+0.051}_{-0.056}$	1539^{+33}_{-32}	5960 ± 100	$1.019^{+0.162}_{-0.129}$	0.24 ± 0.15	$1.157^{+0.043}_{-0.081}$	$2.60^{+2.10}_{-1.40}$	8.10	6,11
HAT-P-60b	4.795	0.492 ± 0.049	$1.116^{+0.150}_{-0.064}$	1662^{+73}_{-42}	6462 ± 50	$0.357^{+0.055}_{-0.082}$	-0.24 ± 0.08	1.310 ± 0.070	2.88 ± 0.56	4.10	162
HAT-P-61b	1.902	$1.103^{+0.052}_{-0.071}$	$0.968^{+0.061}_{-0.047}$	1526 ± 36	5551 ± 50	1.510 ± 0.180	0.40 ± 0.08	1.043 ± 0.022	$2.70^{+1.80}_{-2.50}$	11.95	162
HAT-P-62b	2.645	0.801 ± 0.088	$1.131^{+0.074}_{-0.053}$	1523 ± 31	5601 ± 50	0.840 ± 0.087	0.45 ± 0.08	1.103 ± 0.028	5.40 ± 0.89	9.60	162
HAT-P-63b	3.378	0.638 ± 0.023	1.213 ± 0.094	1246 ± 32	5365 ± 50	1.320 ± 0.180	0.43 ± 0.08	0.976 ± 0.022	7.20 ± 2.00	14.95	162
HAT-P-64b	4.007	0.750 ± 0.160	1.790 ± 0.140	1741^{+48}_{-35}	6302 ± 50	$0.332^{+0.040}_{-0.054}$	-0.01 ± 0.08	1.369 ± 0.046	2.87 ± 0.30	4.10	162
HAT-P-65b	2.605	0.527 ± 0.083	1.890 ± 0.130	1930 ± 45	5835 ± 51	0.266 ± 0.036	0.10 ± 0.08	1.212 ± 0.050	5.46 ± 0.61	6.50	166
HAT-P-66b	2.972	0.783 ± 0.057	$1.590^{+0.160}_{-0.100}$	1897^{+66}_{-42}	6002 ± 50	0.269 ± 0.040	0.04 ± 0.08	$1.255^{+0.107}_{-0.054}$	$4.66^{+0.52}_{-1.12}$	5.60	166
HAT-P-6b	3.853	$1.059^{+0.053}_{-0.052}$	$1.330^{+0.064}_{-0.058}$	1675^{+32}_{-31}	6570 ± 80	$0.581^{+0.088}_{-0.080}$	-0.13 ± 0.08	$1.290^{+0.064}_{-0.066}$	$2.30^{+0.50}_{-0.60}$	4.65	10,11,58
HAT-P-7b	2.205	1.820 ± 0.030	1.500 ± 0.020	2140^{+110}_{-60}	6350 ± 80	0.271 ± 0.003	0.26 ± 0.08	1.530 ± 0.040	2.14 ± 0.26	3.25	12,46,47,48
HAT-P-8b	3.076	$1.520^{+0.180}_{-0.160}$	$1.500^{+0.080}_{-0.060}$	1700 ± 35	6200 ± 80	$0.458^{+0.058}_{-0.063}$	0.01 ± 0.08	1.280 ± 0.040	3.40 ± 1.00	5.20	31
HAT-P-9b	3.923	0.780 ± 0.090	1.400 ± 0.060	1530 ± 40	6350 ± 150	$0.782^{+0.166}_{-0.135}$	0.12 ± 0.20	1.280 ± 0.130	$1.60^{+1.80}_{-1.40}$	5.50	23,103
HATS-10b	3.313	0.526 ± 0.081	$0.969^{+0.061}_{-0.045}$	1407 ± 39	5880 ± 120	$1.150^{+0.120}_{-0.160}$	0.15 ± 0.10	1.101 ± 0.054	3.30 ± 1.70	9.40	138
HATS-11b	3.619	0.850 ± 0.120	1.510 ± 0.078	1637 ± 48	6060 ± 150	$0.471^{+0.037}_{-0.052}$	-0.39 ± 0.06	1.000 ± 0.060	$7.70^{+2.20}_{-1.60}$	9.40	156
HATS-12b	3.143	2.380 ± 0.110	1.350 ± 0.170	2097 ± 89	6408 ± 75	$0.196^{+0.057}_{-0.044}$	-0.10 ± 0.04	1.489 ± 0.071	2.36 ± 0.31	3.00	156
HATS-13b	3.044	0.543 ± 0.072	1.212 ± 0.035	1244 ± 20	5523 ± 69	1.930 ± 0.110	0.05 ± 0.06	0.962 ± 0.029	2.50 ± 1.70	14.55	131
HATS-14b	2.767	1.071 ± 0.070	$1.039^{+0.032}_{-0.022}$	1276 ± 20	5408 ± 65	$1.682^{+0.071}_{-0.126}$	0.28 ± 0.03	0.967 ± 0.024	4.90 ± 1.70	15.70	131,145
HATS-15b	1.747	2.170 ± 0.150	1.105 ± 0.040	1505 ± 30	5311 ± 77	1.570 ± 0.120	0.00 ± 0.05	0.871 ± 0.023	$11.00^{+1.40}_{-2.00}$	19.95	150
HATS-16b	2.687	3.270 ± 0.190	1.300 ± 0.150	1592^{+61}_{-82}	5738 ± 79	$0.720^{+0.260}_{-0.130}$	0.10 ± 0.05	0.970 ± 0.035	9.50 ± 1.80	14.50	150
HATS-17b	16.255	1.338 ± 0.065	0.777 ± 0.056	814 ± 25	5846 ± 78	1.380 ± 0.270	0.30 ± 0.03	1.131 ± 0.030	2.10 ± 1.30	8.95	154
HATS-18b	0.838	1.980 ± 0.077	$1.337^{+0.102}_{-0.049}$	2060 ± 59	5600 ± 120	$1.380^{+0.130}_{-0.210}$	0.28 ± 0.08	1.037 ± 0.047	4.20 ± 2.20	12.25	167
HATS-19b	4.570	0.427 ± 0.071	$1.660^{+0.270}_{-0.210}$	1570 ± 110	5896 ± 77	$0.340^{+0.150}_{-0.110}$	0.24 ± 0.05	1.303 ± 0.083	$3.94^{+0.96}_{-0.50}$	5.40	164
HATS-1b	3.446	$1.855^{+0.262}_{-0.196}$	$1.302^{+0.162}_{-0.098}$	1359^{+89}_{-59}	5870 ± 100	$1.241^{+0.317}_{-0.370}$	-0.06 ± 0.12	0.986 ± 0.054	6.00 ± 2.80	12.50	114
HATS-20b	3.799	0.273 ± 0.035	0.776 ± 0.055	1147 ± 36	5406 ± 49	1.980 ± 0.480	0.03 ± 0.05	0.910 ± 0.026	6.40 ± 3.40	17.50	164
HATS-21b	3.554	$0.332^{+0.040}_{-0.030}$	$1.123^{+0.147}_{-0.054}$	1284^{+55}_{-31}	5695 ± 67	1.550 ± 0.380	0.30 ± 0.04	1.080 ± 0.026	2.30 ± 1.70	10.60	164
HATS-22b	4.723	2.740 ± 0.110	$0.953^{+0.048}_{-0.029}$	858^{+24}_{-17}	4803 ± 55	3.260 ± 0.680	0.00 ± 0.04	0.759 ± 0.019	$4.60^{+5.80}_{-4.00}$	19.95	163
HATS-23b	2.161	1.470 ± 0.072	$1.860^{+0.300}_{-0.400}$	1654 ± 54	5780 ± 120	$0.920^{+0.200}_{-0.110}$	0.28 ± 0.07	1.121 ± 0.046	4.20 ± 1.50	9.20	163
HATS-24b	1.348	2.440 ± 0.180	$1.487^{+0.078}_{-0.054}$	2067 ± 39	6346 ± 81	$1.096^{+0.059}_{-0.085}$	0.00 ± 0.05	1.212 ± 0.033	$0.88^{+0.67}_{-0.45}$	6.15	163
HATS-25b	4.299	0.613 ± 0.042	1.260 ± 0.100	1277 ± 42	5715 ± 73	1.030 ± 0.200	0.02 ± 0.05	0.994 ± 0.035	7.50 ± 1.90	12.70	159

Table 8 — *Continued*

Planet	Period (d)	M_p (M_J)	R_p (R_J)	T_{eq} (K)	$T_{eff\star}$ (K)	$\rho_\star$ (g cm^{-3})	[Fe/H]	$M_\star$ ($M_\odot$)	Age (Gyr)	t_{tot} (Gyr)	Refs.
HATS-26b	3.302	0.650 ± 0.076	1.750 ± 0.210	1918 ± 61	6071 ± 81	0.219 ± 0.033	-0.02 ± 0.05	$1.299^{+0.113}_{-0.056}$	$4.04^{+0.62}_{-0.94}$	4.85	159
HATS-27b	4.637	0.540 ± 0.130	1.520 ± 0.140	1661 ± 50	6438 ± 64	0.370 ± 0.059	0.09 ± 0.04	1.415 ± 0.045	2.31 ± 0.21	3.90	159
HATS-28b	3.181	0.672 ± 0.087	1.194 ± 0.070	1253 ± 35	5498 ± 84	1.680 ± 0.270	0.01 ± 0.06	0.929 ± 0.036	6.20 ± 2.80	16.10	159
HATS-29b	4.606	0.653 ± 0.063	1.251 ± 0.061	1212 ± 30	5670 ± 110	1.170 ± 0.110	0.16 ± 0.08	1.032 ± 0.049	$5.50^{+2.60}_{-1.70}$	11.95	159
HATS-2b	1.354	1.345 ± 0.150	1.168 ± 0.030	1577 ± 31	5227 ± 95	$1.718^{+0.133}_{-0.127}$	0.15 ± 0.05	0.882 ± 0.037	9.70 ± 2.90	19.95	111
HATS-30b	3.174	0.706 ± 0.039	1.175 ± 0.052	1414 ± 32	5943 ± 70	1.340 ± 0.190	0.06 ± 0.05	1.093 ± 0.031	2.30 ± 1.20	9.20	159
HATS-31b	3.378	0.880 ± 0.120	1.640 ± 0.220	1823 ± 81	6050 ± 120	$0.275^{+0.082}_{-0.061}$	0.00 ± 0.07	1.275 ± 0.096	4.30 ± 1.10	5.25	165
HATS-32b	2.813	0.920 ± 0.100	$1.249^{+0.144}_{-0.096}$	1437 ± 58	5700 ± 110	1.190 ± 0.230	0.39 ± 0.05	1.099 ± 0.044	3.50 ± 1.80	9.90	165
HATS-33b	2.550	1.192 ± 0.053	$1.230^{+0.112}_{-0.081}$	1429 ± 38	5659 ± 85	1.420 ± 0.170	0.29 ± 0.05	1.062 ± 0.032	3.00 ± 1.70	11.25	165
HATS-34b	2.106	0.941 ± 0.072	1.430 ± 0.190	1445 ± 42	5380 ± 73	1.440 ± 0.250	0.25 ± 0.07	0.955 ± 0.031	7.70 ± 2.70	16.30	165
HATS-35b	1.821	1.266 ± 0.077	$1.570^{+0.170}_{-0.130}$	2100 ± 100	6300 ± 100	0.530 ± 0.180	0.21 ± 0.06	1.347 ± 0.060	2.29 ± 0.55	4.85	165
HATS-3b	3.548	1.071 ± 0.136	1.381 ± 0.035	1648 ± 24	6351 ± 76	$0.617^{+0.046}_{-0.041}$	-0.16 ± 0.07	1.209 ± 0.036	$3.20^{+0.60}_{-0.40}$	5.70	115
HATS-4b	2.517	1.323 ± 0.028	1.020 ± 0.037	1315 ± 21	5403 ± 50	$1.784^{+0.143}_{-0.122}$	0.43 ± 0.08	1.001 ± 0.020	2.10 ± 1.60	13.65	127
HATS-5b	4.763	0.237 ± 0.012	0.912 ± 0.025	1025 ± 17	5304 ± 50	$2.001^{+0.180}_{-0.165}$	0.19 ± 0.08	0.936 ± 0.028	$3.60^{+2.60}_{-1.90}$	17.25	124
HATS-6b	3.325	0.319 ± 0.070	0.998 ± 0.019	712 ± 5	3770 ± 100	4.360 ± 0.150	0.20 ± 0.09	$0.574^{+0.020}_{-0.027}$	0.00 ± 0.00	19.95	133
HATS-7b	3.185	0.120 ± 0.012	$0.563^{+0.046}_{-0.034}$	1084 ± 32	4985 ± 50	$2.206^{+0.326}_{-0.356}$	0.25 ± 0.08	0.849 ± 0.027	7.80 ± 5.00	19.95	143
HATS-8b	3.584	0.138 ± 0.019	$0.873^{+0.123}_{-0.075}$	1324^{+79}_{-38}	5679 ± 50	$1.159^{+0.220}_{-0.373}$	0.21 ± 0.08	1.056 ± 0.037	5.10 ± 1.70	11.25	139
HATS-9b	1.915	0.837 ± 0.029	1.065 ± 0.098	1823^{+52}_{-35}	5366 ± 70	$0.427^{+0.030}_{-0.070}$	0.34 ± 0.05	1.030 ± 0.039	10.80 ± 1.50	12.55	138
KELT-10b	4.166	$0.679^{+0.039}_{-0.038}$	$1.399^{+0.069}_{-0.049}$	1377^{+28}_{-23}	5948 ± 74	$0.889^{+0.062}_{-0.088}$	$0.09^{+0.11}_{-0.10}$	$1.112^{+0.055}_{-0.061}$	$3.20^{+0.37}_{-0.51}$	7.50	148
KELT-15b	3.329	$0.910^{+0.210}_{-0.220}$	$1.443^{+0.110}_{-0.057}$	1642^{+45}_{-25}	6003^{+56}_{-52}	$0.514^{+0.034}_{-0.076}$	0.05 ± 0.03	$1.181^{+0.051}_{-0.050}$	$3.89^{+0.18}_{-0.19}$	5.95	149
KELT-1b	1.218	$27.230^{+0.500}_{-0.480}$	$1.110^{+0.032}_{-0.022}$	2422^{+32}_{-26}	6518 ± 50	$0.597^{+0.026}_{-0.039}$	0.01 ± 0.07	1.324 ± 0.026	$1.66^{+0.18}_{-0.17}$	4.30	99
KELT-2Ab	4.114	1.486 ± 0.088	$1.306^{+0.081}_{-0.067}$	1716^{+39}_{-33}	6148^{+48}_{-49}	$0.296^{+0.039}_{-0.041}$	-0.01 ± 0.07	$1.310^{+0.032}_{-0.029}$	$3.08^{+0.09}_{-0.12}$	3.95	98
KELT-3b	2.703	$1.462^{+0.067}_{-0.066}$	$1.358^{+0.068}_{-0.069}$	1821^{+35}_{-37}	6304 ± 49	$0.556^{+0.065}_{-0.054}$	$0.05^{+0.08}_{-0.08}$	$1.282^{+0.062}_{-0.060}$	$2.50^{+0.14}_{-0.26}$	4.90	116
KELT-4Ab	2.990	$0.902^{+0.060}_{-0.059}$	$1.699^{+0.046}_{-0.045}$	1823 ± 27	6206 ± 75	$0.411^{+0.018}_{-0.017}$	$-0.12^{+0.07}_{-0.07}$	$1.201^{+0.067}_{-0.061}$	$3.21^{+0.13}_{-0.17}$	4.65	153
KELT-6b	7.846	$0.430^{+0.045}_{-0.046}$	$1.193^{+0.130}_{-0.077}$	1313^{+59}_{-38}	6102 ± 43	$0.387^{+0.068}_{-0.088}$	$-0.28^{+0.04}_{-0.04}$	$1.085^{+0.043}_{-0.040}$	$5.65^{+0.22}_{-0.27}$	7.00	125
KELT-7b	2.735	1.280 ± 0.180	$1.533^{+0.046}_{-0.047}$	2048 ± 27	6789^{+50}_{-49}	$0.419^{+0.027}_{-0.035}$	$0.14^{+0.07}_{-0.08}$	$1.535^{+0.066}_{-0.054}$	$1.15^{+0.06}_{-0.10}$	2.95	134
KELT-8b	3.244	$0.867^{+0.065}_{-0.061}$	$1.860^{+0.180}_{-0.160}$	1675^{+61}_{-55}	5754^{+54}_{-55}	$0.369^{+0.073}_{-0.067}$	0.27 ± 0.04	$1.211^{+0.078}_{-0.066}$	$4.24^{+0.29}_{-0.25}$	5.55	141
TrES-1b	3.030	$0.752^{+0.047}_{-0.046}$	$1.067^{+0.022}_{-0.021}$	1140^{+13}_{-12}	5230 ± 50	$2.400^{+0.014}_{-0.120}$	0.02 ± 0.05	$0.878^{+0.038}_{-0.040}$	$1.50^{+0.82}_{-0.74}$	17.70	11,22
TrES-2b	2.471	$1.200^{+0.051}_{-0.053}$	1.224 ± 0.041	1498 ± 17	5850^{+38}_{-38}	$1.372^{+0.061}_{-0.059}$	$-0.02^{+0.06}_{-0.06}$	$0.983^{+0.059}_{-0.063}$	$2.75^{+0.38}_{-0.50}$	9.85	1,2,11,18,19
TrES-4b	3.554	$0.925^{+0.081}_{-0.082}$	$1.783^{+0.093}_{-0.086}$	1785 ± 29	6200 ± 75	$0.314^{+0.034}_{-0.032}$	0.14 ± 0.09	$1.404^{+0.066}_{-0.134}$	$2.58^{+0.16}_{-0.18}$	3.80	4,25
TrES-5b	1.482	1.778 ± 0.063	1.209 ± 0.021	1484 ± 41	5171 ± 36	$1.938^{+0.104}_{-0.098}$	0.20 ± 0.08	0.893 ± 0.024	$5.30^{+0.84}_{-0.78}$	18.45	83
WASP-100b	2.849	2.030 ± 0.120	1.690 ± 0.290	2190 ± 140	6900 ± 120	$0.280^{+0.140}_{-0.070}$	-0.03 ± 0.10	1.570 ± 0.100	$1.36^{+0.11}_{-0.13}$	2.35	128
WASP-101b	3.586	0.500 ± 0.040	1.410 ± 0.050	1560 ± 35	6380 ± 120	0.884 ± 0.061	0.20 ± 0.12	1.340 ± 0.070	$0.20^{+0.26}_{-0.08}$	4.80	128
WASP-103b	0.926	1.490 ± 0.088	$1.528^{+0.073}_{-0.047}$	2508^{+75}_{-70}	6110 ± 160	$0.584^{+0.030}_{-0.055}$	0.06 ± 0.13	$1.220^{+0.039}_{-0.036}$	$2.73^{+0.47}_{-0.56}$	5.25	118
WASP-104b	1.755	1.272 ± 0.047	1.137 ± 0.037	1516 ± 39	5450 ± 130	1.704 ± 0.099	0.32 ± 0.09	1.076 ± 0.049	$1.28^{+0.74}_{-1.13}$	12.10	121
WASP-106b	9.290	1.925 ± 0.076	$1.085^{+0.046}_{-0.028}$	1140 ± 29	6000 ± 150	$0.628^{+0.014}_{-0.055}$	-0.09 ± 0.09	1.192 ± 0.054	$3.80^{+0.61}_{-0.52}$	6.30	121
WASP-10b	3.093	$3.150^{+0.130}_{-0.110}$	1.080 ± 0.020	1119^{+26}_{-28}	4675 ± 100	3.099 ± 0.088	0.03 ± 0.20	$0.750^{+0.040}_{-0.028}$	$4.79^{+3.96}_{-3.04}$	19.95	26,36,57
WASP-117b	10.022	0.276 ± 0.009	$1.021^{+0.076}_{-0.065}$	1024^{+30}_{-26}	6040 ± 90	0.990 ± 0.140	-0.11 ± 0.14	1.126 ± 0.029	$2.95^{+0.51}_{-0.71}$	7.40	120
WASP-119b	2.500	1.230 ± 0.080	1.400 ± 0.200	1600 ± 80	5650 ± 100	0.760 ± 0.250	0.14 ± 0.10	1.020 ± 0.060	$5.60^{+1.55}_{-0.75}$	8.90	155
WASP-120b	3.611	5.010 ± 0.260	1.515 ± 0.083	1890 ± 50	6450 ± 120	0.285 ± 0.031	-0.05 ± 0.07	1.450 ± 0.110	2.16 ± 0.18	3.20	147
WASP-121b	1.275	$1.183^{+0.064}_{-0.062}$	1.865 ± 0.044	2358 ± 52	6459 ± 140	$0.617^{+0.011}_{-0.013}$	0.13 ± 0.09	$1.353^{+0.080}_{-0.079}$	$1.18^{+0.28}_{-0.36}$	4.05	146
WASP-122b	1.710	1.284 ± 0.051	$1.731^{+0.063}_{-0.062}$	1960 ± 50	5774^{+75}_{-74}	$0.517^{+0.025}_{-0.025}$	$0.32^{+0.06}_{-0.06}$	$1.223^{+0.038}_{-0.043}$	$4.00^{+0.31}_{-0.29}$	6.35	147,149
WASP-123b	2.978	0.920 ± 0.050	1.327 ± 0.074	1510 ± 40	5740 ± 130	0.782 ± 0.080	0.18 ± 0.08	1.207 ± 0.089	$4.46^{+0.58}_{-0.74}$	8.20	147
WASP-124b	3.373	0.600 ± 0.070	1.240 ± 0.030	1400 ± 30	6050 ± 100	1.397 ± 0.071	-0.02 ± 0.11	1.070 ± 0.050	$0.18^{+0.47}_{-0.04}$	7.45	155
WASP-126b	3.289	0.280 ± 0.040	$0.960^{+0.100}_{-0.050}$	1480 ± 60	5800 ± 100	$0.790^{+0.080}_{-0.170}$	0.17 ± 0.08	1.120 ± 0.060	$4.20^{+0.41}_{-0.63}$	8.00	155
WASP-12b	1.091	1.410 ± 0.100	1.790 ± 0.090	2516 ± 36	6300^{+200}_{-100}	0.494 ± 0.042	$0.30^{+0.05}_{-0.15}$	1.350 ± 0.140	$1.61^{+0.31}_{-0.40}$	4.05	27
WASP-130b	11.551	1.230 ± 0.040	0.890 ± 0.030	833 ± 18	5600 ± 100	1.670 ± 0.130	0.26 ± 0.10	1.040 ± 0.040	$0.18^{+0.02}_{-0.03}$	10.60	158
WASP-131b	5.322	0.270 ± 0.020	1.220 ± 0.050	1460 ± 30	5950 ± 100	0.412 ± 0.037	-0.18 ± 0.08	1.060 ± 0.060	$5.80^{+0.47}_{-0.62}$	7.20	158
WASP-132b	7.134	0.410 ± 0.030	0.870 ± 0.030	763 ± 16	4750 ± 100	$2.823^{+0.099}_{-0.200}$	0.22 ± 0.13	0.800 ± 0.040	$3.17^{+1.57}_{-1.92}$	19.95	158
WASP-133b	2.176	1.160 ± 0.090	1.210 ± 0.050	1790 ± 40	5700 ± 100	0.550 ± 0.040	0.29 ± 0.12	1.160 ± 0.080	$4.36^{+0.47}_{-0.54}$	6.75	155
WASP-135b	1.401	1.900 ± 0.080	1.300 ± 0.090	1717^{+46}_{-40}	5680 ± 60	1.580 ± 0.210	0.02 ± 0.13	1.010 ± 0.070	$2.16^{+0.91}_{-1.11}$	10.70	160
WASP-13b	4.353	$0.460^{+0.060}_{-0.050}$	$1.210^{+0.140}_{-0.120}$	1417^{+62}_{-58}	5826 ± 100	$0.610^{+0.170}_{-0.140}$	0.00 ± 0.20	$1.030^{+0.110}_{-0.090}$	$4.49^{+1.97}_{-0.70}$	6.65	17,100
WASP-140b	2.236	2.440 ± 0.070	$1.440^{+0.420}_{-0.180}$	1320 ± 40	5300 ± 100	1.950 ± 0.250	0.12 ± 0.10	0.900 ± 0.040	$2.69^{+1.17}_{-1.22}$	15.10	158
WASP-141b	3.311	2.690 ± 0.150	1.210 ± 0.080	1540 ± 50	6050 ± 120	0.692 ± 0.099	0.29 ± 0.09	1.250 ± 0.060	$2.15^{+0.36}_{-0.50}$	5.65	158
WASP-142b	2.053	0.840 ± 0.090	1.530 ± 0.080	2000 ± 60	6060 ± 150	0.423 ± 0.056	0.26 ± 0.12	1.330 ± 0.080	$2.54^{+0.35}_{-0.43}$	4.50	158
WASP-14b	2.244	$7.341^{+0.508}_{-0.496}$	$1.281^{+0.075}_{-0.082}$	1866^{+37}_{-42}	6475 ± 100	$0.765^{+0.111}_{-0.085}$	0.00 ± 0.20	$1.211^{+0.127}_{-0.122}$	$0.79^{+0.37}_{-0.40}$	4.30	35,39
WASP-157b	3.952	0.574 ± 0.093	1.045 ± 0.044	1339 ± 93	5840 ± 140	1.300 ± 0.320	0.34 ± 0.09	1.260 ± 0.120	$0.18^{+0.67}_{-0.04}$	7.65	157
WASP-15b	3.752	0.542 ± 0.050	1.428 ± 0.077	1652 ± 28	6300 ± 100	0.515 ± 0.052	-0.17 ± 0.11	1.180 ± 0.120	$2.93^{+0.25}_{-0.32}$	4.80	21
WASP-16b	3.119	$0.855^{+0.043}_{-0.076}$	$1.008^{+0.083}_{-0.060}$	1280^{+35}_{-21}	5700 ± 150	$1.710^{+0.180}_{-0.250}$	0.01 ± 0.10	$1.022^{+0.074}_{-0.129}$	$0.20^{+1.45}_{-0.04}$	10.35	30
WASP-17b	3.735	0.486 ± 0.032	1.991 ± 0.081	1771 ± 35	6650 ± 80	0.474 ± 0.042	-0.19 ± 0.09	1.306 ± 0.026	$1.99^{+0.17}_{-0.19}$	3.75	87
WASP-18b	0.941	10.430 ± 0.380	1.165 ± 0.057	2384^{+58}_{-30}	6400 ± 100	0.972 ± 0.088	0.00 ± 0.09	1.281 ± 0.069	$0.45^{+0.20}_{-0.33}$	5.15	33,38
WASP-19b	0.789	1.168 ± 0.023	1.386 ± 0.032	2050 ± 40	5500 ± 100	$1.401^{+0.066}_{-0.059}$	0.02 ± 0.09	0.970 ± 0.020	$6.25^{+1.34}_{-1.39}$	13.65	44,78
WASP-1b	2.520	$0.918^{+0.091}_{-0.090}$	$1.514^{+0.052}_{-0.047}$	1811^{+34}_{-27}	6110 ± 45	$0.549^{+0.009}_{-0.059}$	0.23 ± 0.08	$1.301^{+0.049}_{-0.047}$	$2.69^{+0.16}_{-0.23}$	5.30	8,11,82
WASP-20b	4.900	0.313 ± 0.018	1.458 ± 0.057	1379 ± 32	5950 ± 100	0.631 ± 0.047	-0.01 ± 0.06	1.202 ± 0.040	$4.15^{+0.55}_{-0.45}$	6.75	130
WASP-21b	4.323	0.270 ± 0.010	$1.143^{+0.045}_{-0.030}$	1321^{+30}_{-26}	5800 ± 100	$0.920^{+0.058}_{-0.085}$	-0.40 ± 0.10	0.860 ± 0.040	$9.91^{+1.38}_{-1.58}$	13.00	41,88
WASP-22b	3.533	0.588 ± 0.017	$1.158^{+0.061}_{-0.038}$	1466 ± 34	6000 ± 100	$0.864^{+0.066}_{-0.095}$	-0.05 ± 0.08	1.109 ± 0.026	$3.58^{+0.42}_{-0.60}$	7.45	43,69
WASP-23b	2.944	$0.884^{+0.088}_{-0.099}$	$0.962^{+0.047}_{-0.056}$	1119^{+22}_{-21}	5150 ± 100	$2.601^{+0.035}_{-0.038}$	-0.05 ± 0.13	$0.780^{+0.130}_{-0.120}$	$1.30^{+1.36}_{-0.78}$	18.85	65
WASP-24b	2.341	$1.032^{+0.038}_{-0.037}$	$1.104^{+0.052}_{-0.057}$	1660^{+44}_{-42}	6075 ± 100	$1.054^{+0.140}_{-0.100}$	0.07 ± 0.10	$1.129^{+0.027}_{-0.025}$	$1.27^{+0.50}_{-0.46}$	6.55	53
WASP-25b	3.765	0.580 ± 0.040	$1.220^{+0.060}_{-0.050}$	1212 ± 35	5703 ± 100	1.820 ± 0.140	-0.07 ± 0.10	1.000 ± 0.030	$1.00^{+0.65}_{-0.85}$	11.00	86
WASP-26b	2.757	1.028 ± 0.021	1.281 ± 0.075	1637 ± 45	5950 ± 100	0.709 ± 0.088	-0.02 ± 0.09	1.111 ± 0.028	$4.02^{+0.63}_{-0.42}$	7.00	42,69
WASP-28b	3.409	0.907 ± 0.043	1.213 ± 0.042	1468 ± 37	6150 ± 140	1.107 ± 0.082	-0.29 ± 0.10	1.021 ± 0.050	$2.44^{+0.68}_{-0.81}$	7.20	130

Table 8 — *Continued*

Planet	Period (d)	M_p (M_J)	R_p (R_J)	T_{eq} (K)	$T_{eff\star}$ (K)	$\rho_\star$ (g cm^{-3})	[Fe/H]	$M_\star$ ($M_\odot$)	Age (Gyr)	t_{tot} (Gyr)	Refs.
WASP-29b	3.923	0.244 ± 0.020	$0.792^{+0.056}_{-0.035}$	980 ± 40	4800 ± 150	$2.200^{+0.280}_{-0.320}$	0.11 ± 0.14	0.825 ± 0.033	$11.68^{+3.31}_{-4.10}$	19.95	54
WASP-2b	2.152	$0.915^{+0.090}_{-0.093}$	$1.071^{+0.080}_{-0.083}$	1304 ± 54	5200 ± 200	$2.050^{+0.260}_{-0.150}$	0.02 ± 0.05	0.890 ± 0.120	$4.68^{+2.22}_{-2.38}$	17.65	7,11,82,110
WASP-30b	4.157	60.960 ± 0.890	0.889 ± 0.021	1474 ± 25	6100 ± 100	0.758 ± 0.027	-0.08 ± 0.10	1.166 ± 0.026	$3.26^{+0.36}_{-0.51}$	6.50	76
WASP-31b	3.406	0.478 ± 0.030	1.537 ± 0.060	1568 ± 33	6203 ± 98	0.858 ± 0.073	-0.19 ± 0.09	1.161 ± 0.026	$2.86^{+0.35}_{-0.53}$	6.55	67
WASP-32b	2.719	3.600 ± 0.070	1.180 ± 0.070	1560 ± 50	6100 ± 100	1.130 ± 0.140	-0.13 ± 0.10	1.100 ± 0.030	$1.87^{+0.61}_{-0.69}$	7.15	62
WASP-34b	4.318	0.590 ± 0.010	$1.220^{+0.110}_{-0.080}$	1250 ± 30	5700 ± 100	$1.770^{+0.917}_{-0.563}$	-0.02 ± 0.10	1.010 ± 0.070	$0.20^{+1.31}_{-0.05}$	10.75	64
WASP-35b	3.162	0.720 ± 0.060	1.320 ± 0.030	1450 ± 20	6050 ± 100	1.171 ± 0.042	-0.15 ± 0.09	1.070 ± 0.020	$2.31^{+0.67}_{-0.72}$	7.75	73
WASP-36b	1.537	2.270 ± 0.068	1.269 ± 0.030	1700^{+42}_{-44}	5800 ± 150	$1.719^{+0.075}_{-0.068}$	-0.31 ± 0.12	1.020 ± 0.032	$2.56^{+1.13}_{-1.30}$	10.60	93
WASP-37b	3.577	$1.696^{+0.123}_{-0.128}$	$1.136^{+0.060}_{-0.051}$	1325^{+25}_{-15}	5800 ± 150	$0.923^{+0.064}_{-0.097}$	-0.40 ± 0.12	$0.849^{+0.067}_{-0.040}$	$9.06^{+1.63}_{-2.09}$	12.10	72
WASP-38b	6.872	2.712 ± 0.065	$1.079^{+0.053}_{-0.044}$	1261^{+24}_{-23}	6150 ± 80	0.673 ± 0.058	-0.12 ± 0.07	1.216 ± 0.041	$3.42^{+0.20}_{-0.30}$	6.10	63
WASP-39b	4.055	0.280 ± 0.030	1.270 ± 0.040	1116^{+33}_{-32}	5400 ± 150	$1.830^{+0.120}_{-0.100}$	-0.12 ± 0.10	0.930 ± 0.030	$5.31^{+1.81}_{-2.17}$	15.40	66
WASP-3b	1.847	$1.875^{+0.031}_{-0.036}$	$1.290^{+0.050}_{-0.120}$	1960^{+33}_{-76}	6400 ± 100	$0.780^{+0.210}_{-0.070}$	0.00 ± 0.20	$1.240^{+0.060}_{-0.110}$	$0.98^{+0.46}_{-0.44}$	4.60	9,14,49
WASP-41b	3.052	0.920 ± 0.070	1.210 ± 0.070	1235 ± 50	5450 ± 150	1.790 ± 0.200	-0.08 ± 0.09	0.940 ± 0.030	$4.36^{+1.64}_{-1.78}$	14.30	90
WASP-42b	4.982	0.500 ± 0.035	1.080 ± 0.057	995 ± 34	5200 ± 150	1.930 ± 0.200	0.05 ± 0.13	$0.881^{+0.086}_{-0.081}$	$4.96^{+2.09}_{-2.27}$	16.90	91
WASP-43b	0.813	1.780 ± 0.100	$0.930^{+0.070}_{-0.090}$	1370 ± 70	4400 ± 200	$3.810^{+0.860}_{-0.510}$	-0.05 ± 0.17	0.580 ± 0.050	$6.71^{+6.35}_{-5.61}$	19.95	70
WASP-44b	2.424	$0.893^{+0.071}_{-0.066}$	$1.090^{+0.130}_{-0.140}$	1343 ± 64	5400 ± 150	$1.877^{+0.762}_{-0.423}$	0.06 ± 0.10	0.948 ± 0.034	$2.31^{+1.24}_{-2.11}$	13.65	101
WASP-45b	3.126	1.005 ± 0.053	$1.170^{+0.280}_{-0.140}$	1198 ± 69	5100 ± 200	1.496 ± 0.381	0.36 ± 0.12	$0.910^{+0.060}_{-60.000}$	$8.29^{+2.15}_{-3.22}$	18.05	101
WASP-46b	1.430	2.100 ± 0.073	1.327 ± 0.058	1654 ± 50	5600 ± 150	1.694 ± 0.169	-0.37 ± 0.13	0.957 ± 0.034	$6.97^{+1.90}_{-2.37}$	14.45	101
WASP-47b	4.159	1.164 ± 0.091	1.134 ± 0.039	1220 ± 20	5400 ± 100	1.017 ± 0.013	0.18 ± 0.07	1.084 ± 0.037	$9.83^{+1.10}_{-2.04}$	14.95	102,142,144
WASP-47d	9.031	$0.027^{+0.012}_{-0.011}$	0.321 ± 0.012	943^{+17}_{-17}	5400 ± 100	1.017 ± 0.013	0.18 ± 0.07	1.084 ± 0.037	$9.79^{+1.12}_{-2.01}$	14.95	102,142
WASP-47e	0.790	0.038 ± 0.012	0.162 ± 0.006	2126^{+39}_{-39}	5400 ± 100	1.017 ± 0.013	0.18 ± 0.07	1.084 ± 0.037	$9.86^{+1.06}_{-1.86}$	15.00	102,142,144
WASP-48b	2.144	0.980 ± 0.090	1.670 ± 0.080	2030 ± 70	6000 ± 150	0.310 ± 0.028	-0.12 ± 0.12	1.190 ± 0.040	$4.30^{+0.78}_{-1.18}$	5.50	73
WASP-49b	2.782	0.378 ± 0.027	1.115 ± 0.047	1369 ± 39	5600 ± 150	1.425 ± 0.085	-0.23 ± 0.07	$0.938^{+0.080}_{-0.076}$	$7.84^{+1.28}_{-1.97}$	14.55	91
WASP-4b	1.338	1.237 ± 0.064	1.365 ± 0.021	1650 ± 30	5500 ± 100	$1.728^{+0.016}_{-0.047}$	-0.03 ± 0.09	0.925 ± 0.040	$3.79^{+1.25}_{-1.28}$	13.45	15,20
WASP-50b	1.955	$1.468^{+0.091}_{-0.086}$	1.153 ± 0.048	1393 ± 30	5400 ± 100	$2.090^{+0.140}_{-0.130}$	-0.12 ± 0.08	$0.892^{+0.080}_{-0.074}$	$3.36^{+1.28}_{-1.42}$	15.55	68
WASP-52b	1.750	0.460 ± 0.020	1.270 ± 0.030	1315 ± 35	5000 ± 100	2.480 ± 0.110	0.03 ± 0.12	0.870 ± 0.030	$4.06^{+2.18}_{-2.23}$	19.95	105
WASP-54b	3.694	0.626 ± 0.023	$1.650^{+0.090}_{-0.180}$	1742^{+49}_{-69}	6100 ± 100	$0.296^{+0.085}_{-0.028}$	-0.27 ± 0.08	$1.201^{+0.034}_{-0.036}$	$4.91^{+0.36}_{-0.44}$	5.80	106
WASP-55b	4.466	0.570 ± 0.040	$1.300^{+0.050}_{-0.030}$	1290 ± 25	5900 ± 100	$1.200^{+0.042}_{-0.099}$	-0.20 ± 0.08	1.010 ± 0.040	$4.28^{+1.12}_{-1.03}$	9.80	102
WASP-56b	4.617	$0.571^{+0.034}_{-0.035}$	$1.092^{+0.035}_{-0.033}$	1216^{+25}_{-24}	5600 ± 100	1.040 ± 0.060	0.12 ± 0.06	1.017 ± 0.024	$6.01^{+1.09}_{-0.98}$	11.30	106
WASP-57b	2.839	$0.672^{+0.049}_{-0.046}$	$0.916^{+0.017}_{-0.014}$	1251^{+21}_{-22}	5600 ± 100	$2.319^{+0.062}_{-0.089}$	-0.25 ± 0.10	0.954 ± 0.027	$0.69^{+0.64}_{-0.51}$	13.60	106
WASP-58b	5.017	0.890 ± 0.070	1.370 ± 0.200	1270 ± 80	5800 ± 150	0.820 ± 0.270	-0.45 ± 0.09	0.940 ± 0.100	$10.21^{+1.94}_{-2.11}$	12.75	105
WASP-59b	7.920	0.863 ± 0.045	0.775 ± 0.068	670 ± 35	4650 ± 150	4.390 ± 0.900	-0.15 ± 0.11	0.719 ± 0.035	$0.14^{+0.03}_{-0.03}$	19.95	105
WASP-5b	1.628	1.637 ± 0.082	1.171 ± 0.057	1706^{+52}_{-48}	5700 ± 100	1.130 ± 0.110	0.09 ± 0.09	1.021 ± 0.063	$4.45^{+0.75}_{-0.94}$	10.20	15,37,89
WASP-60b	4.305	0.514 ± 0.034	0.860 ± 0.120	1320 ± 75	5900 ± 100	1.020 ± 0.280	-0.04 ± 0.09	1.078 ± 0.035	$3.72^{+0.68}_{-0.68}$	8.50	105
WASP-61b	3.856	2.060 ± 0.170	1.240 ± 0.030	1565 ± 35	6250 ± 150	$0.687^{+0.011}_{-0.024}$	-0.10 ± 0.12	1.220 ± 0.070	$2.51^{+0.38}_{-0.53}$	5.35	102
WASP-62b	4.412	0.570 ± 0.040	1.390 ± 0.060	1440 ± 30	6230 ± 80	0.833 ± 0.085	0.04 ± 0.06	1.250 ± 0.050	$1.88^{+0.32}_{-0.36}$	5.85	102
WASP-63b	4.378	0.380 ± 0.030	$1.430^{+0.100}_{-0.060}$	1540 ± 40	5550 ± 100	$0.279^{+0.024}_{-0.035}$	0.08 ± 0.07	1.320 ± 0.050	$7.19^{+0.53}_{-0.71}$	8.00	102
WASP-64b	1.573	1.271 ± 0.068	1.271 ± 0.039	1689 ± 49	5550 ± 150	$1.198^{+0.075}_{-0.062}$	-0.08 ± 0.11	1.004 ± 0.028	$7.70^{+1.63}_{-2.08}$	13.30	109
WASP-65b	2.311	1.550 ± 0.160	1.112 ± 0.059	1480 ± 10	5600 ± 100	$1.280^{+0.040}_{-0.060}$	-0.07 ± 0.07	0.930 ± 0.140	$7.25^{+0.94}_{-1.44}$	13.65	113
WASP-66b	4.086	2.320 ± 0.130	1.390 ± 0.090	1790 ± 60	6600 ± 150	$0.342^{+0.051}_{-0.040}$	-0.31 ± 0.10	1.300 ± 0.070	$2.29^{+0.20}_{-0.23}$	3.35	102
WASP-67b	4.614	0.420 ± 0.040	$1.400^{+0.300}_{-0.200}$	1040 ± 30	5200 ± 100	1.860 ± 0.210	-0.07 ± 0.09	0.870 ± 0.040	$9.66^{+1.77}_{-2.28}$	19.95	102
WASP-68b	5.084	0.950 ± 0.030	$1.270^{+0.110}_{-0.060}$	1488^{+49}_{-32}	5910 ± 60	$0.367^{+0.042}_{-0.071}$	0.22 ± 0.08	1.240 ± 0.030	$3.58^{+0.13}_{-0.23}$	4.95	119
WASP-69b	3.868	0.260 ± 0.017	1.057 ± 0.047	963 ± 18	4700 ± 50	2.170 ± 0.180	0.15 ± 0.08	0.826 ± 0.029	$18.46^{+1.12}_{-2.04}$	19.95	129
WASP-6b	3.361	$0.503^{+0.019}_{-0.038}$	$1.224^{+0.051}_{-0.052}$	1194^{+58}_{-57}	5450 ± 100	$1.890^{+0.160}_{-0.140}$	-0.20 ± 0.09	$0.880^{+0.050}_{-0.080}$	$5.94^{+1.37}_{-1.83}$	16.05	16
WASP-70Ab	3.713	0.590 ± 0.022	$1.164^{+0.073}_{-0.102}$	1387 ± 40	5700 ± 80	$0.870^{+0.190}_{-0.110}$	-0.01 ± 0.06	1.106 ± 0.042	$7.57^{+0.80}_{-1.10}$	11.40	129
WASP-71b	2.904	2.258 ± 0.072	1.500 ± 0.110	2066 ± 67	6050 ± 100	0.179 ± 0.030	0.15 ± 0.07	1.572 ± 0.062	$2.50^{+0.18}_{-0.17}$	3.00	108
WASP-72b	2.217	$1.410^{+0.050}_{-0.045}$	$1.010^{+0.120}_{-0.080}$	2064^{+90}_{-62}	6250 ± 100	$0.374^{+0.062}_{-0.080}$	-0.06 ± 0.09	$1.327^{+0.043}_{-0.035}$	$2.87^{+0.18}_{-0.27}$	4.15	109
WASP-73b	4.087	$1.880^{+0.070}_{-0.060}$	$1.160^{+0.120}_{-0.080}$	1790^{+75}_{-51}	6030 ± 120	$0.212^{+0.028}_{-0.056}$	0.14 ± 0.14	$1.340^{+0.050}_{-0.040}$	$2.62^{+0.22}_{-0.29}$	3.25	119
WASP-74b	2.138	0.950 ± 0.060	1.560 ± 0.060	1910 ± 40	5990 ± 110	0.477 ± 0.025	0.39 ± 0.13	1.480 ± 0.120	$2.45^{+0.30}_{-0.35}$	4.90	136
WASP-75b	2.484	1.070 ± 0.050	1.270 ± 0.048	1710 ± 20	6100 ± 100	0.790 ± 0.060	0.07 ± 0.09	1.140 ± 0.070	$2.51^{+0.38}_{-0.53}$	6.20	113
WASP-76b	1.810	0.920 ± 0.030	$1.830^{+0.060}_{-0.040}$	2160 ± 40	6250 ± 100	$0.404^{+0.011}_{-0.025}$	0.23 ± 0.10	1.460 ± 0.070	$2.15^{+0.24}_{-0.25}$	3.95	152
WASP-77Ab	1.360	1.760 ± 0.060	1.210 ± 0.020	1669^{+24}_{-24}	5500 ± 80	$1.633^{+0.023}_{-0.028}$	0.00 ± 0.11	1.002 ± 0.045	$4.40^{+1.15}_{-1.20}$	13.45	117
WASP-78b	2.175	0.890 ± 0.080	1.700 ± 0.110	2350 ± 80	6100 ± 150	0.176 ± 0.025	-0.35 ± 0.14	1.330 ± 0.090	$3.82^{+0.40}_{-0.38}$	4.10	92
WASP-79b	3.662	0.900 ± 0.080	2.090 ± 0.140	1900 ± 50	6600 ± 100	0.310 ± 0.040	0.03 ± 0.10	1.520 ± 0.070	$1.69^{+0.17}_{-0.16}$	2.90	92
WASP-7b	4.955	$0.960^{+0.120}_{-0.180}$	$0.915^{+0.046}_{-0.040}$	1379^{+35}_{-23}	6400 ± 100	$0.929^{+0.152}_{-0.179}$	0.00 ± 0.10	$1.280^{+0.090}_{-0.190}$	$0.57^{+0.26}_{-0.37}$	5.00	24
WASP-80b	3.068	$0.554^{+0.030}_{-0.039}$	$0.952^{+0.026}_{-0.027}$	814^{+19}_{-19}	4145 ± 100	$4.400^{+0.030}_{-0.028}$	-0.14 ± 0.16	0.570 ± 0.050	$15.95^{+3.43}_{-6.17}$	19.95	107
WASP-82b	2.706	1.240 ± 0.040	$1.670^{+0.070}_{-0.050}$	2190 ± 40	6500 ± 80	$0.223^{+0.008}_{-0.020}$	0.12 ± 0.11	1.630 ± 0.080	$1.70^{+0.13}_{-0.14}$	2.55	152
WASP-83b	4.971	0.300 ± 0.030	$1.040^{+0.080}_{-0.050}$	1120 ± 30	5480 ± 110	$1.369^{+0.100}_{-0.180}$	0.29 ± 0.12	1.110 ± 0.090	$3.95^{+0.84}_{-1.13}$	12.20	136
WASP-88b	4.954	0.560 ± 0.080	$1.700^{+0.150}_{-0.070}$	1772^{+54}_{-45}	6430 ± 130	$0.226^{+0.028}_{-0.042}$	-0.08 ± 0.12	1.450 ± 0.050	$2.07^{+0.17}_{-0.19}$	2.80	119
WASP-89b	3.356	5.900 ± 0.400	1.040 ± 0.040	1120 ± 20	4955 ± 100	1.920 ± 0.099	0.15 ± 0.14	0.920 ± 0.080	$10.68^{+2.08}_{-2.64}$	19.95	136
WASP-8b	8.159	$2.247^{+0.083}_{-0.074}$	$1.048^{+0.042}_{-0.079}$	951^{+21}_{-28}	5600 ± 80	$1.680^{+0.310}_{-0.160}$	0.17 ± 0.07	$1.033^{+0.058}_{-0.050}$	$1.04^{+0.64}_{-0.88}$	11.10	40
WASP-90b	3.916	0.630 ± 0.070	1.630 ± 0.090	1840 ± 50	6440 ± 130	0.282 ± 0.028	0.11 ± 0.14	1.550 ± 0.100	$1.79^{+0.20}_{-0.26}$	2.90	152
WASP-94Ab	3.950	$0.452^{+0.035}_{-0.032}$	$1.720^{+0.060}_{-0.050}$	1604^{+25}_{-22}	6153^{+75}_{-76}	$0.486^{+0.016}_{-0.028}$	0.26 ± 0.15	1.450 ± 0.090	$2.27^{+0.28}_{-0.39}$	4.60	122
WASP-95b	2.185	$1.130^{+0.100}_{-0.040}$	1.210 ± 0.060	1570 ± 50	5830 ± 140	$1.100^{+0.060}_{-0.180}$	0.14 ± 0.16	1.110 ± 0.090	$2.35^{+0.80}_{-1.12}$	7.90	128
WASP-96b	3.425	0.480 ± 0.030	1.200 ± 0.060	1285 ± 40	5500 ± 150	1.300 ± 0.100	0.14 ± 0.19	1.060 ± 0.090	$4.46^{+1.36}_{-1.51}$	11.60	128
WASP-97b	2.073	1.320 ± 0.050	1.130 ± 0.060	1555 ± 40	5670 ± 110	1.310 ± 0.130	0.23 ± 0.11	1.120 ± 0.060	$2.40^{+0.77}_{-0.95}$	9.75	128
WASP-98b	2.963	0.830 ± 0.070	1.100 ± 0.040	1180 ± 30	5550 ± 140	2.810 ± 0.100	-0.60 ± 0.19	0.690 ± 0.060	$2.19^{+2.37}_{-1.73}$	16.00	128
WASP-99b	5.753	2.780 ± 0.130	$1.100^{+0.080}_{-0.050}$	1480 ± 40	6150 ± 100	$0.381^{+0.028}_{-0.056}$	0.21 ± 0.15	1.480 ± 0.100	$2.41^{+0.31}_{-0.33}$	4.05	128

Table 8 — *Continued*

Planet	Period (d)	M_p (M_J)	R_p (R_J)	T_{eq} (K)	$T_{eff\star}$ (K)	$\rho_\star$ (g cm^{-3})	[Fe/H]	$M_\star$ ($M_\odot$)	Age (Gyr)	t_{tot} (Gyr)	Refs.

References. — 1–O'Donovan et al. (2006); 2–Sozzetti et al. (2007); 3–Torres et al. (2007); 4–Mandushev et al. (2007); 5–Kovács et al. (2007); 6–Bakos et al. (2007); 7–Collier Cameron et al. (2007); 8–Stempels et al. (2007); 9–Gibson et al. (2008); 10–Noyes et al. (2008); 11–Torres et al. (2008); 12–Pál et al. (2008); 13–Johnson et al. (2008); 14–Pollacco et al. (2008); 15–Gillon et al. (2009b); 16–Gillon et al. (2009a); 17–Skillen et al. (2009); 18–Ammler-von Eiff et al. (2009); 19–Rabus et al. (2009); 20–Winn et al. (2009); 21–West et al. (2009); 22–Raetz et al. (2009); 23–Shporer et al. (2009); 24–Hellier et al. (2009b); 25–Sozzetti et al. (2009); 26–Johnson et al. (2009b); 27–Hebb et al. (2009); 28–Bakos et al. (2009a); 29–Gibson et al. (2009); 30–Lister et al. (2009); 31–Latham et al. (2009); 32–Hartman et al. (2009); 33–Southworth et al. (2009b); 34–Bakos et al. (2009b); 35–Joshi et al. (2009); 36–Christian et al. (2009); 37–Southworth et al. (2009a); 38–Hellier et al. (2009a); 39–Johnson et al. (2009a); 40–Queloz et al. (2010); 41–Bouchy et al. (2010); 42–Smalley et al. (2010); 43–Maxted et al. (2010a); 44–Hebb et al. (2010); 45–Bakos et al. (2010); 46–Christiansen et al. (2010); 47–Welsh et al. (2010); 48–Christensen-Dalsgaard et al. (2010); 49–Tripathi et al. (2010); 50–Torres et al. (2010); 51–Winn et al. (2010); 52–Buchhave et al. (2010); 53–Street et al. (2010); 54–Hellier et al. (2010); 55–Kovács et al. (2010); 56–Kipping et al. (2010); 57–Krejčová et al. (2010); 58–Szabo et al. (2010); 59–Gibson et al. (2010); 60–Pál et al. (2010); 61–Collier Cameron et al. (2010); 62–Maxted et al. (2010b); 63–Barros et al. (2011b); 64–Smalley et al. (2011); 65–Triaud et al. (2011); 66–Faedi et al. (2011); 67–Anderson et al. (2011d); 68–Gillon et al. (2011); 69–Anderson et al. (2011a); 70–Hellier et al. (2011b); 71–Winn et al. (2011); 72–Simpson et al. (2011); 73–Enoch et al. (2011b); 74–Kipping et al. (2011); 75–Hartman et al. (2011a); 76–Anderson et al. (2011c); 77–Hartman et al. (2011b); 78–Hellier et al. (2011a); 79–Buchhave et al. (2011); 80–Béky et al. (2011); 81–Johnson et al. (2011); 82–Albrecht et al. (2011); 83–Mandushev et al. (2011); 84–Bakos et al. (2011); 85–Hartman et al. (2011c); 86–Enoch et al. (2011a); 87–Anderson et al. (2011b); 88–Barros et al. (2011a); 89–Fukui et al. (2011); 90–Maxted et al. (2011); 91–Lendl et al. (2012); 92–Smalley et al. (2012); 93–Smith et al. (2012); 94–Hartman et al. (2012); 95–Bakos et al. (2012); 96–Quinn et al. (2012); 97–Howard et al. (2012); 98–Beatty et al. (2012); 99–Siverd et al. (2012); 100–Barros et al. (2012); 101–Anderson et al. (2012); 102–Hellier et al. (2012); 103–Dittmann et al. (2012); 104–Sato et al. (2012); 105–Hébrard et al. (2013); 106–Faedi et al. (2013); 107–Triaud et al. (2013); 108–Smith et al. (2013); 109–Gillon et al. (2013); 110–Santos et al. (2013); 111–Mohler-Fischer et al. (2013); 112–Boisse et al. (2013); 113–Gómez Maqueo Chew et al. (2013); 114–Penev et al. (2013); 115–Bayliss et al. (2013); 116–Pepper et al. (2013); 117–Maxted et al. (2013); 118–Gillon et al. (2014); 119–Delrez et al. (2014); 120–Lendl et al. (2014); 121–Smith et al. (2014); 122–Neveu-VanMalle et al. (2014); 123–Hartman et al. (2014); 124–Zhou et al. (2014); 125–Collins et al. (2014); 126–Bieryla et al. (2014); 127–Jordán et al. (2014); 128–Hellier et al. (2014); 129–Anderson et al. (2014); 130–Anderson et al. (2015); 131–Mancini et al. (2015); 132–Bakos et al. (2015a); 133–Hartman et al. (2015c); 134–Bieryla et al. (2015); 135–Hartman et al. (2015a); 136–Hellier et al. (2015); 137–Hartman et al. (2015b); 138–Brahm et al. (2015); 139–Bayliss et al. (2015); 140–Huang et al. (2015); 141–Fulton et al. (2015); 142–Becker et al. (2015); 143–Bakos et al. (2015b); 144–Dai et al. (2015); 145–Zhou et al. (2015); 146–Delrez et al. (2015); 147–Turner et al. (2015); 148–Kuhn et al. (2015); 149–Rodriguez et al. (2015); 150–Ciceri et al. (2015); 151–Juncher et al. (2015); 152–West et al. (2016); 153–Eastman et al. (2016); 154–Brahm et al. (2016); 155–Maxted et al. (2016); 156–Rabus et al. (2016); 157–Močnik et al. (2016); 158–Hellier et al. (2016); 159–Espinoza et al. (2016); 160–Spake et al. (2016); 161–Bakos et al. (2016); 162–Bakos et al. (2016b; in prep); 163–Bento et al. (2016); 164–Bhatti et al. (2016); 165–de Val-Borro et al. (2016); 166–this work; 167–Penev et al. (2016);